

1 ***Tectonic evolution and deep mantle structure of the eastern Tethys since the latest***
2 ***Jurassic***

3
4 **Authors**

5 Sabin Zahirovic^{a,*}, Kara J Matthews^{a,#}, Nicolas Flament^a, R Dietmar Müller^a, Kevin C Hill^b, Maria
6 Seton^a and Michael Gurnis^c

7
8 ^a EarthByte Group, School of Geosciences, The University of Sydney, NSW 2006, Australia

9 ^b Oil Search Limited, Sydney, NSW 2000, Australia

10 ^c Seismological Laboratory, California Institute of Technology, Pasadena, California 91125,
11 USA

12
13 * Corresponding author at: EarthByte Group, School of Geosciences, The University of Sydney,
14 NSW 2006, Australia. E-mail address: sabin.zahirovic@sydney.edu.au (S. Zahirovic)

15 # Present address: Department of Earth Sciences, University of Oxford, South Parks Road, Oxford
16 OX1 3AN, UK

17
18 Invited review submitted to *Earth-Science Reviews*

19

21	1	Introduction.....	5
22	1.1	Plate tectonic models of the eastern Tethys	12
23	1.2	Seismic tomography constraints	18
24	1.3	Numerical modelling of Tethyan geodynamics	22
25	1.3.1	Numerical models of India-Eurasia convergence	23
26	1.3.2	Numerical modelling of Southeast Asia and New Guinea geodynamics	27
27	2	Methods	28
28	2.1	Plate tectonic reconstructions.....	28
29	2.2	Insights from seismic tomography.....	36
30	2.3	Coupled plate reconstructions and mantle convection numerical models	38
31	3	Regional tectonic evolution	43
32	3.1	Late Jurassic plate boundary configuration and rifting mechanism along northern Gondwana.....	43
33	3.2	Active margin evolution in the Lhasa segment	51
34	3.3	Convergence along the West Burma and Sumatra margin segment.....	55
35	3.3.1	Development of the Woyla intra-oceanic arc.....	57
36	3.3.2	Subduction of the Woyla back-arc basin	58
37	3.4	Accretionary history of the Java and Borneo margin segment	64
38	3.4.1	Subduction and accretion history of southern Sundaland	64
39	3.4.2	Northern Sundaland collisions.....	70
40	3.4.3	Sundaland oroclinal bending	73
41	3.5	New Guinea and the Philippines	75
42	3.5.1	Origin and evolution of the Philippine Archipelago.....	75
43	3.5.2	Nature of the New Guinea margin since the Late Jurassic	76
44	4	Insights from age-coded slabs in seismic tomography	81
45	5	Numerical modelling results	87
46	5.1	Large-scale post-Jurassic mantle evolution of the Tethyan tectonic domain	87
47	5.2	Regional interpretations of mantle evolution.....	91
48	5.2.1	India-Eurasia convergence.....	91
49	5.2.2	Woyla and Sumatra active margin evolution	95
50	5.2.3	Java and Borneo subduction history.....	98
51	5.2.4	New Guinea margin evolution	101
52	6	Discussion.....	106
53	6.1	Intra-oceanic subduction in the Meso- and Neo-Tethys.....	106
54	6.2	Southeast Asia and New Guinea.....	108
55	6.3	Relevance to global plate reconstructions and geodynamics	111
56	7	Conclusions.....	111
57			

59 **Abstract**

60 The breakup of Pangea in the Jurassic saw the opening of major ocean basins at the expense
61 of older Tethyan and Pacific oceanic plates. Although the Tethyan seafloor spreading history has
62 been lost to subduction, proxy indicators from multiple generations of Tethyan ribbon terranes and
63 the active margin geological histories of volcanism and ophiolite obduction events can be used to
64 reconstruct these ancient oceanic plates. The resulting plate reconstructions reconcile observations
65 from ocean basins and the onshore geological record to provide a regional synthesis, embedded in a
66 global plate motion model, of the India-Eurasia convergence history, the accretionary growth of
67 Southeast Asia and the Tethyan-Pacific tectonic link through the New Guinea margin.

68 The global plate motion model presented in this study captures the time-dependent evolution
69 of plates and their tectonic boundaries since 160 Ma, which are assimilated as surface boundary
70 conditions for numerical experiments of mantle convection. We evaluate subducted slab locations
71 and geometries predicted by forward mantle flow models against P- and S-wave seismic tomography.
72 This approach harnesses modern plate reconstruction techniques, mantle convection models with
73 imposed one-sided subduction, and constraints from the surface geology to address a number of
74 unresolved Tethyan geodynamic controversies. Our synthesis reveals that north-dipping subduction
75 beneath Eurasia in the latest Jurassic consumed the Meso-Tethys, and suggests that northward slab
76 pull opened the younger Neo-Tethyan ocean basin from ~155 Ma. We model the rifting of
77 ‘Argoland’, representing the East Java and West Sulawesi continental fragments, which were
78 transferred northward in latest Jurassic times from the northwest Australian shelf – likely colliding
79 first with parts of the Woyla intra-oceanic arc in the mid-Cretaceous, and accreting to the Borneo
80 (Sundaland) core by ~80 Ma. The Neo-Tethyan ridge was likely consumed along an intra-oceanic
81 subduction zone south of Eurasia from ~105 Ma, leading to a major change in the motion of the
82 Indian Plate by ~100 Ma, as observed in the Wharton Basin fracture zone bends.

83 We investigate the geodynamic consequences of long-lived intra-oceanic subduction within
84 the Neo-Tethys, requiring a two-stage India-Eurasia collision involving first contact between Greater

85 India and the Kohistan-Ladakh Arc sometime between ~60 and 50 Ma, followed by continent-
86 continent collision from ~47 Ma. Our models suggest the Sunda slab kink beneath northwest Sumatra
87 in the mantle transition zone results from the rotation and extrusion of Indochina from ~30 Ma. Our
88 results are also the first to reproduce the enigmatic Proto South China Sea slab beneath northern
89 Borneo, as well as the Tethyan/Woyla slab that is predicted at mid-mantle depths south of Sumatra.
90 Further east, our revised reconstructions of the New Guinea margin, notably the evolution of the
91 Sepik composite terrane and the Maramuni subduction zone, produce a better match with seismic
92 tomography than previous reconstructions, and account for a slab at ~30°S beneath Lake Eyre that
93 has been overridden by the northward advancing Australian continent. Our plate reconstructions
94 provide a framework to study changing patterns of oceanic circulation, long-term sea level driven by
95 changes in ocean basin volume, as well as major biogeographic dispersal pathways that have resulted
96 from Gondwana fragmentation and accretion of Tethyan terranes to south- and southeast-Eurasia.

97

98

99 Keywords:

100 Tethys, Pangea, tectonics, geodynamics, Sundaland, Southeast Asia

101

102

103 **1 Introduction**

104

105 Southern Eurasia, Southeast Asia and New Guinea represent a unique example of long-term
106 tectonic convergence between multiple tectonic domains that has resulted in a complex assemblage
107 of continental fragments, intra-oceanic arcs, ophiolite belts and marginal basins (Figs. 1 and 2). The
108 Southeast Asian continental promontory, known as Sundaland, has grown through successive
109 accretionary episodes resulting from the breakup of Pangea (Acharyya, 1998; Audley-Charles, 1988;
110 Metcalfe, 1994), and subsequent northward transfer of Gondwana-derived continental ribbon terranes
111 and microcontinents on the Tethyan oceanic “conveyors” towards Eurasia. Importantly, the region
112 records a complex interaction between the Tethyan and (proto-) Pacific tectonic domains, which has
113 opened and consumed successive oceanic basins and gateways (Metcalfe, 1999), and has had major
114 consequences for biogeographic dispersal pathways such as the origin of the Wallace Line (Burrett
115 et al., 1991; de Bruyn et al., 2014; Lohman et al., 2011; Monod and Prendini, 2015; Rolland et al.,
116 2015), oceanic circulation (Gaina and Müller, 2007; Gurlan et al., 2008; Heine et al., 2004), global
117 climate and sea level (Herold et al., 2014; Huber and Goldner, 2012; Lee et al., 2013; Morley, 2012b;
118 Müller et al., 2008; Scotese et al., 1999; Spasojevic and Gurnis, 2012; van der Meer et al., 2014;
119 Wang, 2004; Xu et al., 2012), and the development of economic resources (Goldfarb et al., 2014;
120 Zaw et al., 2014).

121 Plate tectonic reconstructions play a pivotal role in unravelling the complexity of this region
122 and provide a platform to address long-standing geological questions in a geodynamic context. We
123 apply a modern approach of modelling entire plates, their evolving plate boundaries and the terranes
124 they carry. This study aims to synthesise previously published onshore and offshore geological
125 constraints, as well as incorporate decades of developments in plate tectonic reconstructions, into a
126 modern plate motion model to document the post-Pangea geodynamic evolution of southern Eurasia,

127 Southeast Asia and New Guinea since the Late Jurassic in a regional and global context. Despite
128 significant technological and methodological advancements in plate reconstruction approaches, very
129 few reconstructions of the eastern Tethys exist in an open-access digital form that can be tested and
130 expanded by the scientific community.

131 As part of this work, we release detailed plate reconstructions for the eastern Tethys (from the
132 India-Eurasia collision zone eastward to Papua New Guinea, Figs. 1-3) that are embedded in a self-
133 consistent global plate motion model, as a collection of digital geometry files and rotation parameters
134 compatible with the open-source and cross-platform plate reconstruction tool, GPlates
135 (www.gplates.org). We provide a brief background to previous regional tectonic reconstructions in
136 Section 1.1, as well as tomographic and numerical modelling approaches in Sections 1.2-1.3 that have
137 been used to gain insight into the tectonic and geodynamic processes controlling the regional
138 evolution. In Sections 2 to 4, we outline our approach of building modern plate reconstructions for
139 the three key regions that comprise the eastern Tethys, including i) the India-Eurasia convergence
140 zone, ii) Southeast Asia, and iii) the New Guinea margin, and compare our approach and findings
141 with previous work. In Section 5, we show how modern plate reconstructions that incorporate
142 evolving plate boundaries can be used with numerical models of mantle flow to predict mantle
143 structure, study the distribution of ancient slabs, and test alternative plate motion scenarios where
144 geological constraints are vague or interpretation is ambiguous. In Sections 6 and 7 we highlight the
145 implications of our work in a regional and global context, and provide some key findings from our
146 modelling of the tectonic and geodynamic evolution of the entire eastern Tethyan domain.

147 The coupled global plate reconstructions and mantle flow models provide a context for better
148 understanding the latest Jurassic rifting events from northern Gondwana (Metcalf, 1994; Pigram and
149 Panggabean, 1984), which opened the Neo-Tethys at the expense of the Meso-Tethys ocean basin
150 (Fig. 4a). This rifting episode transferred the ‘Argoland’ ribbon continent, which included East Java,
151 West Sulawesi and Mangkalihat (Hall, 2012; Zahirovic et al., 2014), north towards Eurasia, while
152 also marking the onset of major intra-oceanic subduction systems along southern Eurasia and

153 northern New Guinea. In the absence of preserved seafloor spreading histories for Neo-Tethyan
154 evolution, we test alternative scenarios of subduction using geodynamic models of mantle flow that
155 are compared with the present-day mantle structure interpreted from seismic tomography.

156 The improvement in the methods applied to plate reconstructions and increasing levels of
157 detail in complex regions have implications for linking plate tectonic evolution with the deep mantle
158 and other Earth systems. Improved plate tectonic reconstruction techniques have enabled the
159 quantification of time-dependent convergence rates (Lee and Lawver, 1995; Sdrolias and Müller,
160 2006; Whittaker et al., 2007), and inferences on regional and global plate re-organization events
161 (Matthews et al., 2011; Matthews et al., 2012), as well as providing insight into the size distribution
162 of tectonic plates (Morra et al., 2013) and factors controlling the speed of tectonic plates (Zahirovic
163 et al., 2015). The plate reconstructions presented in this work have important implications for our
164 understanding of the mid-Cretaceous seafloor spreading pulse (Seton et al., 2009) that may have led
165 to higher eustatic sea levels (Müller et al., 2008), the proposed major regional and global plate
166 reorganization at ~105-100 Ma (Matthews et al., 2012) that may be linked to the subduction of the
167 Neo-Tethyan mid oceanic ridge. In addition, plate reconstructions of the Tethyan domain have
168 consequences for understanding the atmospheric carbon budget resulting from the initiation and
169 abandonment of major Andean-style and intra-oceanic Tethyan subduction zones (Jagoutz et al.,
170 2016; van der Meer et al., 2014).

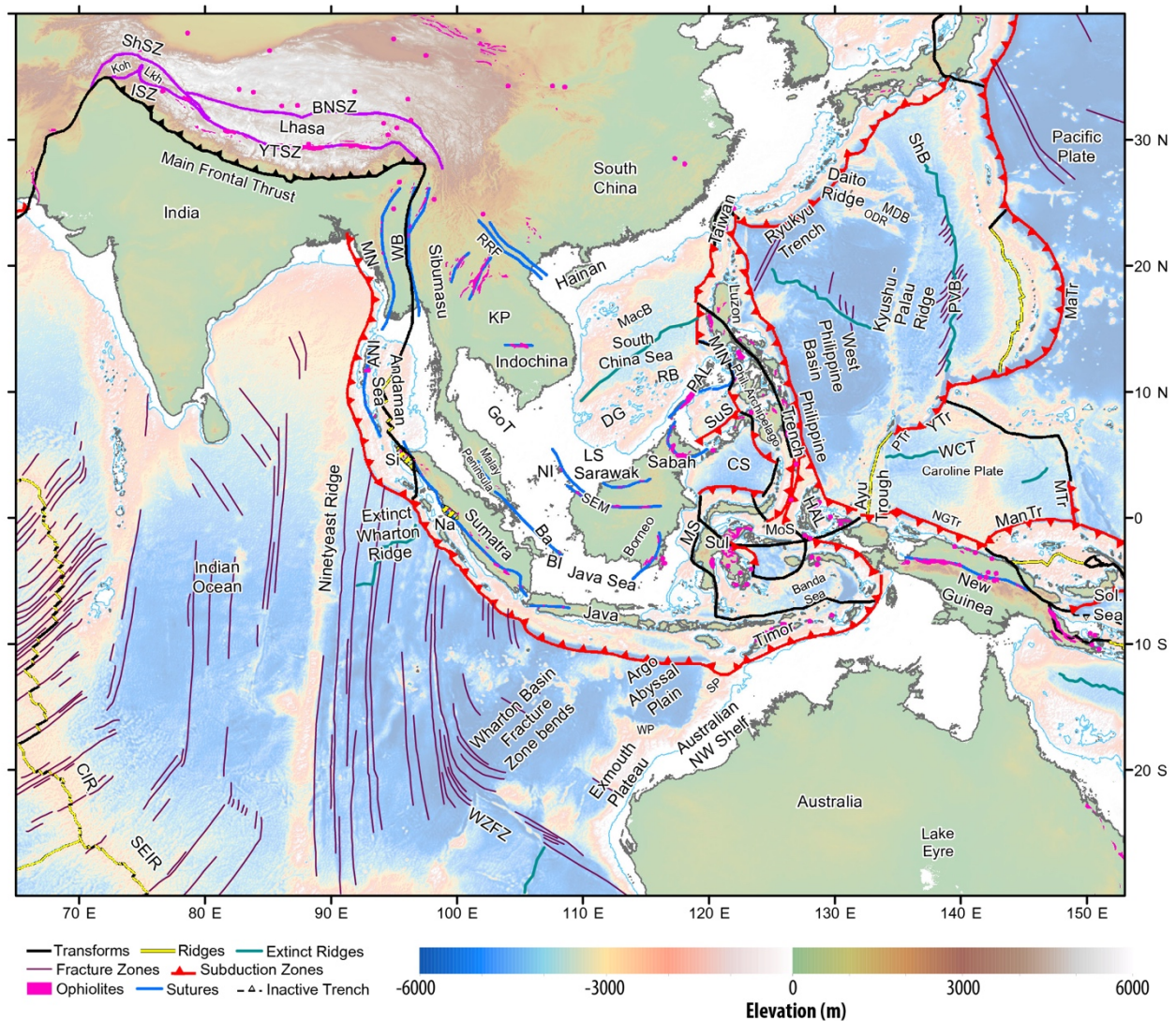
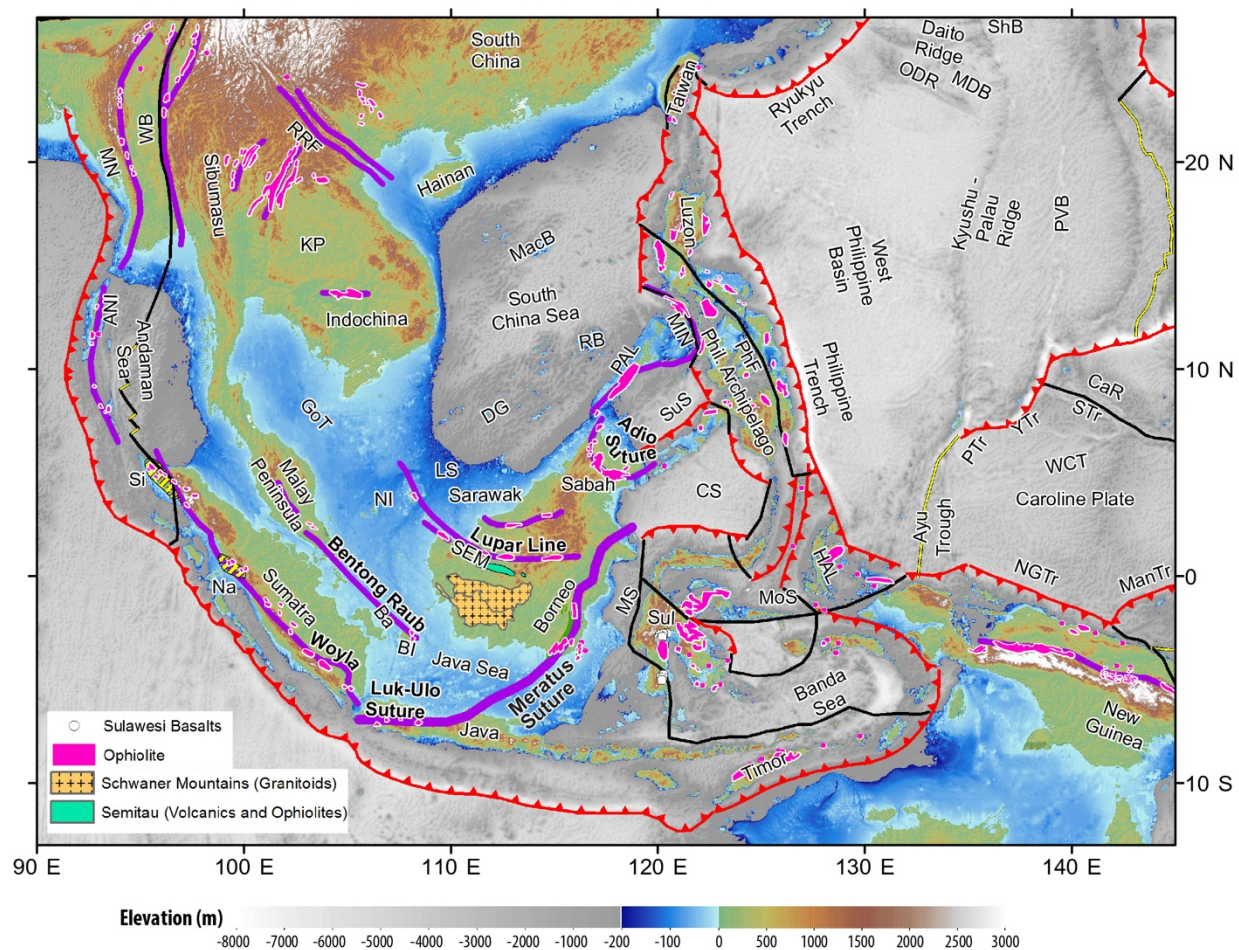


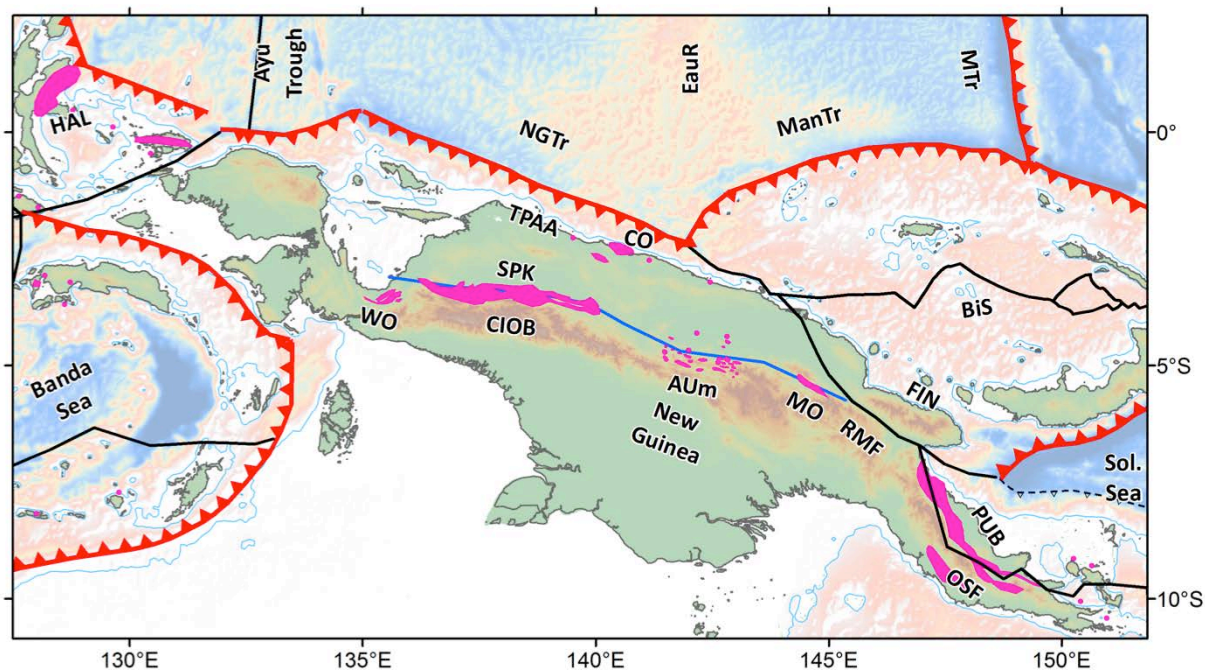
Fig. 1. Regional tectonic setting of southern Eurasia, Southeast Asia and New Guinea. The plate boundaries are modified from Bird (2003), the topography is from Amante et al. (2009), and the seafloor fabric is from Matthews et al. (2011). Southeast Asian sutures (blue) and ophiolites are modified from Hutchison (1975), with additional ophiolites for New Guinea from Baldwin et al. (2012), and for Southeast Asia from Pubellier et al. (2004). The Tethyan sutures in the Indian segment of the margin (violet lines) are from Yin and Harrison (2000). ANI – Andaman-Nicobar Islands, Ba – Bangka Island, BI – Billiton Island, BNSZ – Bangong-Nujiang Suture Zone, CIR – Central Indian Ridge, CS – Celebes Sea, DG – Dangerous Grounds, GoT – Gulf of Thailand, HAL – Halmahera, ISZ – Indus Suture Zone, Koh-Lkh – Kohistan-Ladakh, KP – Khorat Plateau, LS – Luconia Shoals, ManTr – Manus Trench, MaTr – Izu-Bonin-Mariana Trench, MDB – Minami Daito Basin, MIN – Mindoro, MN – Mawgyi Nappe, MoS – Molucca Sea, MP – Malay Peninsula, MS – Makassar Straits,

183 MTr – Mussau Trench, Na – Natal, NGTr – New Guinea Trench, NI – Natuna Island, ODR – Oki
 184 Daito Ridge, PA – Philippine Arc, PAL – Palawan, PTr – Palau Trench, PVB – Parece Vela Basin,
 185 RB – Reed Bank, RRF – Red River Fault, SEIR – Southeast Indian Ridge, SEM – Semitau, ShB –
 186 Shikoku Basin, ShSZ – Shyok Suture Zone, Si – Sikuleh, Sol. Sea – Solomon Sea, SP – Scott Plateau,
 187 Sul – Sulawesi, SuS – Sulu Sea, WB – West Burma, WCT – West Caroline Trough, WP – Wombat
 188 Plateau, WZFZ – Wallaby Zenith Fracture Zone, YTr – Yap Trench, YTSZ – Yarlung-Tsangpo
 189 Suture Zone.



190
 191 **Fig. 2.** Regional tectonic framework of Southeast Asia and New Guinea, with high-resolution Global
 192 Multi-Resolution Topography of depths shallower than 200 m from Ryan et al. (2009). Abbreviations
 193 and plate boundary symbology follow those used in Fig. 1.

194

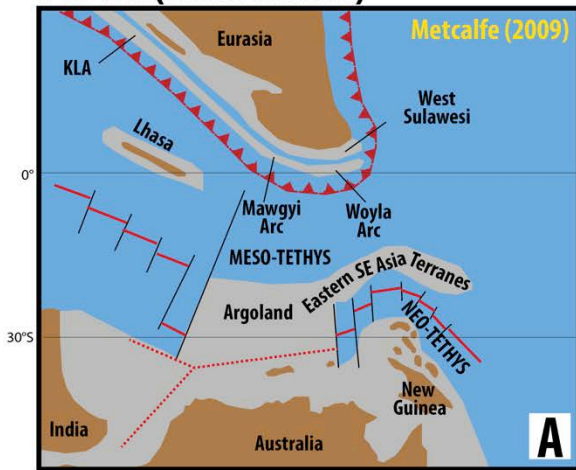


196

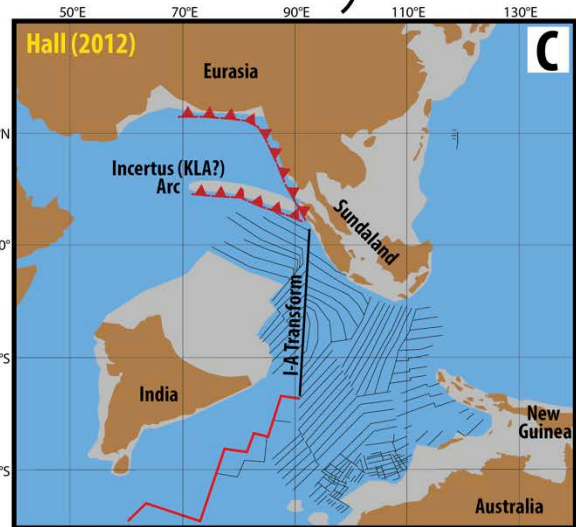
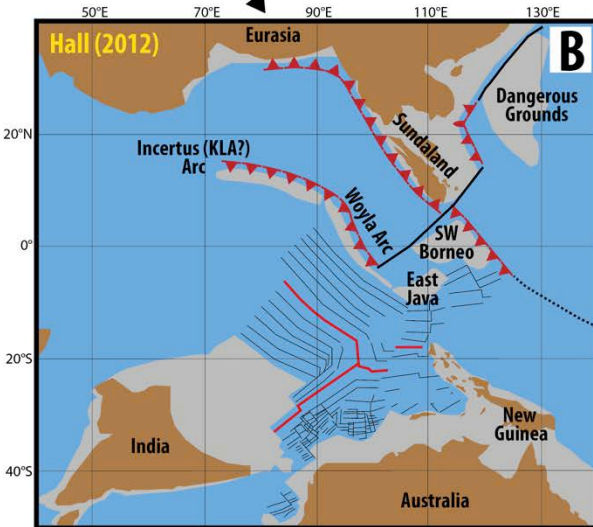
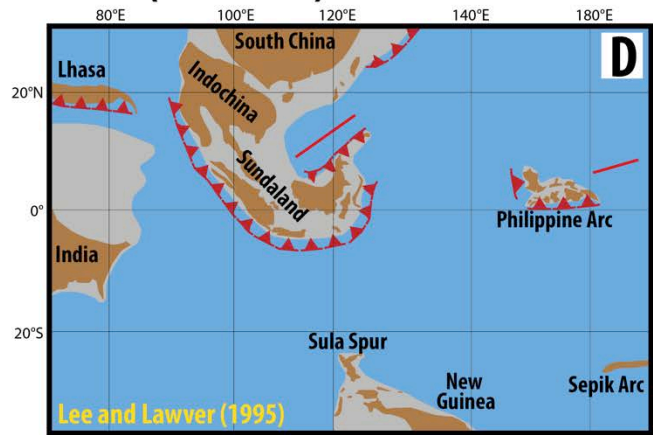
197 **Fig. 3.** Tectonic framework and topography of New Guinea. AUm – April Ultramafics, BiS –
198 Bismarck Sea, CIOB – Central Irian Ophiolite Belt, CO – Cyclops Ophiolite, EauR – Eauripik Rise,
199 FIN – Finisterre Terrane, MO – Marum Ophiolite, OSF – Owen Stanley Fault, PUB – Papuan
200 Ultramafic Belt, SPK – Sepik Terrane, Sol. Sea – Solomon Sea, TPA – Torricelli-Prince Alexander
201 Arc, WO – Weyland Overthrust. Other abbreviations and plate boundary symbology follow those
202 used in Fig. 1.

203

165 Ma (Late Jurassic)



60 Ma (Paleocene)



120 Ma (Early Cretaceous)

70 Ma (Late Cretaceous)

Fig. 4. A wide range of tectonic reconstructions have been proposed for the eastern Tethys between the India-Eurasia convergence zone and New Guinea. A) The Late Jurassic rifting event along northern Gondwana has been modelled as a westward propagating rift from New Guinea towards Argoland, and joining up as a triple junction in between India and Australia in the model of Metcalfe (2009). The rifting mechanism is implied as northward slab pull from Tethyan subduction along southern Eurasia. B) The model of Hall (2012) instead invokes a south-dipping subduction zone along northern Gondwana in the latest Jurassic, leading to the opening of the Neo-Tethys as a large back-arc basin. The related Incertus Arc likely represents the Kohistan-Ladakh (KLA) and Woyla arc systems in the Neo-Tethys. C) By the Late Cretaceous, subduction polarity reverses across the Incertus Arc to produce northward slab pull along a north-dipping intra-oceanic subduction zone. The

215 Hall (2012) model imposes a subduction hiatus along southern Sundaland between 90 and 45 Ma,
216 which requires the segmentation of the Neo-Tethys across a transform that cross-cuts Tethyan
217 seafloor fabric at ~90°E (I-A Transform). D) The model of Lee and Lawver (1995) presents eastern
218 Tethyan plate reconstructions since 60 Ma in a South China fixed reference frame. The size of Greater
219 India is similar as proposed in Hall (2012), but is about twice the northward extent presented in this
220 study, largely to accommodate an India-Eurasia continent-continent collision at ~55 Ma. The Lee and
221 Lawver (1995) model also presents all plate rotation parameters, which enables the reproducibility
222 and testability of this model. A common feature between the models (A-D) is relatively less detail for
223 the New Guinea region, which has been difficult to reconstruct due to the lack of data and the
224 dominance of complex interactions between Asian and Pacific subduction systems.

225

226 **1.1 Plate tectonic models of the eastern Tethys**

227

228 As many generations of plate reconstructions have been proposed for the eastern Tethyan
229 tectonic domain, it is useful to understand the historical context and help categorize successive
230 generations of models that have been proposed. Even before the acceptance of plate tectonic
231 principles, Southeast Asian geology was of great interest due to significant hydrocarbon (Halbouty
232 et al., 1970; Wennekens, 1958) and metallogenic (Brown, 1951; Leith, 1926; Matthews, 1990;
233 Penrose, 1903) discoveries. Early attempts to explain the geology of Southeast Asia led to a large
234 number of competing hypotheses. Fairbridge (1963) explained the geological affinities between
235 Southeast Asia and Gondwana by invoking a range of mechanisms from now-abandoned ideas of
236 mantle contraction, mantle expansion, rising and sinking land bridges, galactic expansion, to then
237 emerging ideas of continental drift. A few years on, Audley-Charles (1966) provided the first
238 synthesis of stratigraphic evidence to describe the region's Mesozoic paleogeographic evolution in
239 the context of continental drift, with special reference to paleo-latitude indicators from paleo-climatic
240 and paleo-magnetic data.

241 It was only in the 1970s that plate tectonic principles of subduction, seafloor spreading and
242 transform tectonic boundaries (Forsyth and Uyeda, 1975; Le Pichon, 1968; McKenzie, 1969;
243 McKenzie and Parker, 1967) were invoked in first-generation continental reconstructions (Table 1)
244 to explain the present-day tectonic complexity of the eastern Tethys (Fitch, 1972; Hamilton, 1979;
245 Katili, 1971). These models were subsequently used to create the first schematic “plate
246 reconstructions” (Katili, 1975) that largely focused on the dominance of active volcanic arcs and
247 associated subduction zones in controlling the tectonic complexity of the region. Importantly, the
248 work of Katili (1975) identified a number of parallel and arcuate paleo-arc systems, which recorded
249 post-Permian subduction of Tethyan oceanic crust. Pioneering work in the 1970s and 1980s applied
250 paleomagnetic techniques to infer that parts of Southeast Asia originated from the northern
251 Gondwana margin (McElhinny et al., 1981), and more specifically somewhere between north Africa
252 and Greater India (the portion of India currently under-thrust beneath Eurasia) (Stauffer, 1983).
253 Although the origin of Southeast Asian continental fragments from Arabia or Africa in the Paleozoic
254 have since been discounted (see Metcalfe, 1988; Metcalfe, 1994; Metcalfe, 1999; Veevers, 2004),
255 these early works established the wider notion of Southeast Asian crustal accretion via the northward
256 transfer of continental fragments originating from the northern Gondwana margins (Fig. 4A).

257 Pioneering reconstructions of Gondwana breakup, and the northward transfer of crustal
258 fragments towards Asia, were largely presented as schematic scenarios portraying the drift of
259 continents with consideration of some major regional plate boundaries. Pigram and Panggabean
260 (1984) and Audley-Charles (1988) combined regional stratigraphic composite wells to identify a
261 major Late Jurassic breakup unconformity across the NW Australian margin, which suggested that a
262 number of continental fragments had detached to form the north Gondwana passive margin and open
263 the “Mesozoic Tethys” ocean basin. Based on the interpretation of rift-drift sedimentary sequences,
264 including the timing of the post-breakup unconformity, Pigram and Panggabean (1984) provided
265 schematic reconstructions of the Late Jurassic drifting episode and concluded that seafloor spreading
266 initiated sometime in the Early Jurassic along New Guinea and Middle Jurassic along the NW

267 Australian shelf. The generally northward transfer of Gondwana terranes opened successive Tethyan
268 ocean basins including the rifting of a ribbon continent comprising Iran, North Tibet (Qiangtang) and
269 Indochina to open “Tethys II” in the late Permian (Audley-Charles, 1988). A subsequent major rifting
270 phase in the Late Jurassic opened the “Tethys III”, detaching fragments including South Tibet
271 (Lhasa), West Burma, Malaya, Borneo, Sulawesi, Sumatra and a number of Banda allochthons
272 (Audley-Charles, 1988). Importantly, the work of Audley-Charles (1988) and Audley-Charles et al.
273 (1988) introduced a paleogeographic reconstruction framework using the computerised University of
274 Cambridge Atlas plotting workflow, which we classify as a second generation reconstruction
275 methodology (Table 1). This early generation of reconstructions assessed the prior continental
276 affinities and inferred major rifting phases using biostratigraphic constraints, as well as made use of
277 paleomagnetic syntheses and structural interpretations from seismic sections to infer rift and drift
278 histories.

279 The third generation of plate reconstructions, largely developed in the late 1980s and
280 throughout the 1990s (e.g., Besse and Courtillot, 1988; Daly et al., 1991; Jolivet et al., 1989; Lee and
281 Lawver, 1994; Lee and Lawver, 1995), made use of extensive identifications of marine magnetic
282 anomalies from the Indian Ocean and West Pacific calibrated to a geological timescale (e.g., Taylor
283 and Hayes, 1980; Taylor and Hayes, 1983). The seafloor spreading histories, supplemented with
284 paleomagnetic data from the continental blocks (e.g., Haile et al., 1977), were applied to make plate
285 reconstructions using rigid body motions on the surface of a sphere (i.e., Euler rotations). The Jurassic
286 to recent plate reconstructions of Besse and Courtillot (1988) and Scotese et al. (1988) were an
287 important benchmark for subsequent plate motion models, as the work synthesised marine magnetic
288 anomalies and continental paleomagnetism, yet also took into account the plate boundary evolution.
289 Pertinent to this study, the work of Besse and Courtillot (1988) and Scotese et al. (1988) enabled
290 reproducibility by providing finite rotation parameters.

291 Although the plate reconstructions of Lee and Lawver (1994) and Lee and Lawver (1995)
292 covered only the Cenozoic evolution of Southeast Asia (Fig. 4d), these were the first detailed regional

293 reconstruction that published testable and reproducible finite rotation parameters that quantitatively
294 described the motion of Southeast Asian crustal elements, building on the more regional approach
295 presented in Jolivet et al. (1989). The relative plate motions, provided as finite rotations, were linked
296 into a plate motion hierarchy that tied back to the South China block, and thus only provide a regional
297 perspective (Lee and Lawver, 1994; Lee and Lawver, 1995). However, the provision of Euler
298 rotations significantly increased their utility even over more recent models as they allow for
299 reproducibility and refinement by subsequent researchers.

300 A major improvement in regional plate reconstructions was presented in Hall (1996), and
301 subsequent works by the same author (Hall, 2002; Hall, 2012) (Fig. 4B-C), where the regional plate
302 reconstructions were embedded in a global plate circuit – that links Australia and India back to Africa,
303 and Asian fragments through Eurasia, North America and Africa. Using a global plate circuit
304 combines relative plate motions with a frame of reference with respect to the mantle using a hotspot
305 frame (e.g., Müller et al., 1993), which enables linkages between the plate-mantle system. In the
306 absence of hotspot tracks (i.e., before ~120 Ma), plate reconstructions make use of paleomagnetic
307 reference frames (e.g., Hall and Spakman, 2015), which enable the reconstruction of paleo-latitudes
308 of climate-sensitive data, and can be corrected for True Polar Wander to create more explicit links
309 between the plate-mantle system in deep time. The reconstructions presented in Hall (1996) and Hall
310 (2002) provide a regional post-Jurassic evolution of the India-Eurasia convergence zone, Southeast
311 Asia and New Guinea embedded in a detailed synthesis of relevant data, and are presented in 1 Myr
312 interval snapshots. Such high temporal resolution is important for capturing major plate boundary
313 reconfigurations and resulting changes in plate motion magnitudes and directions, such as the change
314 in India's plate motions and northward advance from ~100 Ma (Gibbons et al., 2015; Matthews et
315 al., 2012; van Hinsbergen et al., 2011). Although the reconstructions are presented in 1 Myr intervals,
316 no relative or absolute plate rotation parameters have been provided, which limits the testability of
317 such models.

318 These first- to fourth-generation plate reconstructions provide considerable detail and insight
319 into the tectonic evolution of the eastern Tethys, but cannot be easily linked to methods that take into
320 account the geodynamic evolution of the plate-mantle system. Schematic reconstructions cannot be
321 linked to numerical models of convection as they usually lack the continuous network of plate
322 boundaries through time that enables the use of plate velocities as surface boundary conditions. As
323 plate motions are inextricably linked to mantle convection (Hager and O'Connell, 1981; Turcotte and
324 Oxburgh, 1972), and since much of the Tethyan seafloor spreading history has since been subducted
325 (Hutchison, 1975; Şengör et al., 1988), some authors have inferred plate motion histories from high
326 velocity seismic anomalies as given by mantle tomography models (Hall and Spakman, 2003; Hall
327 and Spakman, 2015; Replumaz et al., 2004; van der Voo et al., 1999b; Wu et al., 2016). We expand
328 on these approaches and make use of our most recent plate reconstructions coupled to numerical
329 models of mantle convection that are validated using seismic tomographic images and a suite of
330 onshore and offshore geological constraints.

331

332 Table 1. Generations of continental and plate reconstructions depicting the kinematic and geodynamic evolution of
333 Southeast Asia.

Generation of reconstruction	Description	Examples
First	Schematic reconstructions of continental motions.	Pigram and Panggabean (1984) Metcalfe (1988)
Second	Continental reconstructions are made using digital approaches, with schematic paleo- plate boundaries.	Audley-Charles et al. (1988) Rangin et al. (1990)
Third	Additionally provide regional reconstructions using seafloor spreading histories, constraints from onshore geology (paleomagnetism, stratigraphy, seismic, structural, biogeography, etc.) and an incomplete network of plate boundaries. Although these models are classified as 3 rd generation reconstructions, they	Besse and Courtillot (1988) Scotese et al. (1988) Jolivet et al. (1989) Lee and Lawver (1994) Lee and Lawver (1995)

	have a significant advantage over any other reconstructions that do not provide Euler rotation parameters that are provided in 5 th generation models. These models are important examples of reproducible and testable plate reconstructions of Southeast Asia.	
Fourth	Regional reconstructions embedded in a global rotation hierarchy, constraining relative plate motions using seafloor spreading histories that are tied to an absolute hotspot or paleomagnetic reference frame. Synthetic seafloor spreading histories are generated in regions and times where seafloor has been subducted.	Hall (1996) Hall (2002) Hall (2012) Stampfli and Borel (2002) [#]
Fifth	A continuous global network of evolving plate boundaries is modelled, with complete model rotation parameters and digital geometry files released for testability and reproducibility. Such models can be linked to regional and global geodynamic numerical calculations that link plate tectonics with underlying mantle convection. Some of these models incorporate regional refinements that include retro-deformation of continental crust to provide better full-fit reconstructions of Pangea.	Gurnis et al. (2012) Seton et al. (2012) Zahirovic et al. (2012) Zahirovic et al. (2014) Domeier and Torsvik (2014) [^] Gibbons et al. (2015) This study
Future	Build on previous approaches with stronger emphasis on quantifying uncertainties, and using ensemble computer modelling that incorporates all constraints (offshore and onshore) simultaneously and all relevant uncertainties to derive a quantitative “best-fit” plate reconstruction that is fully consistent with plate boundary forces and mantle convection models. Global plate reconstructions incorporate all major regions of deformation to provide better full-fit reconstructions and address the oversimplification of plate rigidity assumptions.	Such models are not yet available, and represent an aspirational goal to produce better plate tectonic reconstructions.

334 [^] The Domeier and Torsvik (2014) reconstructions cover the Late Paleozoic global plate motion history, and include
335 major blocks of Southeast Asia.

336 [#] The model of Stampfli and Borel (2002) has linked plate boundaries and synthetic seafloor spreading histories, which
337 are important components of 5th-generation models, but only provides snapshots without rotation parameters or
338 (evolving plate boundary) geometries.

340 1.2 Seismic tomography constraints

341

342 Seismic tomographic techniques have provided an important link between the present-day
343 arrangement of plate boundaries and deep mantle structure around Southeast Asia resulting from
344 long-term subduction of Tethyan and Pacific lithosphere. High-resolution P-wave seismic
345 tomographic models have demonstrated that the Sunda slab from the subduction of the Indo-
346 Australian oceanic plate penetrates to depths of ~1500 km (Li et al., 2008; Widiyantoro and van der
347 Hilst, 1996), and that it is distinct from the older and deeper Tethyan slabs (Widiyantoro and van der
348 Hilst, 1996). Due to the complexity of Tethyan convergence, and the lack of preserved seafloor
349 spreading histories, interpretations of mantle structure provide an important additional insight into
350 the past geometry and evolution of active margins in the region. For example, Hall and Spakman
351 (2002) and Hall and Spakman (2003) used a P-wave seismic tomographic model to infer Cenozoic
352 subduction histories in the vicinity of the northern Australian margin. Hall and Spakman (2003)
353 interpreted the Bijwaard and Spakman (2000) P-wave seismic tomographic model to suggest north-
354 dipping subduction north of Australia along the Philippine Archipelago occurred between 45 and
355 25 Ma, and inferred that little subduction occurred north of Australia since 25 Ma due to the likelihood
356 of a margin dominated by strike-slip motion rather than convergence. Hall and Spakman (2015)
357 recently attributed the 1600 km deep Sunda slab to subduction since 45 Ma, but discounted the
358 possibility that the Proto South China Sea slab is in the upper mantle, and concluded that it is instead
359 likely in the lower mantle at ~1200 km depth. Further south, a large east-west slab beneath Australia
360 (including Lake Eyre) at ~800-1200 km depths has been interpreted to be the result of north-dipping
361 subduction that ceased following accretion of the Sepik Terrane along New Guinea at ~50 Ma
362 (Schellart and Spakman, 2015).

363 The India-Eurasia Tethyan mantle structure was interpreted in van der Voo et al. (1999b)
364 where a global P-wave seismic tomographic model (Bijwaard et al., 1998) was used to infer the

365 subduction history related to post-Jurassic subduction (Fig. 5). The large slabs, with a generally
366 northwest-southeast trend and largely at mid-mantle depths, were interpreted to be the result of two
367 simultaneous north-dipping subduction zones in the Neo-Tethys (van der Voo et al., 1999b), a
368 scenario which requires a two-stage India-Eurasia collision. Hafkenscheid et al. (2006) elaborated on
369 this approach by quantifying Tethyan slab volumes and inferring average slab sinking rates in the
370 mantle. Hafkenscheid et al. (2006) tested end-member scenarios of Neo-Tethyan convergence,
371 including a model for long-lived Andean-style subduction along southern Eurasia following Norton
372 (1999) and Şengör and Natal'in (1996). Instead, the analysis by Hafkenscheid et al. (2006) suggested
373 that an additional intra-oceanic subduction zone, following Stampfli and Borel (2002), could better
374 reproduce the volume and distributions of slabs interpreted from 3D seismic tomography. The
375 preferred scenario in Hafkenscheid et al. (2006) invoked an arc-continent collision between Greater
376 India and the Spong Arc, likely contemporaneous with the Kohistan-Ladakh Arc (McDermid et al.,
377 2002), at ~65-60 Ma, with continent-continent collision occurring at ~48 Ma, and infer a “free sinking
378 rate” (i.e., when not attached to a subducting plate) of 3 and 2 cm/yr in the upper and lower mantle,
379 respectively.

380

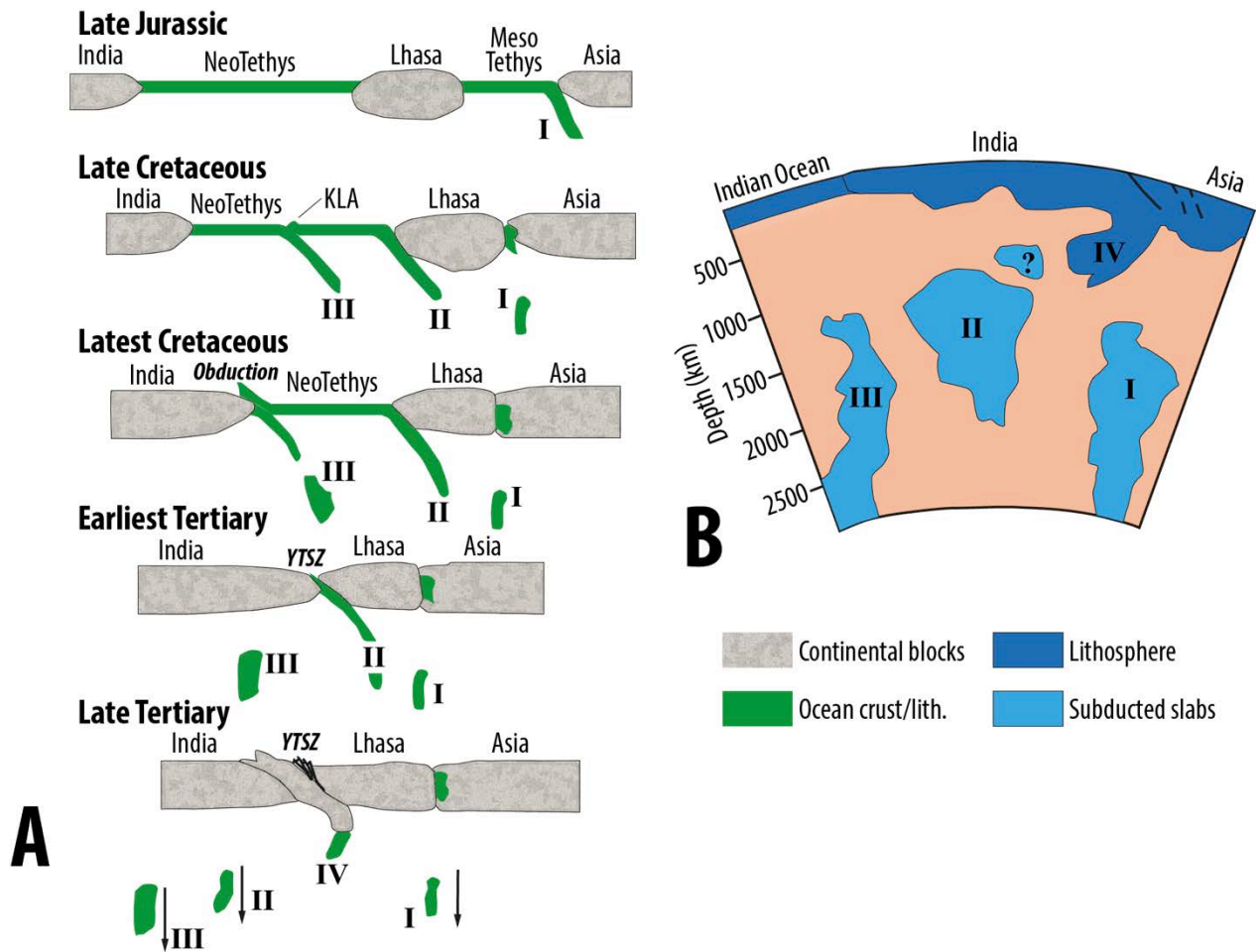


Fig. 5. A) Schematic synthesis of Tethyan subduction history accommodating India-Eurasia convergence, as interpreted from P-wave seismic tomography by van der Voo et al. (1999b). B) The three slab volumes in the lower mantle are interpreted as representing intra-oceanic subduction and a two-stage India-Eurasia collision. Figure adapted from van der Voo et al. (1999b). Note that the Tethyan ocean basin nomenclature in van der Voo et al. (1999b) differs slightly from the terminology used in this study. KLA – Kohistan-Ladakh Arc, YTSZ – Yarlung Tsangpo Suture Zone.

Incorporating 3D seismic tomographic interpretations, Replumaz et al. (2004) combined an assumption of vertical slab sinking with a tectonic reconstruction of Southeast Asia in a Siberia reference frame, and interpreted the pre-collision geometry of the southern Eurasian active margin using tomographic depth slices. The analysis of tomography linked to a “retro-deformation” model of block motions in Southeast Asia (using available fault offsets and slip rates) for Cenozoic times

394 suggests that the India-Eurasia continental collision occurred sometime between 55 and 40 Ma, based
395 on changes in slab morphology, and suggests a sinking rate of 5 cm/yr in the upper mantle and 2
396 cm/yr in the lower mantle. The resulting upper mantle sinking rates are slightly higher than the values
397 suggested by Hafkenscheid et al. (2006). A similar approach of age-coding slabs in P- and S-wave
398 seismic tomographic depth slices, assuming constant and vertical slab sinking was used in Zahirovic
399 et al. (2012) and Zahirovic et al. (2014) as a general estimate of the location of Tethyan subduction
400 zones that were then implemented into a global plate motion model. One important distinction was
401 the use of multiple P- and S-wave seismic tomographic models, which is an important consideration
402 in determining the distribution of Tethyan slabs. To supplement the assumption of vertical slab
403 sinking, Zahirovic et al. (2012) used numerical mantle convection models kinematically driven by
404 time-dependent plate reconstructions, and found that an intra-oceanic subduction scenario, as
405 suggested by van der Voo et al. (1999b), Hafkenscheid et al. (2006) and Aitchison et al. (2007), better
406 reproduced the Tethyan mantle structure than Andean-style subduction alone.

407 More generally, the approach of age-coding slabs in seismic tomographic depth slices has
408 been applied globally to derive average slab sinking rates (Butterworth et al., 2014; van der Meer et
409 al., 2010), and to propose a subduction reference frame using the assumption of vertical sinking and
410 constant sinking rates (van der Meer et al., 2010). The cataloguing of global slab volumes by van der
411 Meer et al. (2010) suggests that a ~ 15 to 20° longitudinal global shift of all continents is required to
412 account for the observed distribution of post-Jurassic slabs in the mantle. Such an observation is an
413 important first-order constraint of paleo-longitude in the absence of preserved hotspot tracks during
414 the Late Jurassic and Early Cretaceous, and provides an estimated average global slab-sinking rate of
415 1.2 ± 0.3 cm/yr. A similar synthesis of slabs interpreted from seismic tomography in Butterworth et
416 al. (2014) suggests a comparable average sinking rate of 1.3 ± 0.3 cm/yr for the whole mantle.
417 However, such an approach does not take into account the contrasting viscosities of the upper and
418 lower mantle, or the effects of slab stagnation and lateral slab advection from mantle flow, which
419 may be an important factor contributing to Tethyan mantle structure (Becker and Faccenna, 2011;

420 Zahirovic et al., 2012). To address this, Butterworth et al. (2014) made use of global numerical
421 modelling of mantle flow to test competing absolute reference frames against present-day seismic
422 tomographic constraints, and suggest that the longitudinal correction argued in van der Meer et al.
423 (2010) is likely too large. The numerical modelling approach in Butterworth et al. (2014) highlighted
424 the need to account for variable slab sinking rates resulting from factors such as oblique convergence,
425 diachronous collisions and suturing, as well as two orders of magnitude increase in viscosity between
426 the upper and lower mantle. The slab sinking rates from numerical mantle convection models in
427 Butterworth et al. (2014) suggests a global mantle sinking rate of 1.5 to 2.0 cm/yr, which is also
428 consistent with the 2.0 ± 0.8 cm/yr mantle sinking rate inferred from mantle flow modelling
429 (Steinberger et al., 2012). However, other work applying mantle flow modelling highlights the time-
430 varying nature of slab sinking rates, which is an important consideration when interpreting slabs from
431 the present-day snapshot in seismic tomography (Bower et al., 2013).

432

433 **1.3 Numerical modelling of Tethyan geodynamics**

434

435 The evolution of the Tethyan realm has been the focus of decades of research to better
436 understand the India-Eurasia collision and the complex tectonics of Southeast Asia and New Guinea.
437 A wide range of physical (analogue) and numerical experiments at crustal, lithosphere and mantle
438 scales have revealed important aspects of the plate-mantle system that are responsible for the
439 geodynamics of the Tethyan, Eurasian and Pacific tectonic domains. Since our approach requires
440 modelling in a spherical domain with assimilation of plate reconstructions, only numerical methods
441 are appropriate to study the long-term eastern Tethyan subduction history in a regional and global
442 framework.

443 Wide ranges of numerical approaches exist to model mantle behaviour – including forward or
444 backward advection models (including inverse and adjoint approaches), forward models with data
445 assimilation, and fully geodynamic models that do not have imposed boundary conditions. Forward

models assume that the plate motion histories are a reasonably good recorder of plate-mantle evolution, and use the plate motions as a surface kinematic boundary condition to predict mantle structure that can be compared to seismic tomography (Bower et al., 2015; Bunge et al., 2002; Richards et al., 2000; Zahirovic et al., 2012). Backward advection models use seismic tomography (as a present-day snapshot of the mantle) as an input where the seismic velocity anomalies are converted to density perturbations, assuming that the bulk of the anomaly has a thermal source, and the sign of gravity and time reversed to compute the past position of the mantle material (Bunge et al., 2003; Conrad and Gurnis, 2003; Glišović and Forte, 2014; Liu and Gurnis, 2008; Steinberger and O'Connell, 1998). The backward advection models take into account the complex present-day mantle structure, but can only be successfully used for times since ~ 70 Ma due to the inherent issues of irreversible thermal diffusion and the interaction of the boundary layers with internal flow (Bunge et al., 2003; Conrad and Gurnis, 2003; Steinberger and O'Connell, 1998). More advanced approaches using adjoint models overcome the limitations of irreversible backward advection (Liu and Gurnis, 2008; Spasojevic et al., 2009), but have yet to be applied to the Tethyan domain. Since our region of interest requires deeper time considerations, we use forward geodynamic flow experiments that are tested against mantle tomography.

1.3.1 Numerical models of India-Eurasia convergence

Following the interpretation of discrete Tethyan slab volumes at mid-mantle depths beneath India in P-wave seismic tomographic models by van der Voo et al. (1999b), a numerical approach using a 2D box (with 16.5 km mesh resolution) was used by Jarvis and Lowman (2005) to interpret the inferred Tethyan mantle structure (Fig. 6). A number of experiments were conducted, specifically varying the poorly-constrained viscosity contrast between the upper and lower mantle, with the results requiring a lower mantle that was at least 30 times more viscous than the upper mantle to maintain Tethyan slabs at mid-mantle depths (Jarvis and Lowman, 2005). The resulting upper and lower mantle

viscosity contrast from Jarvis and Lowman (2005) was also consistent with earlier estimates of a 10 to 30 times more viscous lower mantle from global models fitting geoid anomalies over slabs (Hager, 1984).

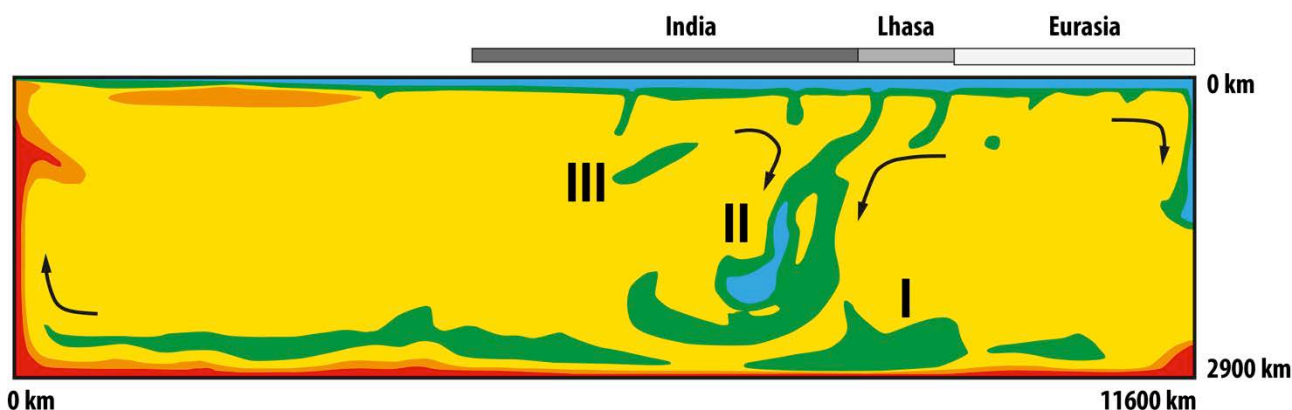


Fig. 6. Numerical 2D box model of India-Eurasia convergence, adapted from Jarvis and Lowman (2005), provided an important benchmark for quantifying and testing tectonic reconstruction scenarios of India-Eurasia convergence and Tethyan geodynamics.

Due to the limitation of a 2D box set-up, the India-Eurasia convergence modelled by Jarvis and Lowman (2005) required a simplified convergence history along a single transect despite a complex active margin with periods of oblique convergence. The applied velocity boundary condition led to symmetric downwellings rather than one-sided subduction. However, the work of Jarvis and Lowman (2005) highlighted the need for quantitative approaches to test plate reconstructions, while suggesting a lower limit on the viscosity contrast between the upper and lower mantle. The approach utilised simple kinematic boundary conditions for the convergence velocities, which were assumed to be ~ 17 and 6 cm/yr (Besse and Courtillot, 1988) before and after the India-Eurasia collision, respectively, at 42 Ma. Their subsequent numerical approach made use of a simple sinking slab in a 2D and 3D Cartesian box (Jarvis and Lowman, 2007), which suggested a viscosity contrast of a factor of 100 to 300 between the upper and lower mantle to maintain Tethyan slabs in the mid-mantle. These

492 results suggested that Jurassic slabs likely retain a thermally anomalous signature with respect to the
493 ambient mantle, enabling their detection by seismic tomographic techniques.

494 Becker and Faccenna (2011) used a 3D global approach to investigate the plate driving forces
495 acting on the circum-Tethyan regions, and converted P- and S-wave seismic tomographic models to
496 density anomalies driving instantaneous mantle flow models. They found that there was a dominant
497 first-order mantle conveyor belt with northward velocities in the shallow mantle beneath India,
498 sinking of mantle material near the suture zone, and accompanying southward flow that is interrupted
499 by mantle upwelling in the region of the Carlsberg and Central Indian ridges. The work highlights
500 the power of global models in capturing the complexity of slab interactions from circum-Tethyan
501 subduction, with results suggesting that large-scale mantle flow and an associated Tethyan conveyor
502 supports ongoing indentation by India. Similarly, a 3D global spherical approach using CitcomS
503 (Zhong et al., 2000) was applied in Zahirovic et al. (2012), where plate kinematic boundary conditions
504 were applied from 140 Ma to test end-member subduction scenarios accommodating India-Eurasia
505 convergence. The forward numerical model predictions were compared to slabs interpreted from
506 seismic tomography (Zahirovic et al., 2012), and showed that the mantle structure could be better
507 reproduced when taking into account intra-oceanic subduction and a two-stage India-Eurasia collision
508 (Aitchison et al., 2007; Hafkenscheid et al., 2006; van der Voo et al., 1999b). This earlier work
509 highlights the need to test end-member plate reconstruction scenarios using mantle flow models, and
510 comparisons to mantle structure from seismic tomography as an additional criterion for reconciling
511 surface geology.

512 More recently, a 3D approach was also employed in Yoshida and Hamano (2015), who ran a
513 forward convection model from Pangea times, but without applying a kinematic boundary condition
514 or being able to incorporate one-sided subduction. Although many of the experiments failed to
515 reproduce present-day arrangements of continents (such as predicting a problematic fit of Antarctica
516 with South America), one aspect of the models reproduced the approximate present position of India
517 and highlights the requirement of long-lived subduction along southern Eurasia since Pangea breakup

518 (Yoshida and Hamano, 2015). When considering the motion of India towards Eurasia, the
519 anomalously high velocities (more than 14 cm/yr) of India between ~80 and 65 Ma can be modelled
520 numerically through a viscous coupling mechanism between two simultaneous north-dipping
521 subduction zones in the Neo-Tethys prior to India-Eurasia collision (Jagoutz et al., 2015). This
522 modelling approach suggests that two subduction zones in the Neo-Tethys are required to account for
523 the high convergence rates as long-lived (~20 Myr) accelerations cannot be explained by plume
524 influences, which are likely to diminish over a shorter timeframe of several millions of years (van
525 Hinsbergen et al., 2011).

526 When considering the mantle-surface interaction from Tethyan tectonics, the work of Pusok
527 and Kaus (2015) used a 3D numerical box model that captured both subduction processes and the
528 resulting topographic response to the India-Eurasia collision, providing insight on the formation of
529 oroclinal in the eastern and western syntaxes of the convergence zone, as well as the uplift of the
530 Tibetan Plateau and lateral expulsion of continental material. Major advances are also being made in
531 reducing the uncertainties in the rheology of the mantle and lithosphere in such numerical models,
532 with the recent work (Baumann and Kaus, 2015) highlighting a new, and currently computationally-
533 intensive, approach of parallel inversion of observables including the gravity field, topography and
534 GPS velocities to better model the lithospheric and crustal rheology. Other advances in inverse
535 methods have the potential to fully incorporate the details of slabs and their coupling to lithospheric
536 plates with fault-zones between plates with fully non-linear rheologies, which remains one of the
537 largest uncertainties in mantle convection modelling (Ratnaswamy et al., 2015; Worthen et al., 2014).
538 Such approaches provide a framework for geodynamic computations that capture realistic non-linear
539 rheologies, including strain rate weakening and yielding, to better account for plate velocity
540 observations, complex slab-trench interactions, and intra-plate deformation that goes beyond the
541 simplifying assumption of plate rigidity (Alisic et al., 2012; Alisic et al., 2010).

542

543 *1.3.2 Numerical modelling of Southeast Asia and New Guinea geodynamics*

544

545 Few geodynamic models of mantle-, lithospheric- and crustal-scale evolution exist for the
546 tectonically complex and less constrained Sundaland and New Guinea regions than for other parts of
547 the Tethyan tectonic domain. For example, the synthesis by van Ufford and Cloos (2005) of at least
548 six competing proposed scenarios for the Cenozoic evolution of New Guinea highlights the uncertain
549 chronology of major tectonic events, as well as poorly-constrained subduction polarities. As a result,
550 much of the numerical modelling has been restricted to understanding the present-day geodynamic
551 character of the region. Ghose et al. (1990) used focal mechanism solutions to build a 3D finite
552 element numerical experiment of subducted slabs and generalised mantle structure in the Sundaland
553 region to compute the flow and stress field acting on the overriding continental promontory. The
554 results indicate significantly higher plate coupling across the Sumatra segment of the Sunda Trench,
555 resulting in a higher seismogenic potential than the Java region. This may be due to lower coupling
556 assumed to be due to the lubricating effect of soft sediments in the trench (e.g., Clements and Hall,
557 2011), as well as the subduction of older Indian Ocean crust than along the Sumatra segment (Ghose
558 et al., 1990).

559 North of New Guinea, the geodynamic significance of the Philippine Sea Plate has been the
560 subject of a number of studies that employ numerical modelling to quantify the effects of Izu-Bonin-
561 Mariana subduction initiation (Gurnis et al., 2004; Hall et al., 2003; Leng and Gurnis, 2015) on the
562 Pacific Plate boundary forces, and its contribution to a change in Pacific Plate motion between ~50
563 and 40 Ma based on force balance calculations (Faccenna et al., 2012). Temporally linked to the
564 inception of (proto-) Izu-Bonin-Mariana subduction, major changes in subduction along New Guinea
565 in the Eocene have been invoked to explain the acceleration of Australia's northward motion
566 (Schellart and Spakman, 2015; Zahirovic et al., 2014) from ~43 Ma (Williams et al., 2011). Schellart
567 and Spakman (2015) identified a subducted slab at depths between ~800 and 1200 km beneath Lake
568 Eyre in eastern Australia, and argued based on a simple Stokes flow model that the topographic

depression is caused by dynamic subsidence induced by the sinking of a slab that detached along New Guinea at ~55-45 Ma. However, the complex interaction of slabs from regional subduction zones plays an important role that can only be tested in regional and global geodynamic numerical simulations that capture the time-dependent evolution of Southeast Asian plate boundaries.

2 Methods

2.1 Plate tectonic reconstructions

Reconstructions of the Tethyan domain have taken many forms over decades of research (see Section 1.1, Table 1, Fig. 4), with the post-Pangea plate reconstruction timeframe (since ~200 Ma) generally associated with lower uncertainties than earlier times due to greater preservation of oceanic crust (Zahirovic et al., 2015). Due to the ambiguity in reconstructing regions with no preserved seafloor spreading records and/or poor geological constraints, testing alternative scenarios becomes an avenue to evaluate the uncertainty inherent in plate reconstructions. In this study we present a new post-Jurassic plate motion model spanning the Tethyan region from the westernmost India-Eurasia convergence segment, in the vicinity of Kohistan-Ladakh, eastward to Southeast Asia (including Sundaland and the proto-South China Sea) and Papua New Guinea. The model is also compared to the previous synthesis of the region presented in Zahirovic et al. (2014) for Southeast Asia and New Guinea, and in Gibbons et al. (2015) for the India-Eurasia convergence zone, highlighting the alternative kinematic scenarios that can account for the constraints from marine and onshore data (Supplementary Animation 1). The refinements presented in this study focus on an alternative model for the Neo-Tethys, transferring the East Java-West Sulawesi blocks from the Argo Abyssal Plain on the NW Australian shelf towards Sundaland, as well as refinements to the evolution of the Kohistan-

593 Ladakh, Woyla, and Philippine intra-oceanic arcs, in the context of the evolving Sundaland and New
594 Guinea continental margins (see Section 3).

595 Relative plate motions are derived from preserved seafloor spreading histories (as in third and
596 fourth generation reconstructions from Table 2), where seafloor magnetic anomalies are identified
597 and combined with directional constraints from fracture zones to compute the Euler rotation that
598 defines the relative rigid body motions on the surface of a sphere. We use the Global Seafloor and
599 Magnetic Lineation Database of previously-published magnetic anomaly picks (Seton et al., 2014)
600 and fracture zone geometries (Matthews et al., 2011), which were combined to compute relative plate
601 motion parameters in previous studies (see discussion and references in Seton et al., 2012), preferably
602 using the least-squares best-fit statistical method following Hellinger (1981) and Royer and Chang
603 (1991). The rotation parameters are calibrated to the geomagnetic polarity reversal timescale of Gee
604 and Kent (2007), which is an updated timescale compared to the one used in our previous plate
605 reconstruction of the Tethyan region in Zahirovic et al. (2014) and Gibbons et al. (2015). In the
606 absence of preserved seafloor spreading histories, we use onshore geological constraints to estimate
607 the pre-rift position of continental fragments, the timing and trajectory of rifting, as well as the age
608 and location of the accretion events (Tables 2-3). We construct synthetic oceanic plates that are
609 consistent with plate tectonic driving mechanisms and reasonable relative plate motions across plate
610 boundaries (e.g., convergence across subduction zones, divergence across mid-oceanic ridges, strike-
611 slip motion along transform faults).

612 The relative plate motions form a chain that is hierarchical and typically ties all plate motions
613 back to Africa, largely due to the central position of Africa within Pangea and relative stability
614 because it is surrounded by mid-oceanic ridges (Torsvik et al., 2008). The motion of Africa is
615 expressed with respect to the underlying mantle, using Indo-Atlantic or global hotspot tracks since
616 ~100 Ma to derive a frame of reference for the global plate motion model. For earlier times when no
617 hotspot tracks are available, the True Polar Wander- (TPW) corrected paleomagnetic reference frame
618 of Steinberger and Torsvik (2008) is used. Due to the lack of paleo-longitudinal constraints in a

619 paleomagnetic reference frame resulting from the radial symmetry of the Earth's magnetic dipole, we
620 apply a 10° longitudinal shift gradually between 70 and 105 Ma to the TPW-corrected reference
621 frame, following Butterworth et al. (2014) and van der Meer et al. (2010) to provide a better paleo-
622 longitudinal link between subduction zones and Jurassic and Cretaceous subducted slabs interpreted
623 from seismic tomography.

624 The combination of relative plate motions with an absolute reference frame enables the
625 computation of absolute plate motions through time, modelled using the GPlates software (Boyden
626 et al., 2011). Evolving plate boundaries are constructed using continuously-closing plate polygon
627 algorithm (Gurnis et al., 2012), which provides global coverage of plates through time in 1 Myr
628 intervals. The Tethyan plate motions are embedded in a global model, which is based on the synthesis
629 in Seton et al. (2012) with regional refinements that are documented in Müller et al. (2016). The time-
630 dependent plate boundaries, seafloor age-grids and plate velocities are assimilated into the numerical
631 models of mantle convection, described in Section 2.3. By considering the evolution of the entire
632 plate (Gurnis et al., 2012; Stampfli and Borel, 2002) rather than only focusing on continental blocks,
633 plate reconstructions can be linked to geodynamic models (Conrad and Lithgow - Bertelloni, 2004;
634 Lithgow - Bertelloni and Richards, 1998). The coupling of plate kinematics to geodynamic models
635 provides the opportunity to reproduce the mantle structure interpreted from seismic tomography as
636 well as reconstruct past mantle flow using the present-day surface geology and tectonics as
637 constraints.

638

639 Table 3. Constraints used to construct plate motion model.

Region	Event	Timing	Dating method/ interpretation	Interpretations based on data and models
Australian NW Shelf	Onset of rifting	Sometime in Late Jurassic	Stratigraphic rift-drift sequences	Pigram and Panggabean (1984)

	Triple junction mid-oceanic ridge configuration	Latest Jurassic	Geometrical requirement, and evidence of possible plume influence	Audley-Charles (1988), Audley-Charles et al. (1988), Gibbons et al. (2012), Rohrman (2015)
	Onset of seafloor spreading	155 ± 3.4 Ma	K-Ar of basaltic basement	Gradstein and Ludden (1992)
West Sulawesi, East Java, Mangkalihat and easternmost Borneo	Onset of rifting	Late Jurassic	Biostratigraphic constraints in Paremba Sandstone and shallow marine sandstones in Bantimala Complex	Sukamoto and Westermann (1992), Wakita (2000)
	Onset of seafloor spreading	~158-155 Ma	K-Ar of diorite, microgabbro and basaltic dyke	Polvé et al. (1997)
	Oldest seafloor spreading magnetic anomalies	M25A M26 (~153-155 Ma)	Magnetic anomaly identifications from shiptracks	Heine and Müller (2005) Gibbons et al. (2012)
	Youngest preserved seafloor spreading magnetic anomaly in the Argo Abyssal Plain region	M10Ny, 128.9 Ma	Magnetic anomaly identifications from shiptracks	Gibbons et al. (2012)
	Suturing of 'Argoland' to southwest Borneo core	~80 Ma	Stratigraphy, K-Ar and U-Pb of metamorphics, synthesis of previous studies	Wakita (2000) Clements and Hall (2011)

New Guinea	Rifting on northern New Guinea (opening of Sepik ocean basin)	Late Jurassic 172 Ma ~157 ± 16 Ma	Jurassic granite in Bena Bena Terrane SSZ ophiolites in Central Ophiolite Belt	Davies (2012) Permana (1998)
	Subduction influence on eastern New Guinea	Early Cretaceous	Kondaku Tuffs	Dow (1977), Rickwood (1954)
	Onset of Sepik ocean basin subduction	Maastrichtian (~71 to 66 Ma) 68 Ma	Stratigraphic correlation and dating using foraminifera High-temperature metabasites on West Papuan Ophiolite	Worthing and Crawford (1996) Davies (2012)
	Sepik Terrane docking with New Guinea	35-31 Ma ~30 Ma	Ar-Ar age of Emo metamorphics Cooling histories from exhumation	Worthing and Crawford (1996) Crowhurst et al. (1996)
	South-dipping subduction	~18-8 Ma	Maramuni Arc volcanics	Hill and Hall (2003), Page (1976)
	Halmahera Arc collision	~14 Ma	Compression in PNG Mobile Belt, apatite fission track geochronology	Hill and Raza, (1999), Kendrick (2000)
	Onset of Neo-Tethyan subduction	~170 Ma (to 137 Ma)	Calc-alkaline granites and granitoids	Zhang et al. (2012)
Lhasa	Onset of intra-oceanic subduction	~154 Ma	Matum Das tonalite	Schaltegger et al. (2003)

	along Kohistan-Ladakh Arc			
	Subduction along Zedong Terrane	161.0 ± 2.3 Ma, ~156 Ma, 152.2 ± 3.3 Ma	Dacite breccia, Andesite dyke/breccia, Quartz diorite, Andesitic dyke	McDermid et al. (2002)
	Magmatic hiatus on Lhasa	~137 to 109 Ma, ~75 to 60 Ma	Magmatic gap in Gangdese Batholith	Ji et al. (2009), Wen et al. (2008), Chung et al. (2005)
	Initiation of Kohistan-Ladakh back-arc basin subduction along Lhasa	~109 Ma	Resumption of arc volcanism in Gangdese Batholith	Ji et al. (2009), Wen et al. (2008)
	Maximum southward position of Kohistan-Ladakh Arc	~100 Ma	Equatorial paleolatitudes from mid- to Late Cretaceous red beds	Zaman and Torii (1999)
	Kohistan-Ladakh collision with Greater India	~60 to 50 Ma	Cessation of calc-alkaline magmatism, stratigraphic constraints of collision, slowdown in Indian Ocean seafloor spreading at ~52 Ma, change in arc magma chemistry by ~50 Ma	Khan et al. (2009) Hu et al. (2015) Cande et al. (2010) Bouilhol et al. (2013)

	Kohistan-Ladakh collision with Eurasia	~47 to 40 Ma	Slowdown in India-Africa seafloor spreading, Indian Ocean microplate formation, completion of Andean-style subduction (Linzizong), change in arc magma chemistry by ~40 Ma	Cande and Patriat (2015) Matthews et al. (2016) Chung et al. (2005) Bouilhol et al. (2013)
West Burma	Onset of Neo-Tethyan subduction	~163-152 Ma	Jadeite geochronology	Shi et al. (2008, 2014)
	Onset of Neo-Tethyan intra-oceanic subduction	~156-150 Ma	Biostratigraphic ages of cherts constraining age of Naga Ophiolite formation	Baxter et al. (2011)
	Subduction of Woyla back-arc basin	~113-110 Ma (Albian) ~105-90 Ma 95 ± 2 Ma	Albian unconformity on West Burma Wuntho-Popa Arc SSZ formation of Andaman Ophiolite	Morley (2012a) Mitchell et al. (2012) Pedersen et al. (2010)
Sumatra	Onset of Neo-Tethyan subduction	~170 Ma ~165-140 Ma (?)	Onset of arc volcanism in Sumatra segment Minor UHP/VHP metamorphism	McCourt et al. (1996) Parkinson et al. (1998)

	Subduction of Woyla back-arc basin	From ~115 Ma ~105-75 Ma	Peak in UHP/VHP metamorphism in Meratus and Luk Ulo sutures Wuntho-Popa Arc volcanism to the west, and Woyla intrusions	Parkinson et al. (1998) Mitchell et al. (2012), McCourt et al. (1996), Wajzer et al. (1991)
	Woyla Arc accretion	~75-62 Ma	Magmatic gap of arc volcanics on Sumatra	McCourt et al. (1996)
	Onset of Sunda subduction	62 Ma	Arc volcanism on Sumatra	McCourt et al. (1996)
West Java/ East Borneo	Onset of NeoTethyan subduction	~180-165 Ma	Schist in Meratus Complex	Wakita et al. (1998)
		~170 Ma (Bajocian)	Radiolarians	Wakita et al. (1998)
		~160 Ma	Zircon age spectra	Clements and Hall (2007)
	Late stage of Woyla/Barito back-arc basin subduction along Sunda continental margin	~100 Ma	Peak in zircon age spectra	Clements and Hall (2007)
		~100-93 Ma	Cenomanian/Turonian Meratus Ophiolite obduction	Pubellier et al. (2004), Yuwono et al. (1988)
	Suturing of East Java	~80 Ma	Stratigraphy, K–Ar and U–Pb of metamorphics,	Wakita (2000) Clements and Hall (2011)

			synthesis of previous studies	
	Onset of Sunda subduction	65 Ma	Subduction-related rocks on Sulawesi	Guntoro (1999), van Leeuwen (1981)
Philippine Arc	Onset of south-dipping subduction along New Guinea (Sepik)	156.3 \pm 2.0 Ma and 150.9 \pm 3.3 Ma 142 \pm 4 Ma	SSZ ophiolitic crust from the Lagonoy Ophiolite Ophiolite crystallisation from Gag Island, Halmahera	Encarnación (2004)
	Continued arc volcanism	126 \pm 3 Ma and 119 \pm 2 Ma 99.9 \pm 7.0 Ma 100 \pm 4 Ma	SSZ volcanics from Cebu Island Ar-Ar age of the Calaguas Ophiolite Arc rocks reported from Obi Island on Halmahera	Deng et al. (2015) Geary et al. (1988), Geary and Kay (1989) Hall et al. (1995b)

2.2 Insights from seismic tomography

The distribution of ophiolites, intra-oceanic arc fragments and a complex network of sutures within southern Eurasia (Figs. 1-3), Southeast Asia and New Guinea preserve the remnants of oceanic basins that have been lost to subduction. Although the consumption of oceanic basins leaves physical evidence in the form of arc volcanics, accreted seamounts and ocean floor sediments, and ophiolites, the present-day mantle structure illuminated using seismic tomographic methods holds additional

648 clues to the geodynamic evolution of these regions (Hafkenscheid et al., 2006; Replumaz et al., 2004;
649 van der Voo et al., 1999a; van der Voo et al., 1999b).

650 As an estimate of the location of subduction through time, depth slices of fast seismic velocity
651 anomalies are age-coded according to an assumption of vertical slab sinking with an average sinking
652 rate. In this study we compare our revised plate reconstructions with the publicly-available P-wave
653 seismic tomography depth slices from Li et al. (2008), assuming a sinking rate of 3 and 2 cm/yr in
654 the upper and lower mantle, respectively, following Hafkenscheid et al. (2006). Hafkenscheid et al.
655 (2006) also noted that the upper mantle sinking rates are likely to be similar to the convergence rate
656 at the trenches, which may suggest even higher sinking rates for the circum-Tethyan region in the
657 context of Australia's 6-8 cm/yr, the Pacific's ~8 cm/yr, and India's ~5 cm/yr root mean square
658 velocities since ~40 Ma (Zahirovic et al., 2015). To investigate, we test a higher end-member sinking
659 rate of 8 cm/yr in the upper mantle, which is likely only meaningful for the Cenozoic as constrained
660 by seafloor spreading histories and detailed hotspot tracks for the Pacific. The sinking rates applied
661 in this study are significantly higher than the ~1.2-1.3 cm/yr whole-mantle average global slab sinking
662 rates (Butterworth et al., 2014; van der Meer et al., 2010), with a similar slower and constant sinking
663 rate scenario applied to age-coding of slabs in P- and S-wave seismic tomography in Zahirovic et al.
664 (2014). However, a faster sinking rate, with differential rates in the upper and lower mantle, was
665 found to better reproduce the evolution of major Tethyan and Southeast Asian subduction zones
666 (Zahirovic et al., 2014). Importantly, we note that the assumption of vertical and temporally constant
667 sinking rates along a single subduction zone, not to mention across a range of subduction zones in a
668 region, is likely an oversimplification and requires testing using numerical simulations of mantle
669 flow, as was carried out in Butterworth et al. (2014).

670 We compare our numerical mantle flow predictions to a number of P- and S-wave seismic
671 tomography models, because tomographic models are typically constructed using a variety of
672 methods, which incorporate different seismic phases and parameterisations (Grand, 2002;
673 Romanowicz, 2008). P-wave models tend to have higher resolutions than S-wave models, due to the

674 limited number of S-wave phases that can be used in seismic tomographic inversions (Widiyantoro
675 et al., 1998). Beyond the inherent higher resolution of P-wave models in well-sampled continental
676 regions, the Li et al. (2008) global seismic tomography model has additional coverage by
677 incorporating coverage using the Chinese Seismographic Network, leading to a better sampling of
678 the Tethyan and Asian mantle.

679 The limitation of P-wave models is that they tend to bias their sampling of the mantle beneath
680 continental crust, leading to lower seismic velocity anomaly amplitudes in oceanic regions. For
681 example, a subducted slab that may straddle oceanic and continental regions (such as the Tethyan
682 slabs) may appear “faded” beneath the oceanic regions. Although S-wave models tend to have lower
683 resolution, they offer more equal sampling of the mantle beneath oceans and continents (Grand,
684 2002). Due to the lack of permanent seismic stations in the oceans (except for some stations located
685 on islands) and over Antarctica, the coverage and sampling for both P- and S-wave seismic
686 tomography models is poorer for the southern hemisphere and all oceanic regions (Romanowicz,
687 2008). As regional tomographic models can have edge artefacts (Foulger et al., 2013), and typically
688 are not represented as seismic velocity anomalies with respect to the global mantle, we focus on using
689 only global tomographic models in our comparisons.

690

691 **2.3 Coupled plate reconstructions and mantle convection numerical models**

692

693 To better understand the geodynamic implications of the plate reconstructions, and go beyond
694 the assumption of constant and vertical slab sinking used in simple interpretations of mantle structure,
695 we couple the plate kinematics to computations of mantle flow. We use the mantle convection
696 modelling code CitcomS (Zhong et al., 2000) (<https://geodynamics.org/cig/software/citcoms/>),
697 modified to incorporate a time-dependent surface boundary condition using plate velocities from our
698 plate motion model, and progressively assimilate the thermal structure of the lithosphere and the
699 shallow thermal structure of subducting slabs (Bower et al., 2015) (Fig. 7a). The temperature and

700 thickness of the lithosphere is derived using a half-space cooling model and the synthetic age of the
701 ocean floor. Slabs are assimilated into the mantle to a depth of 350 km but convection is entirely
702 dynamic away from slabs and below the lithosphere. We computed numerical models from 230 Ma
703 to the present to capture the post-Pangea mantle evolution, with global plate reconstructions of the
704 pre-Late Jurassic described in Müller et al. (2016). However, we analyse the mantle evolution since
705 the latest Jurassic (~160 Ma) for which time the plate reconstructions are regionally refined, and the
706 mantle flow models have reached a dynamic equilibrium from the synthetic initial condition (Flament
707 et al., 2014). Initially at 230 Ma, slabs are inserted down to 1400 km depth, with a 45° dip down to
708 425 km and 90° below 425 km. In the initial conditions, slabs are twice as thick in the lower mantle
709 than in the upper mantle to account for advective thickening observed in tests in which slabs are only
710 initially inserted in the upper mantle. The initial condition includes a basal thermochemical layer 113
711 km thick just above the core–mantle boundary (CMB) that consists of material 3.6% denser than
712 ambient mantle. This condition suppresses the formation of plumes, but does not impede the
713 formation of large-scale mantle upwellings. The surface and CMB are isothermal at 273 K and 3100
714 K, respectively (Fig. 7b). Subduction zones that appear (initiate) during the model run are
715 progressively inserted as slabs in the uppermost mantle (Bower et al., 2015). The kinematic boundary
716 conditions, generated in GPlates, and the thermal volume conditions for the lithosphere and shallow
717 subduction, are assimilated in 1 Myr intervals, as described in Bower et al. (2015). The average model
718 resolution, obtained with $\sim 13 \times 10^6$ nodes and radial mesh refinement, is $\sim 50 \times 50 \times 15$ km at the
719 surface, $\sim 28 \times 28 \times 27$ km at the core–mantle boundary (CMB), and $\sim 40 \times 40 \times 100$ km in the mid-
720 mantle.

721

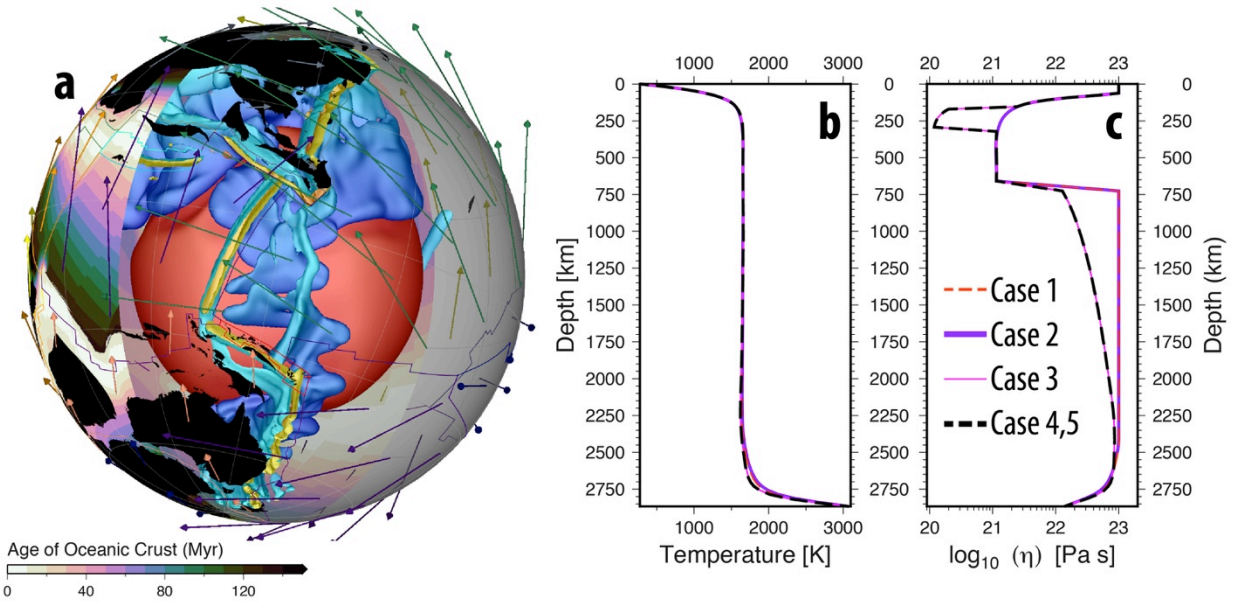


Fig. 7. a) Assimilation of plate velocities (arrows), subduction zones (yellow) and thermal lithospheric thickness based on the age of the seafloor from plate reconstructions in GPlates, with 3D volume contours of dynamic cold slabs (blue) and hotter upwellings (red) predicted by the mantle convection code CitcomS (here using Case 5, see Section 2.3). Reconstructed present-day coastlines (black) are provided as a reference. Slab colouring is a function of depth from light blue (shallow mantle) to darker blue (deep mantle). Seafloor age-grid is applied globally, but is cut out in this schematic to highlight the internal mantle structure. b) Horizontally-averaged present-day mantle temperature, and c) present-day average viscosity in the five numerical cases (see Section 2.3).

The vigour of mantle convection is defined by the Rayleigh number, Ra , where:

$$Ra = \frac{\alpha_0 \rho_0 g_0 \Delta T h_M^3}{\kappa_0 \eta_0},$$

in which α is the coefficient of thermal expansion, ρ the density, g the acceleration of gravity, ΔT the temperature difference between surface and CMB, h_M the thickness of the mantle, κ the thermal diffusivity, and η the viscosity; the subscript “0” indicates reference values (see Table 4). The viscosity of the slabs and mantle are stress- and temperature-dependent, following

$$\eta = \eta_0(r) \exp \left(\frac{E_\eta}{R(T + T_\eta)} - \frac{E_\eta}{R(T_b + T_\eta)} \right)$$

739 where $\eta_0(r)$ is a depth-dependent pre-factor defined with respect to the reference viscosity, η_0 , E_η is
 740 the dimensional activation energy (E_{UM} in the upper mantle and E_{LM} in the lower mantle), R is the
 741 universal gas constant, T is the temperature, T_η is a temperature offset, and T_b is the ambient mantle
 742 temperature outside the thermal lithosphere, slabs or the basal thermal boundary layer (see Table 4).
 743 Although the viscosity of the upper mantle can be estimated in studies of post-glacial rebound
 744 (Fjeldskaar et al., 2000; Gasperini and Sabadini, 1989; Lambeck et al., 1998), the viscosity of the
 745 lower mantle is less well constrained, which has resulted in a wide range of proposed viscosity
 746 profiles. Previous approaches have argued for a factor of 10 increase in viscosity between the upper
 747 and lower mantle (Paulson et al., 2007), while others have argued for a factor of 30 (Hager, 1984) or
 748 100 (Forte and Mitrovica, 1996; Steinberger and Calderwood, 2006). We vary the viscosity profile
 749 (Fig. 7c, Table 5) with cases 1 to 4 based on the plate reconstructions from Zahirovic et al. (2014)
 750 and Gibbons et al. (2015), and a fifth case based on the refined plate reconstructions presented in this
 751 study. The viscosity of the lower mantle in each cases is either 100 times more viscous than the upper
 752 mantle, or increases gradually with depth from a factor of 10 at the base of the transition zone (660
 753 km) to a maximum of 100 in the lowermost mantle (Steinberger and Calderwood, 2006). Cases 3, 4
 754 and 5 also incorporate a low-viscosity asthenosphere, which has been suggested to be an important
 755 decoupling layer that enables the elevated velocities of typically oceanic plates (Becker, 2006;
 756 Debayle and Ricard, 2013). Since paleo-longitudes are less well constrained earlier than ~ 100 Ma,
 757 we incorporate the van der Meer et al. (2010) subduction reference frame and their time-dependent
 758 longitudinal shift into Case 3. Using a variety of radial viscosity profiles, different absolute reference
 759 frames, and plate reconstructions between the five cases, allows us to capture some of the
 760 uncertainties involved in our approach of modelling deep-time plate reconstructions and mantle
 761 convection, and help test end-member plate reconstructions of the Tethyan region.

762 The time-dependent mantle structure is presented in 3D visualisations made with GPlates and
 763 as a series of vertical cross-sections that are reconstructed with the overriding plate to capture the
 764 evolution of subduction, plotted using Generic Mapping Tools (Wessel et al., 2013). The predicted

765 present-day mantle structure is qualitatively compared to equivalent slices of P- and S-wave seismic
766 tomography models, where fast seismic velocity anomalies are compared to slab contours (10%
767 colder than ambient mantle, representing temperatures colder than $\sim 1270^\circ\text{C}$) from the mantle
768 convection models.

769

770 **Table 4.** Parameters common to all model cases. Subscript “0” denotes reference values.

Parameter	Symbol	Value	Units
Rayleigh Number	Ra	7.84×10^7	
Thermal expansion coefficient	α_0	3×10^{-5}	K^{-1}
Density	ρ_0	4000	kg m^{-3}
Gravity acceleration	g_0	9.81	m s^{-2}
Temperature change	ΔT	2825	K
Temperature offset	T_η	452	K
Background mantle temperature	T_b	1685	K
Mantle thickness	h_M	2867	km
Thermal diffusivity	κ_0	1×10^{-6}	$\text{m}^2 \text{s}^{-1}$
Reference viscosity	η_0	1×10^{21}	Pa s
Activation energy (upper mantle)	E_{UM}	100	kJ mol^{-1}
Activation energy (lower mantle)	E_{LM}	33	kJ mol^{-1}
Activation temperature	T_η	452	K
Universal gas constant	R	8.31	$\text{J mol}^{-1} \text{K}^{-1}$
Radius of the Earth	R_0	6371	km

771

772 **Table 5.** Model set-up for Case 1 – 5. Also refer to Fig. 7b-c.

	Case 1	Case 2	Case 3	Case 4	Case 5
Mesh nodes	129 × 129 × 12 (nodes on the surface) × 65 (depth levels)				
Viscosity relative to Reference Viscosity (Lithosphere 0-160 km depth, Asthenosphere 160- 310 km depth, Upper mantle 310-660 km depth, Lower Mantle > 660 km depth)	1,0.1,1,100	1,1,1,100	1,0.1,1,10→100 linear increase of viscosity from 10 to 100 with depth in the lower mantle to approximate the viscosity profile of Steinberger and Calderwood (2006)		
Plate reconstructions for the eastern Tethys	Zahirovic et al. (2014)		Slab-calibrated longitudinal positions from Zahirovic et al. (2014)	Zahirovic et al. (2014)	This Study

773

774 **3 Regional tectonic evolution**

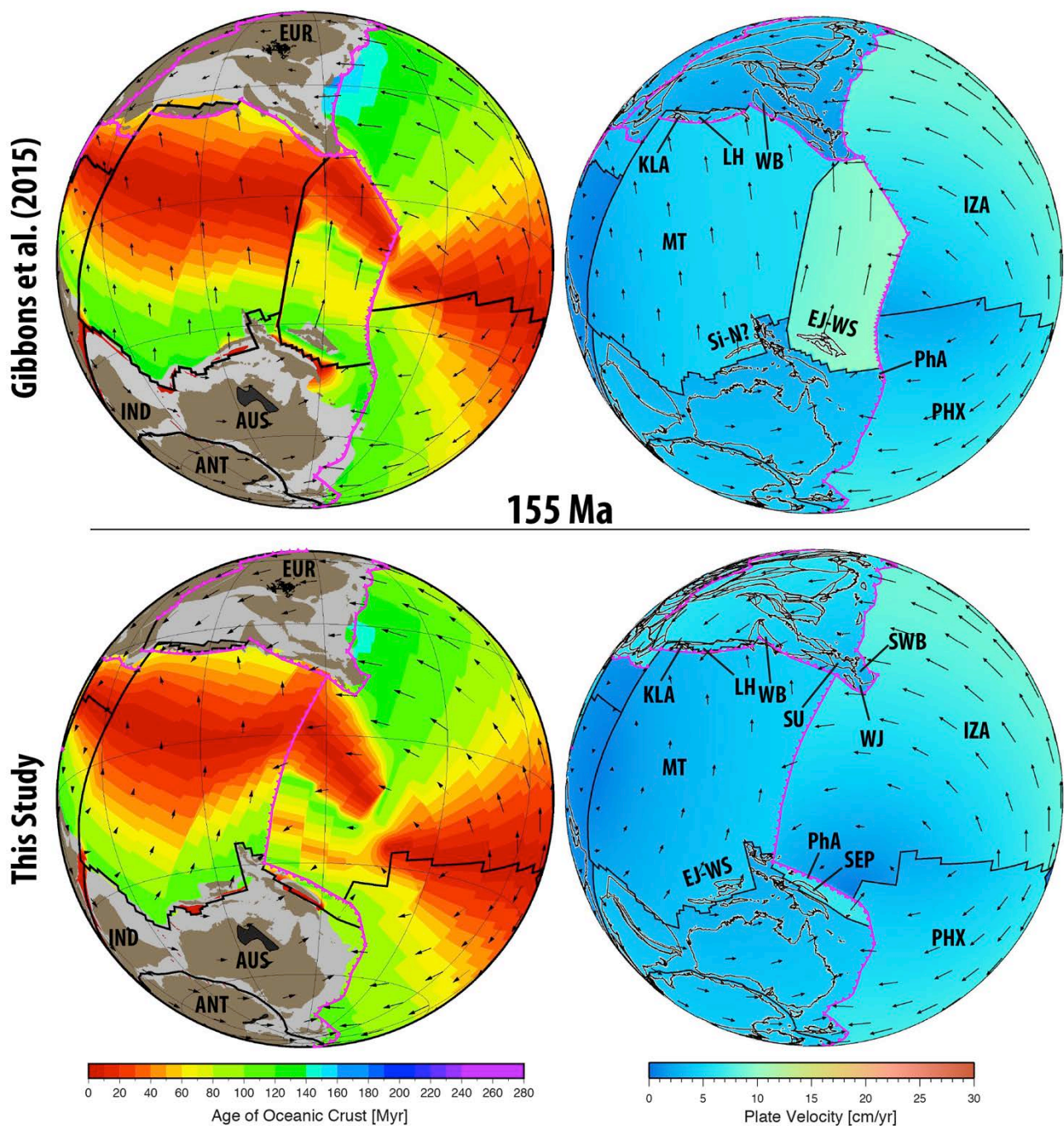
775 **3.1 Late Jurassic plate boundary configuration and rifting mechanism along northern**
776 **Gondwana**

777

778 The Late Jurassic is marked by a major rifting event along northern Gondwana (Pigram and
779 Panggabean, 1984) (Figs. 4a and 8), which transferred a number of continental blocks (including East
780 Java, West Sulawesi, Mangkalihat and east Borneo) northward towards Eurasia (Hall, 2012;
781 Zahirovic et al., 2014), with the only portions of the seafloor spreading system preserved in the Argo

782 Abyssal Plain on the NW Australian shelf (Gibbons et al., 2013). Beyond the oldest preserved oceanic
783 crust, the plate configuration can only be inferred from proxy indicators found on continents. One
784 pertinent argument is that Audley-Charles (1988) and Audley-Charles et al. (1988) required a triple
785 junction plate boundary configuration in the Late Jurassic and Early Cretaceous in the vicinity of the
786 NW Australian shelf where northward slab pull from subduction along southern Eurasia was the
787 driving mechanism for detaching the Neo-Tethyan ribbon terrane (also in Fig. 4a). This northward
788 slab pull detached the continental fragments forming passive margins along the northern and southern
789 boundaries of the ribbon terrane, the preferred scenario presented here. An alternative scenario has
790 south-dipping subduction along northern Gondwana in the Late Jurassic, leading to the opening of
791 the Neo-Tethys and transfer of continental fragments northward through slab rollback (Hall, 2012)
792 (Fig. 4b). Both mechanisms are thought to be capable of detaching continental fragments (see
793 Stampfli and Borel, 2002), but, the south-dipping subduction end-member requires continuous arc
794 volcanism, some of which ought to be preserved on the drifting ribbon terranes.

795



796

797 **Fig. 8.** Reconstruction of Neo-Tethyan ocean basin opening along northern Gondwana in the latest
 798 Jurassic. Both the Zahirovic et al. (2014) and Gibbons et al. (2015) models (top) invoke East Java
 799 and West Sulawesi rifting from New Guinea, as the simplest tectonic scenario to transfer the blocks
 800 northwards toward Southeast Asia, and a possible origin of the Sikuleh and Natal (Si-N) fragments
 801 from the Argo Abyssal Plain. Southwest Borneo (SWB), West Java (WJ), Sumatra (SU), West Burma
 802 (WB) and Lhasa (LH) form the active Eurasian continental margin. Seafloor spreading in the Neo-
 803 Tethys is driven by north-dipping subduction along southern Eurasia (EUR), consuming the Meso-

804 Tethyan (MT) oceanic crust and resulting in the incipient formation of the Kohistan-Ladakh Arc
805 (KLA). In the revised reconstructions, East Java and West Sulawesi (EJ-WS) are the ‘Argoland’
806 continental fragment originating in the Argo Abyssal Plain on the NW Australian shelf. South-
807 dipping subduction along New Guinea is modelled to detach the Sepik Terrane (SEP) from the New
808 Guinea margin through slab rollback, generating the embryonic components of the Philippine
809 Archipelago (PhA). The scale bars are relevant to all plate reconstruction figures. Grey regions
810 represent the extent of continental crust, dark grey represents large igneous provinces and other plume
811 products, and thin brown lines represent reconstructed fracture zones. ANT – Antarctica, AUS –
812 Australia, IND – India, IZA – Izanagi Plate, PHX – Phoenix Plate. Orthographic reconstructions are
813 centred on 115°E, 15°S. See Supplementary Animation 2, 3 and 4.

814

815 The NW Australian shelf, the putative source of the Argoland ribbon terrane records some Late
816 Jurassic and Early Cretaceous volcanic plateaus (e.g., Scott and Wombat plateaux, Joey Rise, etc. –
817 see Fig. 1), rift-related volcanics and seaward dipping reflectors (Heine and Müller, 2005; Rohrman,
818 2015; von Rad et al., 1992). An earlier phase of rhyolitic volcanism between ~213 and 190 Ma erupted
819 on the Wombat Plateau (von Rad and Exon, 1983; von Rad et al., 1992), but cannot be temporally
820 linked to the latest Jurassic (~155 Ma) rifting and seafloor spreading phase recorded on the NW
821 Australian shelf. Although the latest Jurassic NW Australian margin was volcanic, little evidence
822 exists that it was dominated by an Andean-style active margin (von Rad and Exon, 1983; von Rad et
823 al., 1992). Although the seismic interpretations by Hopper et al. (1992) of the margin’s volcanic
824 history do not indicate widespread plume activity, the recent work of Rohrman (2015) suggests a
825 plume origin for the large volume of underplated material and widespread sills interpreted from
826 seismic sections in the Exmouth Plateau region (Fig. 1). One critical aspect of the latest Jurassic event
827 is that the onset of seafloor spreading is well-constrained by a 155 ± 3.4 Ma K-Ar age of the oldest
828 seafloor in the Argo Abyssal Plain (Gradstein and Ludden, 1992), consistent with rapid tectonic
829 subsidence in the latest Jurassic on the NW Australian shelf (Heine and Müller, 2005; Rohrman,

830 2015; Tovaglieri and George, 2014), and the identification of M25A (Heine and Müller, 2005) or
831 M26 (Gibbons et al., 2012) as the oldest magnetic anomalies (~153-155 Ma) in the seafloor spreading
832 record.

833 Due to the lack of latest Jurassic arc volcanics on the NW Australian Shelf, together with strong
834 indicators of north-dipping subduction initiation along southern Eurasia (see following sections), we
835 prefer northward slab pull as the driving mechanism for rifting and seafloor spreading to open the
836 Neo-Tethys from ~155 Ma. Although more work is required to test whether a plume model can
837 explain the volcanism on the NW Australian shelf in the latest Jurassic (Rohrman, 2015), such a
838 scenario would be consistent with the triple junction scenario invoked for this region (Audley-
839 Charles, 1988; Audley-Charles et al., 1988; Gibbons et al., 2015; Gibbons et al., 2012; Zahirovic et
840 al., 2014), and the similarity to the East African rift-plume interaction (Burke and Dewey, 1973;
841 Montelli et al., 2006; Yirgu et al., 2006). Since the Neo-Tethyan seafloor spreading history is
842 incomplete, it remains difficult to ascertain which continental blocks rifted from the Argo segment of
843 the Australian margin (Table 2). Rifting of East Java and West Sulawesi from New Guinea was
844 invoked as a preferred scenario in our base models in the Late Jurassic (Gibbons et al., 2015;
845 Zahirovic et al., 2014), with the possibility that micro-continental fragments along Sumatra (such as
846 the now-disputed Natal and Sikuleh fragments, Fig. 2) had an origin in the Argo Abyssal Plain,
847 following Audley-Charles et al. (1988), Metcalfe (1994) and Heine and Müller (2005). However,
848 recent zircon age spectra analyses from East Java suggesting strong affinities with the NW Australian
849 Shelf (Sevastjanova et al., 2015; Smyth et al., 2007), led Hall (2012) to argue that East Java was the
850 enigmatic “Argoland” fragment (Table 2). We present both a NW Australian shelf and a New Guinea
851 origin for Argoland in our alternative plate reconstruction scenarios, and evaluate their plate
852 kinematic and geodynamic consequences on the Neo-Tethyan tectonic evolution.

853

854 Table 2. Previously-interpreted continental fragments originating from northern Gondwana in the eastern Tethys in the
855 Late Jurassic.

<i>Model</i>	<i>All continental fragments originating from northern Gondwana in the Late Jurassic eastern Tethys</i>	<i>Argoland fragment</i>
Audley-Charles et al. (1988)	South Tibet (Lhasa), West Burma, Malaya, Sumatra, East and West Borneo fragments, West Sulawesi	West Burma
Metcalf (1994)	West Burma, Sikuleh, Natal, West Sulawesi, Mangkalihat, Banda Allochthons	West Burma
Heine and Müller (2005)	West Burma	West Burma
Hall (2012)	Southwest Borneo core, East Java, West Sulawesi	East Java and West Sulawesi
Zahirovic et al. (2014) Gibbons et al. (2015)	Sikuleh, Natal, East Java, Southeast Borneo, West Sulawesi	Sikuleh, Natal and other possible fragments that may be in the Mawgyi Nappe along West Burma
This Study	East Java, Eastern Borneo, Mangkalihat, West Sulawesi and Sepik (New Guinea)	East Java, Eastern Borneo, Mangkalihat and West Sulawesi

856

857

858

859

860

861

862

863

864

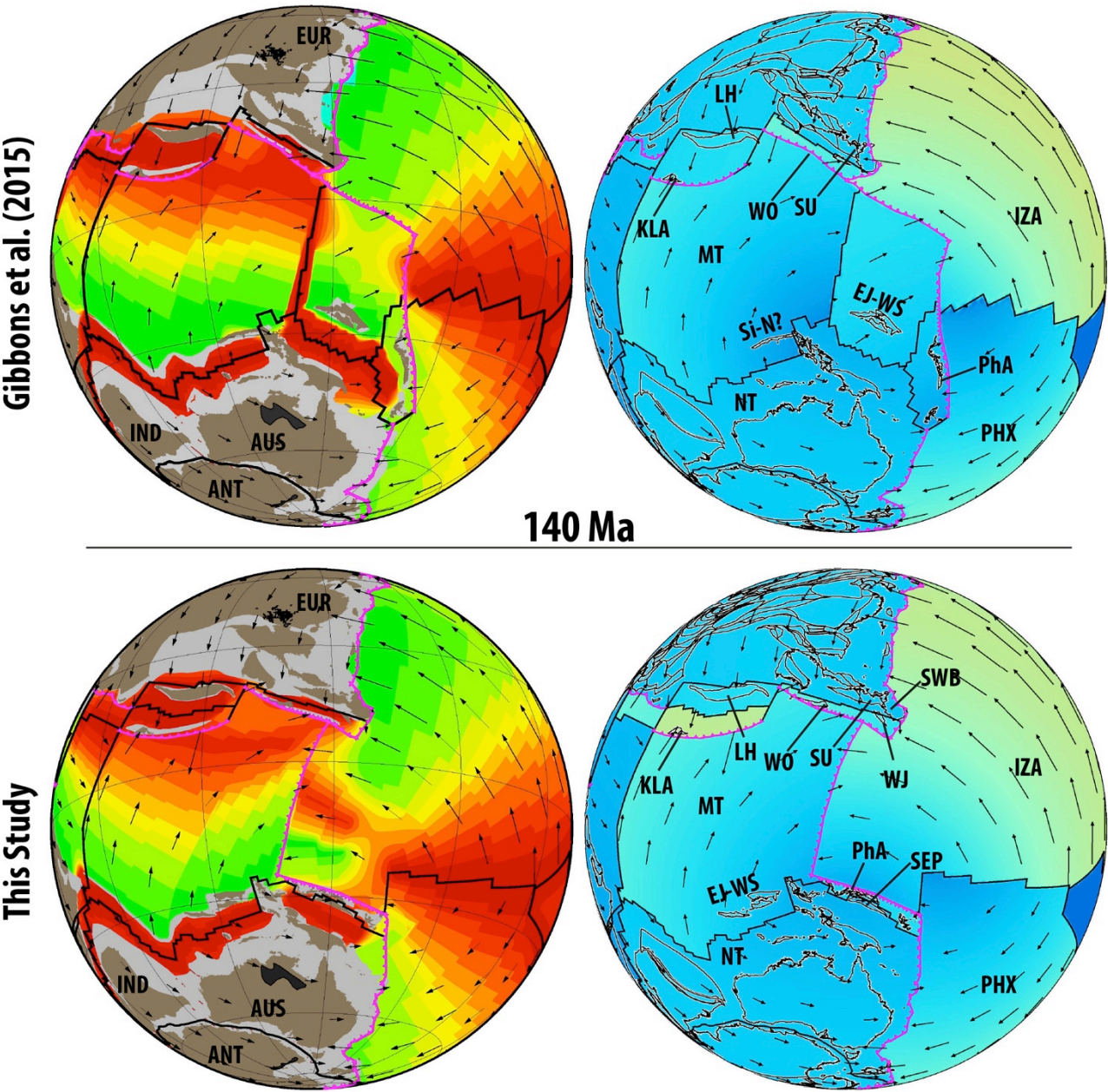
865

866

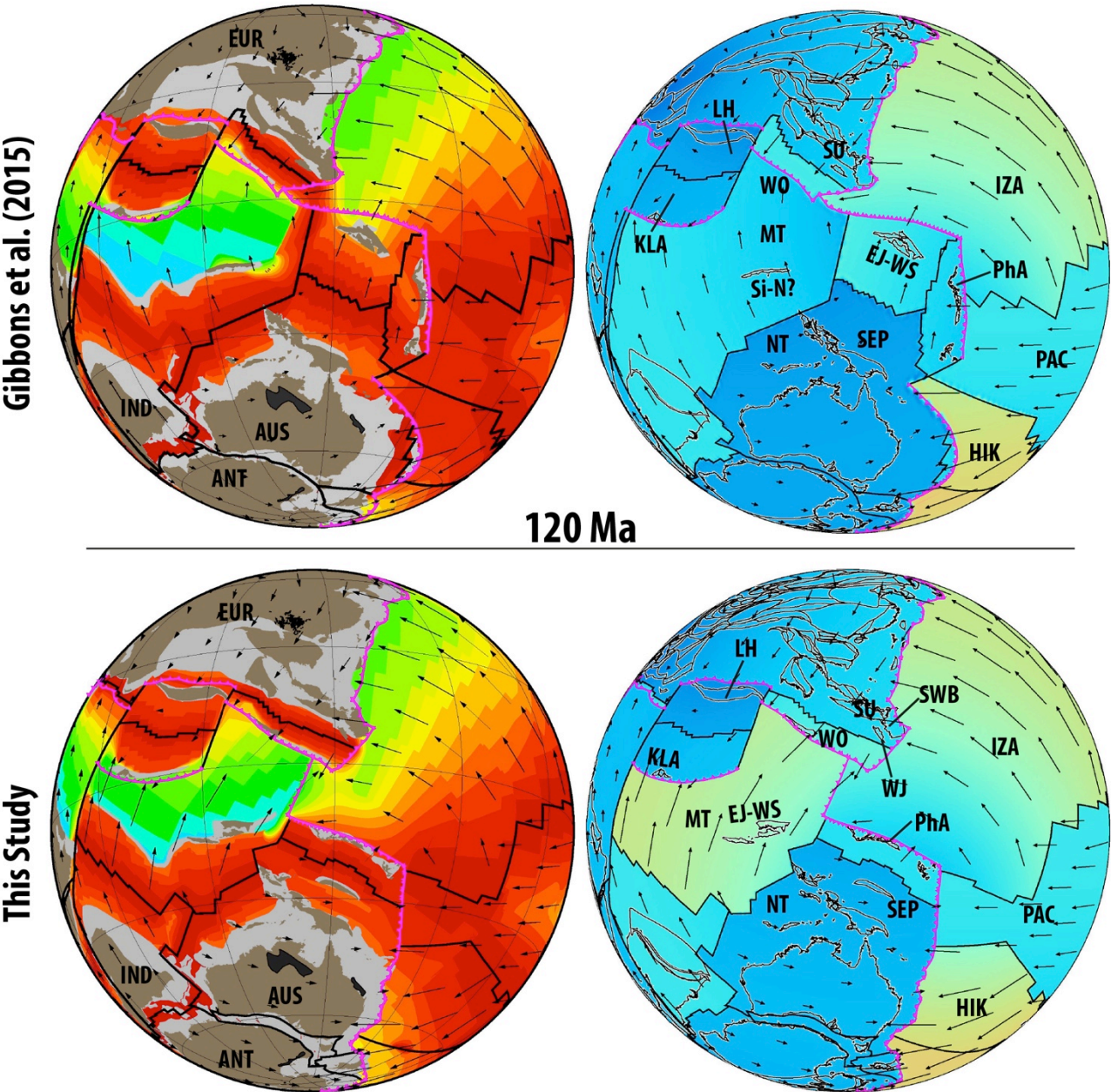
867

The ~155 Ma onset of seafloor spreading in the Argo segment of the north Gondwana margin is consistent with Jurassic sedimentary rift-drift sequences (Pigram and Panggabean, 1984), and mafic rocks that are as old as 158 Ma on West Sulawesi (Polvé et al., 1997), likely representing the drift of the East Java and West Sulawesi continental fragments (Zahirovic et al., 2014). The early seafloor spreading history is preserved in the Argo Abyssal Plain, with the youngest marine magnetic anomaly of M10Ny (Gibbons et al., 2013) representing an age of 128.9 Ma, after which the seafloor spreading history is unconstrained. As discussed extensively in Zahirovic et al. (2014), and summarised below in Section 3.4, the East Java and West Sulawesi fragments may have collided with an intra-oceanic arc in the mid-Cretaceous (Wakita, 2000), and sutured to Sundaland by 80 Ma. However, the Neotethyan full seafloor spreading velocity required by the ~115 Ma arc-continent collision approaches ~25 cm/yr between ~128 and 115 Ma (see Supplementary Fig. 1), which is likely to be an upper limit

868 for plate velocities in the post-Pangea timeframe (Stampfli and Borel, 2002; V  rard et al., 2012;
869 Zahirovic et al., 2015). An alternative explanation for the ~115 Ma peak in very high pressure (VHP)
870 metamorphic rocks in the Luk Ulo-Meratus Suture Zone (Parkinson et al., 1998) (Fig. 2), includes
871 the initiation of subduction of the Woyla/Barito back-arc basins, which reduces the synthetic seafloor
872 spreading velocities to ~11 cm/yr (Figs. 10-11). We adopt the latter option that does not introduce a
873 geodynamically implausible velocity spike in Tethyan plate velocities.
874



876 **Fig. 9.** Ongoing Meso-Tethyan subduction leads to the opening of the Kohistan-Ladakh (KLA) and
877 Woyla (WO) back-arc basins, as well as the Neo-Tethys (NT) along northern Gondwana. The
878 Philippine Archipelago (PhA) is detached from the Sepik Terrane (SEP) through a northward ridge
879 jump and continued rollback of the Izanagi slab.
880



881
882 **Fig. 10.** In the models of Zahirovic et al. (2014) and Gibbons et al. (2015) the Neo-Tethyan ridge
883 system is abandoned by 120 Ma. In this study, seafloor spreading continues because of ongoing
884 subduction of the Meso-Tethyan Plate. Although the oldest preserved seafloor spreading constraints

885 for the Neo-Tethys are ~128 Ma in the Argo Abyssal Plain, we impose continued seafloor spreading
886 in the Neo-Tethys that is driven by northward slab pull. HIK – Hikurangi Plate.

887

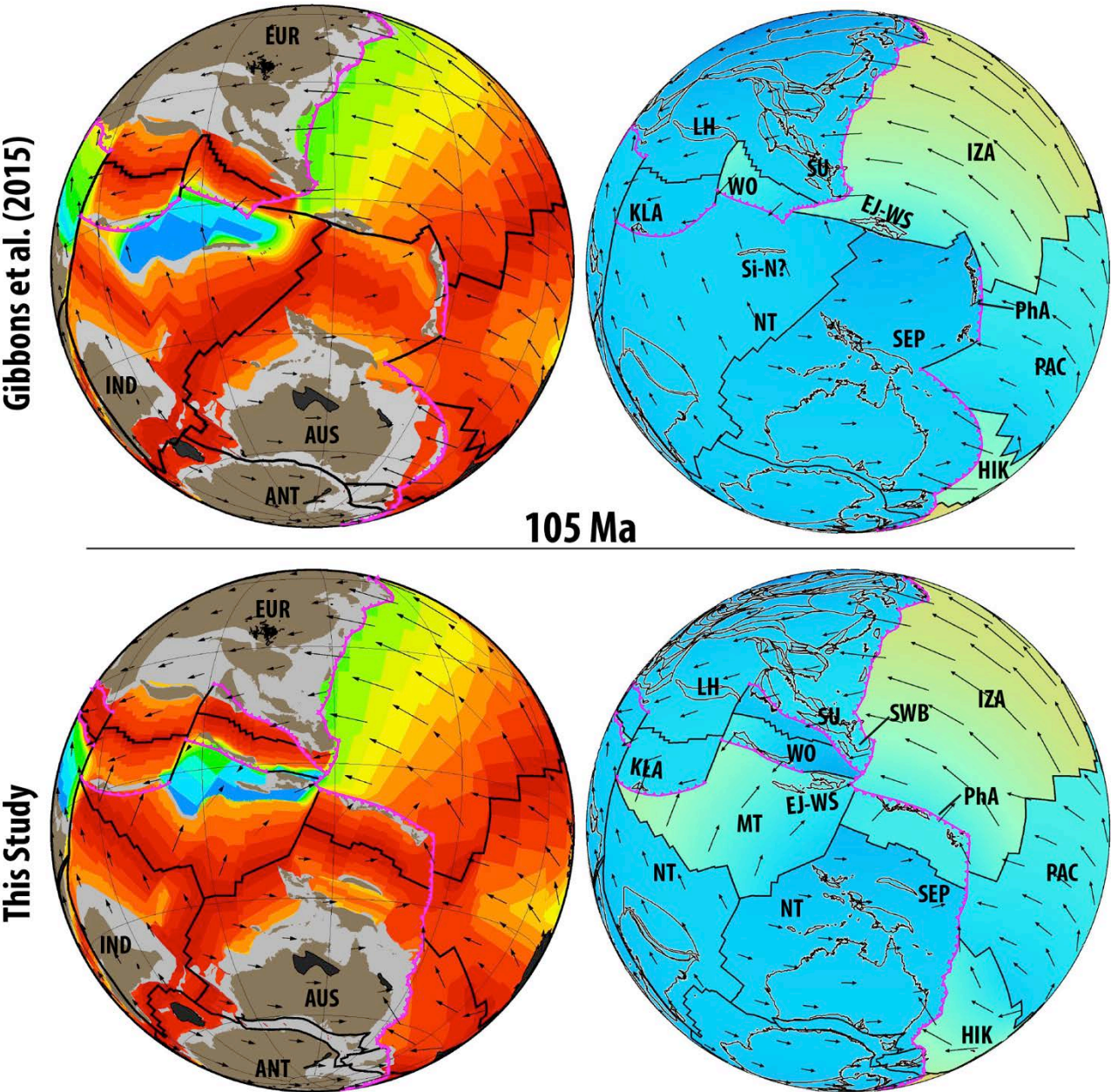
888

889 **3.2 Active margin evolution in the Lhasa segment**

890

891 The Late Jurassic is characterized by the asynchronous development of an active margin along
892 southern Eurasia that was consuming the Meso-Tethyan ocean basin along a north-dipping
893 subduction zone (Fig. 8). Along southern Lhasa, subduction-related calc-alkaline granites and
894 granitoids ranging in age from ~170 to 137 Ma indicate the onset of north-dipping Meso-Tethyan
895 Andean-style subduction (Zhang et al., 2012). The onset of subduction-related magmatism within the
896 Kohistan Arc, which has no continental basement (Burg, 2011; Jagoutz and Schmidt, 2012), at ~154
897 Ma in the form of the Matum Das tonalite (Schaltegger et al., 2003) suggests the rollback of a Meso-
898 Tethyan slab (e.g., Petterson and Windley, 1985; Pudsey, 1986) and the possible origin of Kohistan
899 and Ladakh as fore-arc oceanic crust, following the generic model of forearc formation proposed by
900 Flower and Dilek (2003) and Stern et al. (2012). Further east along the present-day suture zone, the
901 interpreted intra-oceanic Zedong Terrane records latest Jurassic ages of subduction-related igneous
902 suites including a dacite breccia dated as 161.0 ± 2.3 Ma, a number of samples with an age of ~156
903 Ma (andesite dyke, andesite breccia and quartz diorite), and an andesitic dyke with an age of $152.2 \pm$
904 3.3 Ma (McDermid et al., 2002). The Kohistan-Ladakh, Zedong and more-broadly Neo-Tethyan
905 intra-oceanic subduction zone likely became established through continued southward slab rollback
906 between ~150 and 120 Ma, which is marked by a magmatic hiatus in the Gangdese Batholith on
907 Lhasa until ~110 Ma (Ji et al., 2009; Wen et al., 2008b). However, while the magmatic evolution of
908 the Kohistan-Ladakh intra-oceanic arc is well-studied, its paleo-latitudinal position remains
909 controversial and poorly constrained. Burg (2011) and Gibbons et al. (2015) place Kohistan on the
910 equator at ~100 Ma (Fig. 11) based on the magnetisation of mid-Late Cretaceous red beds (Zaman

911 and Torii, 1999), suggesting a maximum southward extent for the Neo-Tethyan intra-oceanic arc. In
 912 addition, although Kohistan and Ladakh form the only significant preserved remnants of the Early
 913 Cretaceous intra-oceanic arc within the Yarlung-Tsangpo Suture Zone, additional ophiolites with
 914 intra-oceanic affinity are embedded in the suture zone east of Kohistan and Ladakh (Aitchison et al.,
 915 2000; Hébert et al., 2012).



916
 917 **Fig. 11.** The change in the motion of India from largely counterclockwise in the Early Cretaceous to
 918 largely northward, is recorded in fracture zone bends in the Wharton Basin at ~105-100 Ma
 919 (Matthews et al., 2012). In this study, the Neo-Tethyan ridge is consumed at the Kohistan-Ladakh

920 (KLA) intra-oceanic subduction zone from ~105 Ma, leading to a greater northward slab pull acting
921 on the Indian Plate (IND), which we interpret as causing the change in India Plate motion. The
922 collision of the East Java-West Sulawesi continental fragments possibly impeded subduction at the
923 Woyla Arc at ~105 Ma, and led to obduction of the Meratus ophiolite in the Cenomanian-Turonian
924 (~100-93 Ma) (Pubellier et al., 2004; Yuwono et al., 1988). The Kohistan-Ladakh and Woyla arcs
925 likely occupied near-equatorial latitudes by ~100 Ma, with both back-arc systems subducted
926 northward from ~115 Ma in the Sunda segment and from ~110 Ma along Lhasa, resulting in two
927 coeval north-dipping subduction zones in the Neo-Tethys (see Section 3.2).

928

929 The Aptian to Albian (~126-100 Ma) Yasin Group sedimentary sequence on the Kohistan-
930 Ladakh Arc are intercalated with syn-tectonic arc volcanics, and subsequent intrusions of diorites and
931 granodiorites (Pudsey et al., 1985; Rehman et al., 2011). A large portion of the magmatic products
932 were emplaced during a key timeframe between ~110 and 90 Ma (Petterson and Windley, 1985;
933 Rehman et al., 2011; Schärer et al., 1984), with significant magmatic accretion forming the Sapat
934 Complex on the Kohistan Arc between ~105 and 99 Ma (Bouilhol et al., 2011). This short-lived
935 “trenchward migration of the hot mantle source” (Bouilhol et al., 2011) may indicate the arrival of
936 the Neo-Tethyan mid-oceanic ridge with slab window formation, consistent with the ~95 Ma high-
937 temperature granulite metamorphism in the Jijal Complex and the peak metamorphic event in the
938 Kamila Amphibolite unit (Petterson, 2010). The demise of the Neo-Tethyan mid-oceanic ridge
939 between ~110 and 90 Ma along the Kohistan-Ladakh intra-oceanic arc (Fig. 11) likely had substantial
940 geodynamic implications for the region at the time, resulting in stronger northward slab pull acting
941 on the Indian Plate. Although the slab window likely temporarily impeded subduction, the
942 progressively increasing northward slab pull from ~105 Ma likely resulted in a major change in the
943 direction and speed of the Indian Plate, observable in the significant bends observed in the Wharton
944 Basin fracture zones (e.g., Wallaby-Zenith Fracture Zone) at ~105-100 Ma that required a ~50°
945 clockwise reorientation of the Indo-Australian spreading system (Matthews et al., 2012), and possibly

946 triggered a regional plate-reorganization event (Matthews et al., 2011). In addition, the onset of
947 northward slab pull on the Indian Plate from ~100 Ma may explain the paleomagnetic observations
948 of rifting within Greater India in the Late Cretaceous (van Hinsbergen et al., 2012).

949 The intersection of the Neo-Tethyan ridge with the Kohistan-Ladakh intra-oceanic subduction
950 zone, as modelled in this study, may have temporarily interrupted subduction due to the decrease of
951 negatively buoyant oceanic lithosphere entering the trench, with convergence accommodated along
952 the active continental Eurasian margin from ~110 Ma rather than along the intra-oceanic subduction
953 zone. The Gangdese Batholith recorded a major pulse of granitic magmatism from ~109 to 80 Ma (Ji
954 et al., 2009), indicating the resumption of Andean-style subduction along Lhasa that is
955 contemporaneous with intra-oceanic subduction along Kohistan-Ladakh, and hence signifies the
956 onset of two simultaneous north-dipping subduction zones in the Neo-Tethys from ~110 Ma.

957 The Late Cretaceous evolution of the Kohistan-Ladakh Arc has conflicting interpretations.
958 Conventional models suggest a Late Cretaceous collision and suturing of Kohistan-Ladakh to Eurasia
959 (Clift et al., 2002; Debon et al., 1987; Treloar et al., 1996), whereas more recent works, which have
960 incorporated detailed geochronology and structural interpretations of Kohistan, have concluded that
961 instead of suturing to Eurasia, the Late Cretaceous is punctuated by an arc rifting and splitting episode
962 by ~85 Ma (Bouilhol et al., 2011; Burg, 2011; Burg et al., 2006), which suggests Neo-Tethyan slab
963 rollback rather than collisional processes. The ~75-60 Ma magmatic gap in the Gangdese Batholith
964 (Chung et al., 2005; Wen et al., 2008b) may imply that the majority of India-Eurasia convergence
965 was accommodated by subduction along Kohistan-Ladakh rather than by subduction along Lhasa. A
966 scenario that precludes Kohistan-Ladakh collision with Eurasia in the Late Cretaceous requires that
967 an intra-oceanic arc first accreted onto Greater India (Chatterjee et al., 2013). A similar model
968 proposes that the Muslim Bagh Ophiolite represents the Kohistan-Ladakh forearc and was obducted
969 onto the leading edge of Greater India at ~65 Ma in near-equatorial latitudes, which resulted in the
970 cessation of calc-alkaline magmatism on Kohistan-Ladakh during ~65-61 Ma (Khan et al., 2009).
971 This scenario requires the accompanying suturing between Kohistan-Ladakh and Greater India along

972 the Indus Suture to occur earlier than the closure of Shyok Suture. Such a scenario is consistent with
973 the plate reconstructions presented in this study, in which Greater India reaches equatorial latitudes
974 at ~65 Ma. A recent stratigraphic analysis presented in Hu et al. (2015) suggests the India-Eurasia
975 collision was underway by 59 ± 1 Ma, which we interpret as the initial arc-continent collision,
976 consistent with the tectonic evolution of the Kohistan-Ladakh Arc. The major slowdown in spreading
977 across the Central and Southeast Indian Ridges at ~52 Ma (Chron 23o, Cande et al., 2010) may
978 indicate the complete abandonment of the intra-oceanic subduction zone, and the completion of the
979 initial arc-continent collision between Greater India and the Neo-Tethyan intra-oceanic arc. Recent
980 geochemical analyses of granitoids from the Kohistan-Ladakh Arc indicate a major change in magma
981 chemistry (Nd and Hf isotopes) and the arrival of the Greater Indian continental margin into the
982 subduction zone by 50.2 ± 1.5 Ma (Bouilhol et al., 2013), which is consistent with the cessation of
983 intra-oceanic subduction by this time.

984 The continent-continent collision between Greater India and Eurasia likely occurred at
985 ~47 Ma, recorded in the marked slowdown of seafloor spreading at Chron 21o along the Southeast
986 Indian Ridge (Cande and Patriat, 2015) and the contemporaneous formation of an Indian Ocean
987 microplate near the Ninetyeast Ridge (Matthews et al., 2016). Suturing along the Shyok Suture Zone
988 between the two continents was likely complete by 40.4 ± 1.3 Ma (Bouilhol et al., 2013), which
989 accounts for the ~60-40 Ma Andean-style emplacement of the Linzizong Volcanics in Lhasa (Chung
990 et al., 2005). The ~47-40 Ma continent-continent collision timing is consistent with an additional
991 slowdown and change in spreading direction along the Central and Southeast Indian Ridges, the
992 inception of a short-lived Indian Ocean microplate (Matthews et al., 2016), and the abandonment of
993 the Wharton Ridge sometime between ~43 and 36 Ma (see discussion in Gibbons et al., 2015).

994

995 **3.3 Convergence along the West Burma and Sumatra margin segment**

996

997 Eastern Sumatra, as part of the Sibumasu ribbon terrane, docked with the Eurasian margin
998 sometime in the Late Triassic to Early Jurassic (Metcalf, 2011), and has since recorded Meso- and
999 Neo-Tethyan subduction and accretion histories. The Woyla Terrane, which accreted to Sumatra in
1000 the Late Cretaceous (Morley, 2012a), plays a key role in elucidating the geodynamic setting of the
1001 Sumatran active margin since the Late Jurassic. However, the nature of the Woyla Terrane crust and
1002 the subduction polarity and history has given rise to a number of competing models for the tectonic
1003 evolution of Sumatra. The Jurassic to Cretaceous Woyla Group of sedimentary and volcanic units has
1004 previously been interpreted as an arc built on re-worked continental basement (Barber and Crow,
1005 2003; Cameron et al., 1980), largely due to the presence of a tin geochemical signature in the Sikuleh
1006 granitoids (Fig. 2) that may have been interpreted as analogous to the Southeast Asian tin belts that
1007 were built on continental crust (e.g., Bangka and Billiton Islands; Searle et al., 2012). Parts of the
1008 Woyla basement near Sikuleh, Natal and Bengkulu are composed of quartzite and phyllite (Acharyya,
1009 1998), and overprinted by widespread granitoid intrusions largely Late Cretaceous in age (Barber and
1010 Crow, 2003), leading some authors to interpret these micro-blocks as Gondwana-derived continental
1011 fragments (Görür and Sengör, 1992; Haile, 1979; Metcalfe, 1994; Metcalfe, 2002; Metcalfe and
1012 Irving, 1990). The paleomagnetic study of a Jurassic limestone sample by Haile (1979) suggests that
1013 the crust in the vicinity of Sikuleh (Locality H in Haile, 1979) was at 26°S in the Jurassic. This result
1014 was used by Metcalfe (1994) to suggest a Gondwana origin for the proposed micro-continental
1015 fragment.

1016 The continental nature of the Sikuleh part of the Woyla Terrane (Si, Fig. 2) is rejected by
1017 Barber and Crow (2003), who instead propose an intra-oceanic arc origin. The Woyla Group consists,
1018 at least in part, of accreted fragments that include seamounts, reef fragments, ophiolites and
1019 associated ocean floor sedimentary sequences (Barber and Crow, 2003; Wajzer et al., 1991), but no
1020 clear continental basement can be identified, much like the Kohistan-Ladakh Arc in the central Neo-
1021 Tethys. Paleontological constraints from a single foraminifera specimen within the Batang Natal
1022 Megabreccia provide a Late Triassic age (Wajzer et al., 1991), and suggest that the oceanic crust that

1023 was consumed in the Woyla intra-oceanic subduction system in the Cretaceous was at least Late
1024 Triassic in age, consistent with the age of Meso-Tethyan oceanic crust subducted along the Sumatra
1025 segment predicted by our reconstructions for the Cretaceous (Fig. 10). In addition, the accretion of
1026 highly disrupted lenses of oceanic crust and sedimentary sequences onto the Woyla Terrane is
1027 consistent with the observations of accreted oceanic plate stratigraphy further east in the Luk Ulo-
1028 Meratus Suture Zone between East Java-West Sulawesi and the core of Borneo (Wakita, 2000;
1029 Wakita and Metcalfe, 2005).

1030

1031 **3.3.1 Development of the Woyla intra-oceanic arc**

1032

1033 The Woyla Terrane, largely represented by the Woyla Group of sedimentary sequences and
1034 intrusions, likely developed on an active intra-oceanic margin (with possible continental basement)
1035 in the Early Cretaceous (Figs. 9-11), separated from mainland Sumatra by a marginal sea (Rock et
1036 al., 1983; Wajzer et al., 1991). However, the origin of the Woyla Arc has recently been debated, with
1037 a model proposing a Gondwana origin for both the Woyla and the Kohistan-Ladakh Arc (Hall, 2012)
1038 as the result of continued rollback of a south-dipping subduction zone (Fig. 4b-c). Alternatively, the
1039 model of Zahirovic et al. (2014), and the one presented here, invoke a southern Eurasia origin of the
1040 Kohistan-Ladakh and Woyla intra-oceanic island arcs. The scenario invoking south-dipping
1041 subduction along northern Gondwana in the Late Jurassic could be corroborated by the preservation
1042 of contemporaneous arc rocks on Greater India (Tethyan Himalayas) or the NW Australian Shelf,
1043 which are not yet documented. The scenario invoking north-dipping Meso-Tethyan subduction to
1044 detach the Argoland continental fragments and open the Neo-Tethys in the latest Jurassic can be
1045 corroborated by the subduction history along Lhasa, West Burma (Myanmar) and Sundaland.
1046 Subduction is suggested to have initiated along the West Burma block at ~163-152 Ma by jadeite
1047 geochronology (Shi et al., 2008; Shi et al., 2014). This age is similar to that of the 154 Ma Matum
1048 Das tonalite within the Kohistan-Ladakh arc (Schaltegger et al., 2003) to the west. The formation of

1049 the Naga Ophiolite during ~156-150 Ma, based on Kimmeridgian-lower Tithonian cherts (Baxter et
1050 al., 2011), suggests a close temporal and geodynamic association between the Kohistan-Ladakh
1051 (Lhasa segment), Mawgyi (West Burma segment) and Woyla (Sumatra segment) intra-oceanic arcs
1052 along which Meso-Tethyan oceanic crust began subducting in the latest Jurassic.

1053

1054 **3.3.2 Subduction of the Woyla back-arc basin**

1055

1056 The resumption of Andean-style subduction in the central Neo-Tethys along Lhasa is well-
1057 constrained to ~109 Ma, based on the onset of subduction-related magmatism in the Gangdese
1058 Batholith (Ji et al., 2009). However, the timings of subduction initiation along West Burma and
1059 Sumatra are less well constrained. An Albian (~113-100 Ma) unconformity on West Burma (Morley,
1060 2012a) may indicate compression related to subduction initiation, which is contemporaneous with
1061 observations in Lhasa, and the supra-subduction formation of the Andaman Ophiolite at 95 ± 2 Ma
1062 (Pedersen et al., 2010) may suggest the onset of rollback and extension in the overriding plate. Here
1063 we interpret the ~115 Ma peak in Ultra- and Very-High Pressure metamorphics in the Luk-Ulo Suture
1064 Zone (Figs. 10-12) (Parkinson et al., 1998) as indicators of subduction initiation of the Woyla back-
1065 arc basin to account for the Albian unconformity on West Burma. The 105 to 90 Ma dioritic and
1066 granodioritic intrusions into the Wuntho-Popa Arc (Mitchell et al., 2012), west of the Sagaing Fault,
1067 suggest continuity of the contemporaneous Lhasa subduction zone into the West Burma segment of
1068 the margin. However, subduction to consume the Woyla back-arc basin may (also) have been south-
1069 dipping as argued in Morley (2012a).

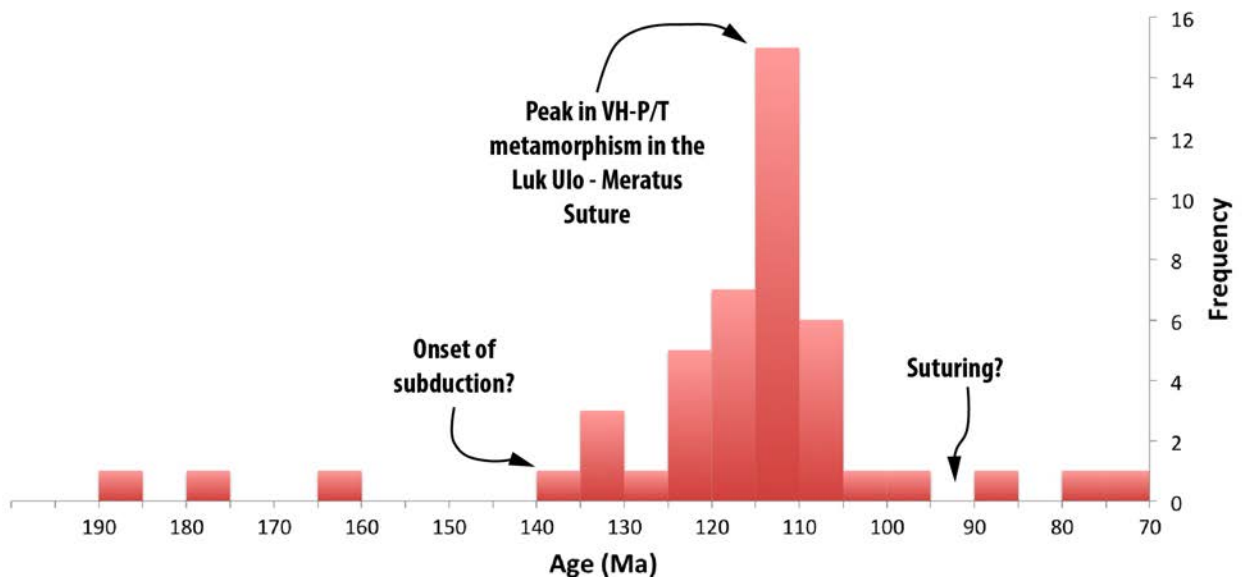


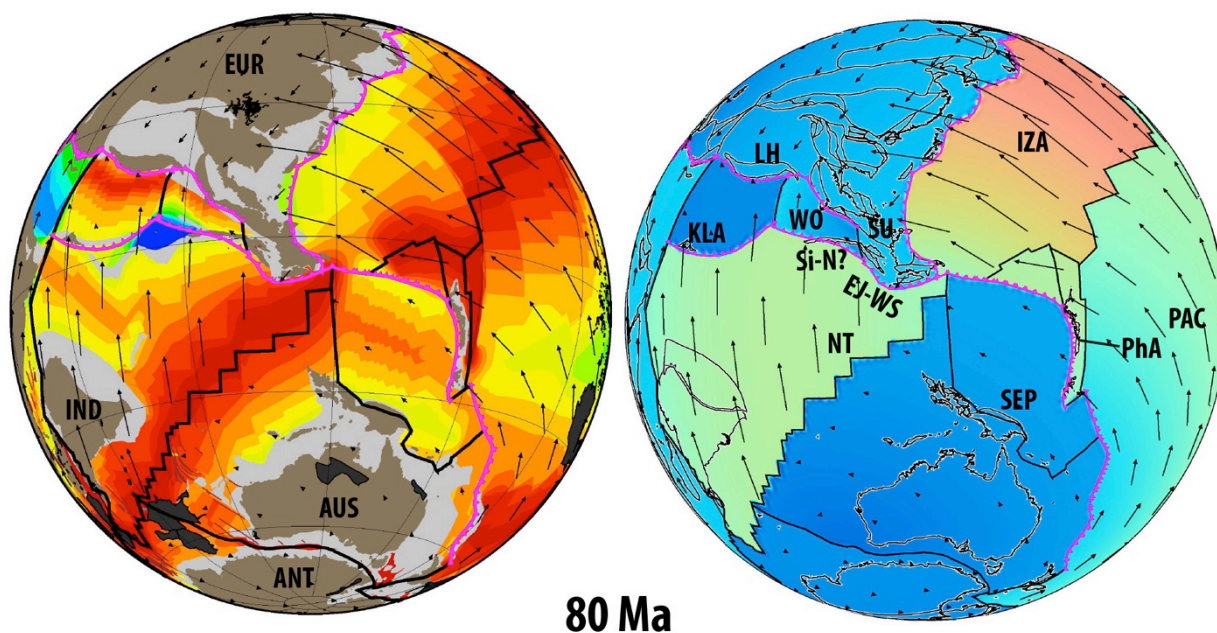
Fig. 12. Very High and Ultra High Pressure (VHP/UHP) metamorphic rocks in the Luk Ulo-Meratus suture on Java and Borneo (Fig. 2) record well-established subduction from at least ~140 Ma. A significant spike at ~115 Ma has been previously interpreted as a collision between East Java-West Sulawesi and the Woyla intra-oceanic arc (Gibbons et al., 2015; Zahirovic et al., 2014). However, in the refined plate reconstructions presented herein, the origin of East Java from the Argo Abyssal Plain would require excessive seafloor spreading rates, and instead we interpret the peak in VHP/UHP metamorphism to represent the onset of Woyla back-arc subduction along West Burma and Sundaland. Figure modified from Parkinson et al. (1998).

Although the Kohistan-Ladakh Arc is loosely constrained to near-equatorial paleo-latitudes during the mid-Cretaceous (Burg, 2011), no latitudinal constraints exist for the Woyla Arc. However, some constraints are available for the closure of the Woyla back-arc basin, and the collision of the intra-oceanic arc with Sumatra (Figs. 13-14). The Woyla Group is intruded by a number of Late Cretaceous igneous bodies, including the 84.7 ± 3.6 Ma (K-Ar) Batu Madingding diorite and the 78.4 ± 2.5 Ma (K-Ar) andesite in the southwest Batang Natal section (Wajzer et al., 1991), after which a significant magmatic gap is interpreted to represent collision of the Woyla Terrane with Sumatra. Hall (2012) argued that no subduction occurred on the Woyla/Sumatra segment of the Tethyan margin

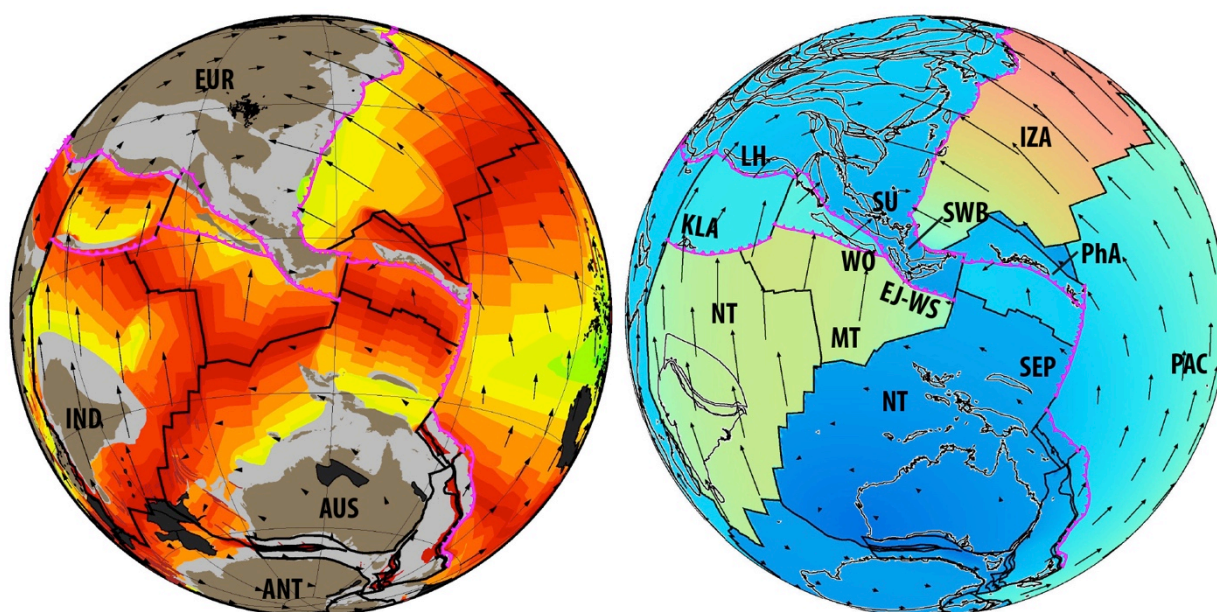
1088 between 90 and 45 Ma (Fig. 4c), largely due to the presence of a regional unconformity that was
1089 interpreted to signify the absence of subduction-related dynamic subsidence on the overriding plate
1090 (Clements et al., 2011). However, only a ~10-15 Myr magmatic gap associated with a hiatus in
1091 subduction between ~75 and 62 Ma (Fig. 15) can be accounted for in the volcanic record on Sumatra
1092 (McCourt et al., 1996; Zahirovic et al., 2014). However, some of these (~10 Myr) magmatic gaps
1093 may be due to sampling issues, and future work may reveal more continuous subduction histories.
1094 The choice to impose a ~45 Myr (Hall, 2012) rather than a ~10-15 Myr (Zahirovic et al., 2014)
1095 subduction hiatus has significant geodynamic implications for the region, where the continued
1096 northward motion of the Indian Plate needs to be accommodated by an oceanic transform that cuts
1097 across older oceanic lithosphere and pre-existing structural fabric in the reconstructions of Hall
1098 (2012) (Fig. 4c).

1099

Gibbons et al. (2015)



This Study



1100

1101

1102

1103

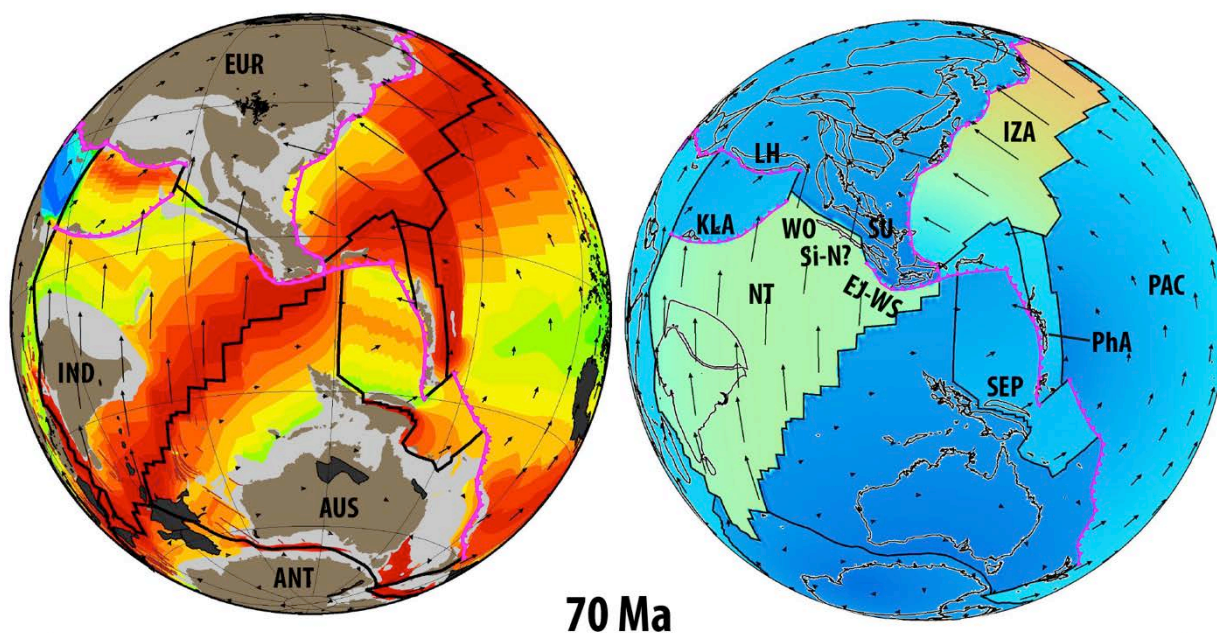
1104

1105

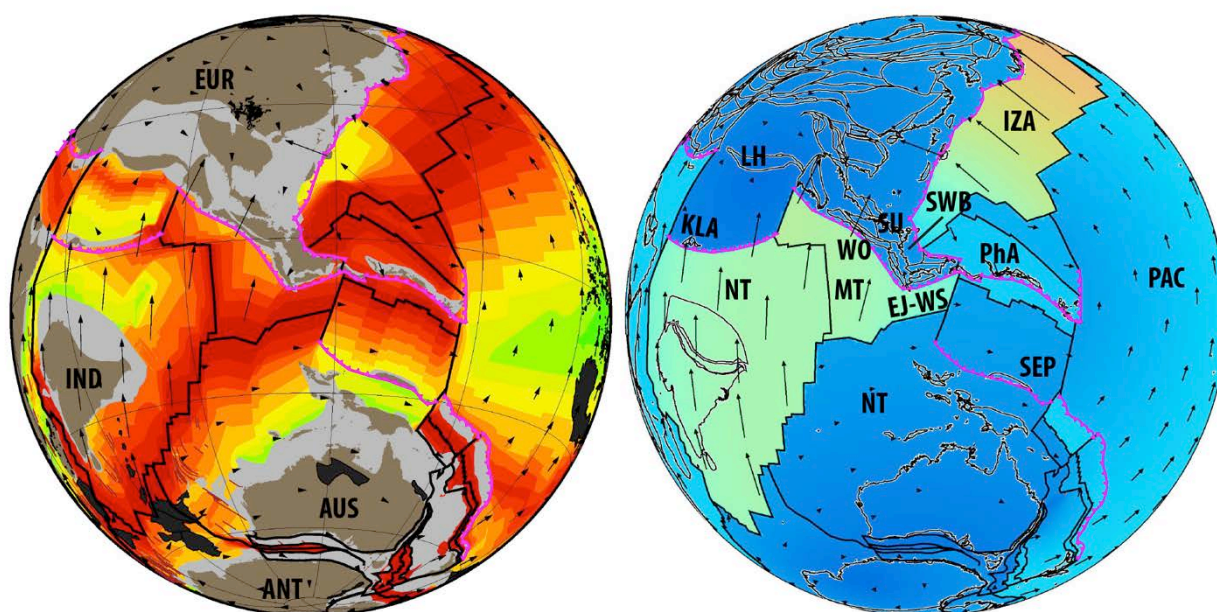
1106

Fig. 13. India's northward motion accelerated from ~80 Ma. The subduction polarity likely reversed along the Philippine Arc and suturing of the East Java and West Sulawesi continental fragments to the Southwest Borneo Core was complete by this time. The Woyla Terrane was approaching the Sumatran margin by this time. Additional polygons in the lower panels for Australian-Antarctic and Lord Howe-Tasman Sea regions represent areas of deforming continental crust.

Gibbons et al. (2015)



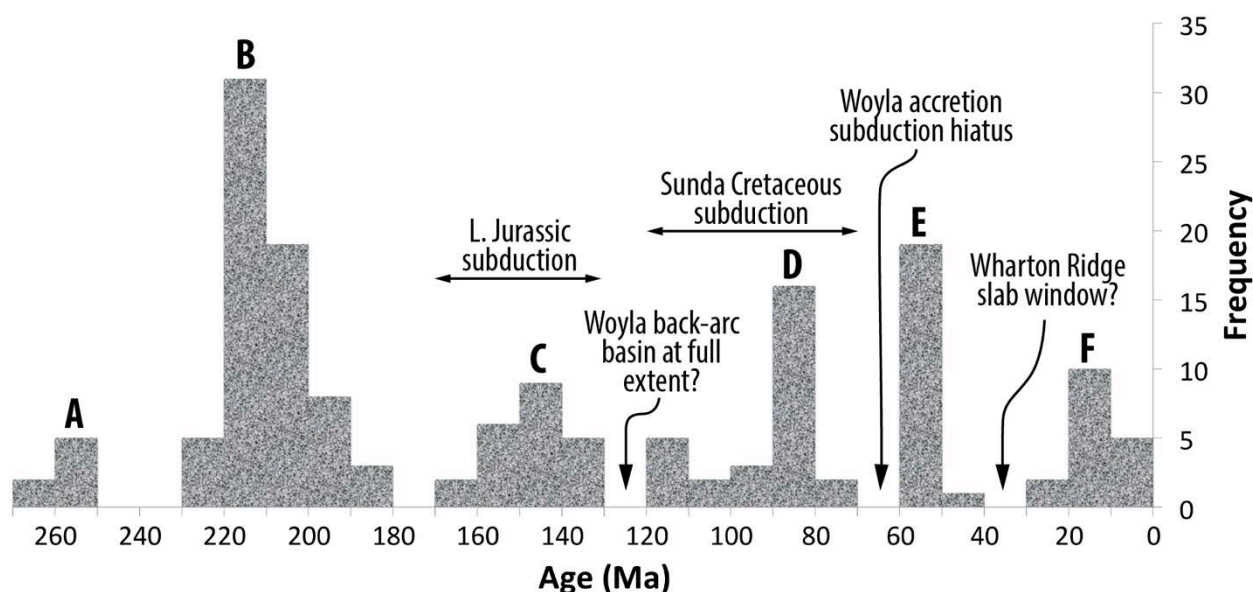
This Study



1107

1108 **Fig. 14.** The Woyla Arc collided with Sundaland (SU) by ~75 Ma, and impeded subduction in this
 1109 segment of the margin for ~10 Myr. The Meso-Tethyan Plate was still likely being subducted along
 1110 the Sunda Trench based on the refined plate reconstructions, with Wharton Ridge arrival near eastern
 1111 Sundaland between ~70 and 60 Ma in both reconstructions. In this study, we reconstruct the
 1112 subduction of the Sepik oceanic gateway from ~71 Ma based on the age of the Emo volcanics
 1113 (Worthing and Crawford, 1996).

1114



1115

1116 **Fig. 15.** A synthesis of arc volcanism on Sumatra, adapted from McCourt et al. (1996), highlights a
 1117 number of short-lived magmatic hiatuses likely related to back-arc basin rifting and/or collisional
 1118 processes that impeded subduction along the Sumatran continental margin.

1119

1120 The post-Cretaceous history of the Sumatran margin is less controversial, with magmatism
 1121 related to the subduction of the Neo-Tethys and Indian oceans (Mccourt et al., 1996), and widespread
 1122 basin rifting and flooding occurring since Paleocene times on Sundaland (Doust and Sumner, 2007).
 1123 One important geodynamic consideration for the Sumatra margin is the interaction of the (extinct)
 1124 Wharton Ridge with the Java-Sunda trench, with the model of Whittaker et al. (2007) suggesting a
 1125 long-lived slab window sweeping westward from eastern Sundaland (near Java) from ~75 Ma to the
 1126 present. Such a scenario implies a time-dependent along-trench thermal anomaly affecting the
 1127 Sundaland continent, and more importantly, the subduction of young oceanic crust (and hence thinner
 1128 oceanic lithosphere) has important implications on the long-wavelength mantle-driven topography
 1129 on the overriding plate (e.g., Flament et al., 2015, for Patagonian uplift associated with the Chile
 1130 Triple Junction; Guillaume et al., 2009). The combination of a subduction hiatus in the Late
 1131 Cretaceous, as well as the subduction of very young oceanic crust in the Eocene along the Java-Sunda
 1132 trench would likely result in widespread regional dynamic uplift that has been proposed by Clements

1133 et al. (2011) to account for a widespread Late Cretaceous to Paleocene regional unconformity across
1134 Sundaland, as explored in Zahirovic et al. (In Press).

1135

1136 **3.4 Accretionary history of the Java and Borneo margin segment**

1137

1138 A key region recording the evolution of Southeast Asia in the context of Eurasian, Tethyan
1139 and (proto-) Pacific convergence is the Sundaland continental promontory. The core of Sundaland is
1140 composed of north-eastern Sumatra, West Java and the Southwest Borneo block (Hall, 2012;
1141 Metcalfe, 1988; Metcalfe, 2011; Zahirovic et al., 2014). The promontory is largely Phanerozoic
1142 continental crust (Hall, 2011), with accreted intra-oceanic and allochthonous continental fragments –
1143 some, like East Java, carrying Archean zircon signatures (Smyth et al., 2007). The continental
1144 fragments making up Sundaland have largely Tethyan-Gondwanan affinities based on
1145 paleontological, stratigraphic and paleo-magnetic constraints, as reviewed in Metcalfe (2006).

1146

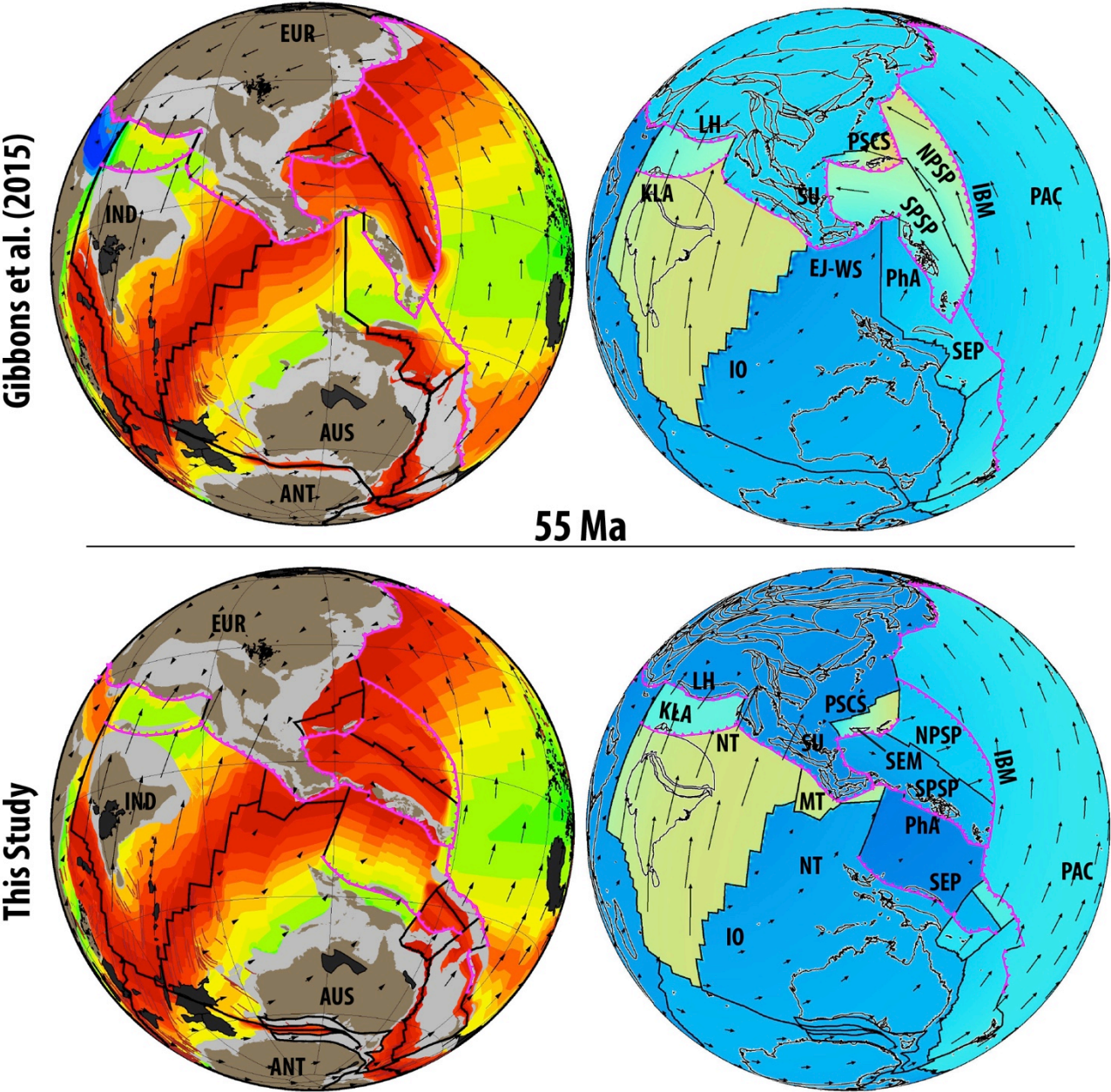
1147 **3.4.1 Subduction and accretion history of southern Sundaland**

1148

1149 The onset of Late Jurassic subduction in the eastern Tethys is best represented by the ~180-
1150 165 Ma schists found within the Meratus Complex on the eastern periphery of the Southwest Borneo
1151 core, as well as the presence of Bajocian (~170 Ma) and younger radiolarians embedded in the
1152 Meratus Suture Zone (Wakita et al., 1998). Zircons shed into the Ciemas and Bayah Formations on
1153 West Java, have ages of 160 Ma and younger (Clements and Hall, 2007), and likely represent the
1154 onset of subduction along this margin. The Late Jurassic-Early Cretaceous age of subduction onset
1155 on this segment is consistent with the establishment of a major subduction system along southern
1156 Eurasia, spanning at least from western Lhasa to the easternmost Tethyan margin on eastern
1157 Sundaland (see previous sections for full chronology). A continuous record of very-high-pressure
1158 (VHP) metamorphic rocks (Fig. 12), including greenschists, blueschists, granulites, eclogites and

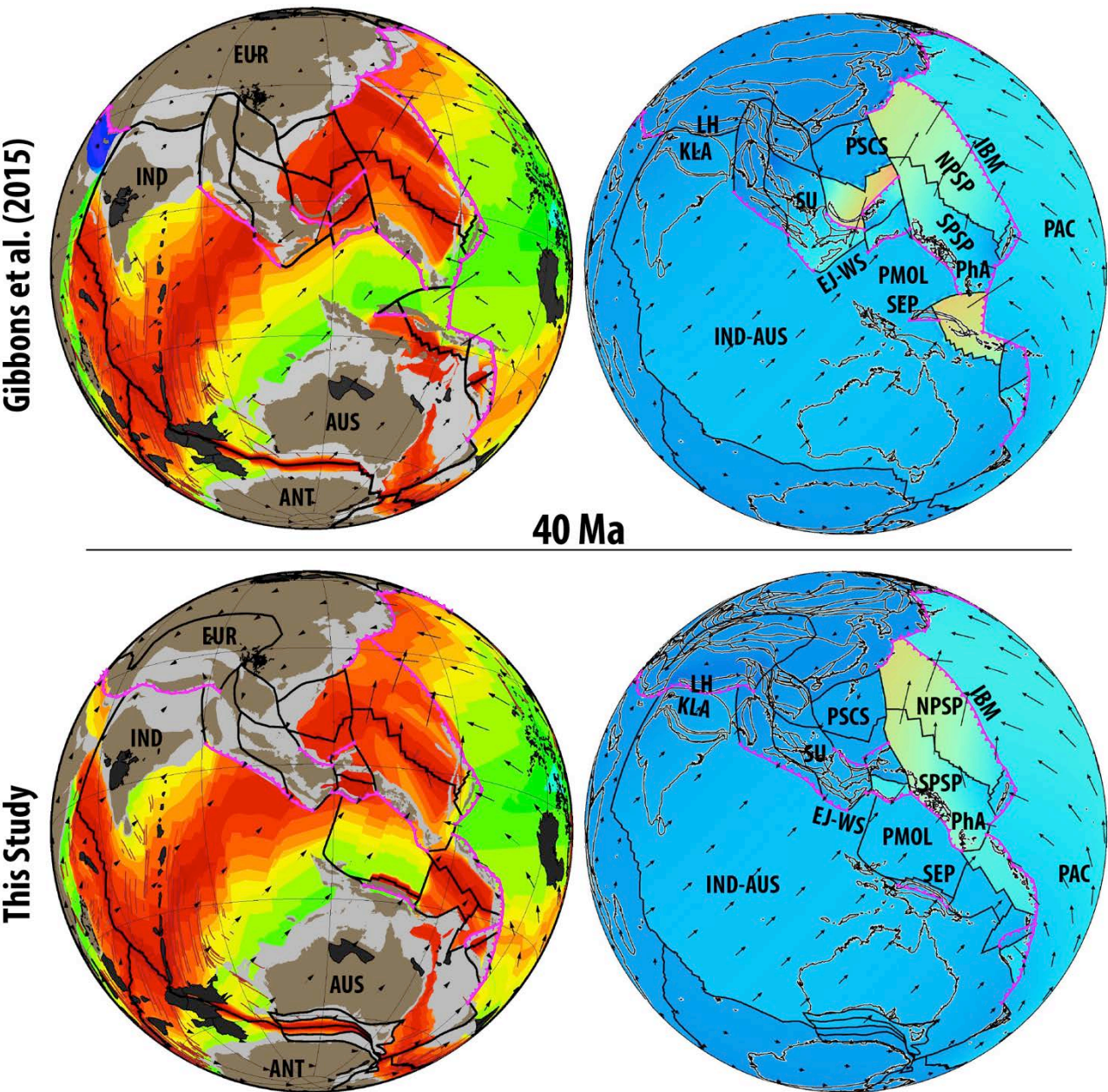
1159 jadeite-bearing metamorphics from ~140 Ma in the Luk-Ulo and Meratus region of Sundaland
1160 (Parkinson et al., 1998) suggests a well-established subduction zone in the Early Cretaceous. The
1161 VHP metamorphic peak at ~115 Ma has previously been interpreted as an arc-continent collision of
1162 Gondwana-derived continental fragments (including East Java, West Sulawesi, Mangkalihat, and
1163 eastern Borneo) with the eastward continuation of the Woyla Arc (Zahirovic et al., 2014). However,
1164 in this study we prefer an interpretation of Woyla back-arc basin subduction initiation at this time to
1165 account for the UHP/VHP metamorphism, as discussed in earlier sections.

1166 A significant spike in the zircon age spectra at ~100 Ma (Clements and Hall, 2007) may
1167 indicate the arrival of the East Java-West Sulawesi in the vicinity of Sundaland. The obduction of the
1168 Meratus Ophiolite in the Cenomanian/Turonian between ~100 and 93 Ma (Pubellier et al., 2004;
1169 Yuwono et al., 1988) is consistent with the Cenomanian radiolarians found in the Meratus Complex
1170 (Wakita et al., 1998). The final closure of the Barito Sea back-arc basin along southern Sundaland
1171 occurred by ~80 Ma based on the lack of volcanic-derived zircons in fore-arc sandstones (Clements
1172 and Hall, 2011; Wakita, 2000). A Late Cretaceous to Paleocene (~72 to 65 Ma) unconformity on
1173 southwest Sulawesi (Milsom, 2000) may indicate collisional (uplift/denudation) processes, a
1174 subduction hiatus, or a combination of both. A resumption of subduction likely occurred in the
1175 Paleocene (Yuwono et al., 1988), with ~65-58 Ma (K-Ar) subduction related rocks (Guntoro, 1999),
1176 a 63 Ma tuff reported on South Sulawesi (van Leeuwen, 1981), and continuous calc-alkaline and
1177 tholeiitic volcanism occurring between 51 and 17 Ma on the western and northern arm of Sulawesi
1178 (Elburg et al., 2003). Ongoing subduction and major deformation (Figs. 16-17), largely due to the
1179 arrival of the Australian continental margin, namely the Sula Spur (Figs. 18-19), started with the
1180 obduction of the East Sulawesi Ophiolite at ~20 Ma (Oligocene to Miocene) in a continent-continent
1181 collision setting (Bergman et al., 1996). The subsequent compressional deformation, and widespread
1182 oroclinal bending of Sundaland are discussed at length in Hutchison (2010) and Zahirovic et al.
1183 (2014), and are summarised in the following sections.



1185

1186 **Fig. 16.** The 55 Ma reconstruction marks the initial stages of contact between Greater India and the
1187 Kohistan-Ladakh Arc to close the Indus Suture Zone, leading to major changes in spreading rate and
1188 direction on the India-Antarctica ridge system. The rollback of the Izanagi slab opens the Proto South
1189 China Sea (PSCS) from ~60 Ma in a Tyrrhenian-style back-arc system. Subduction is initiated at ~55
1190 Ma along the Izu-Bonin-Mariana Arc (IBM) to consume Pacific (PAC) oceanic crust. IO – Indian
1191 Ocean, NPSP – North Philippine Sea Plate, SPSP – South Philippine Sea Plate, SEM – Semitau
1192 Block.

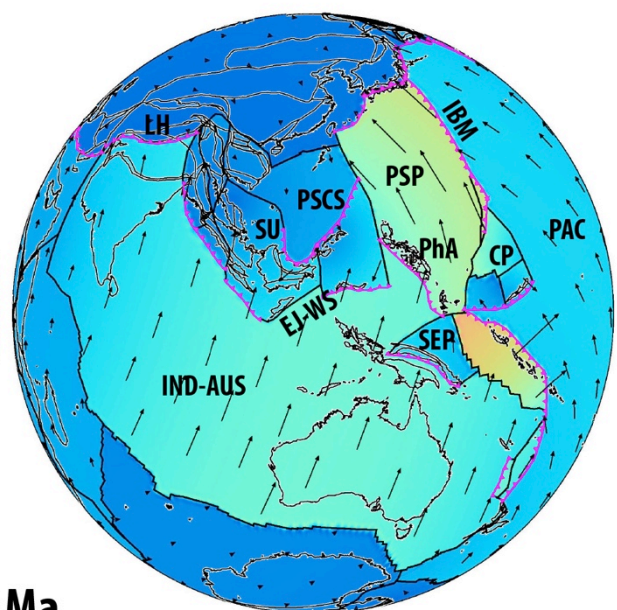
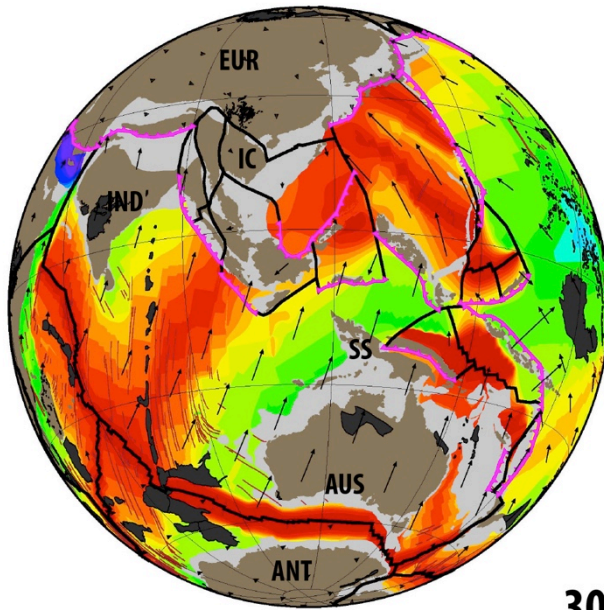


1194

1195 **Fig. 17.** Continent-continent collision between India and Eurasia likely initiated by ~47 Ma, leading
1196 to final closure of the Yarlung-Tansgpo and Shyok suture zones (see Fig. 1). The rollback of the
1197 Izanagi slab opens the Proto South China Sea and transfers the Semitau and Mindoro continental
1198 fragments from the South China margin onto northern Borneo, leading to a mid Eocene collision. The
1199 Sepik oceanic gateway is almost consumed along a north-dipping subduction zone, north of which
1200 the Proto Molucca Plate (PMOL) is consumed contemporaneously along the Philippine Arc.

1201

Gibbons et al. (2015)



30 Ma

This Study

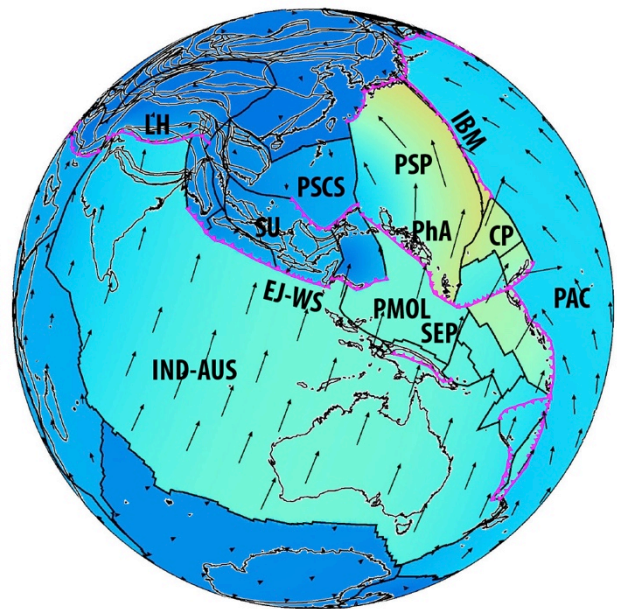
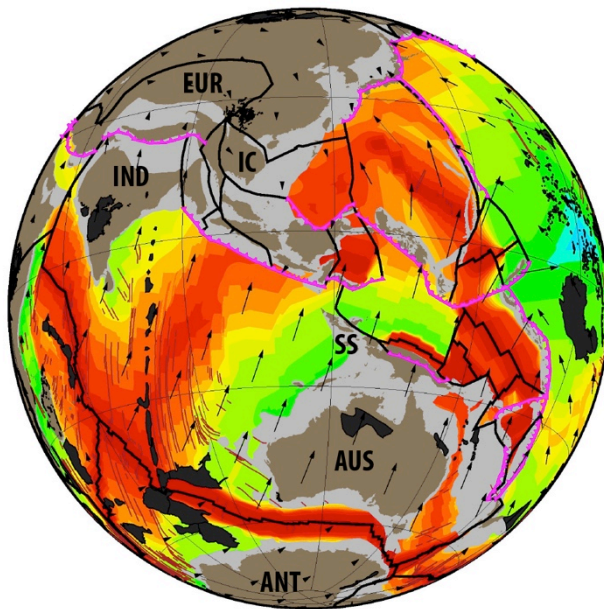
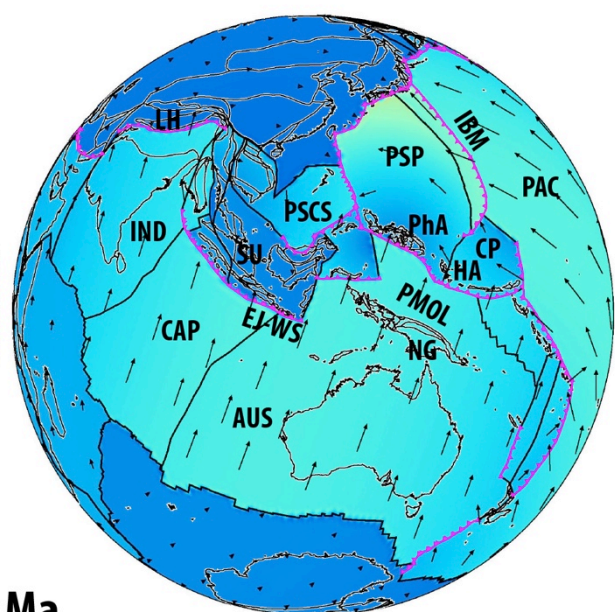
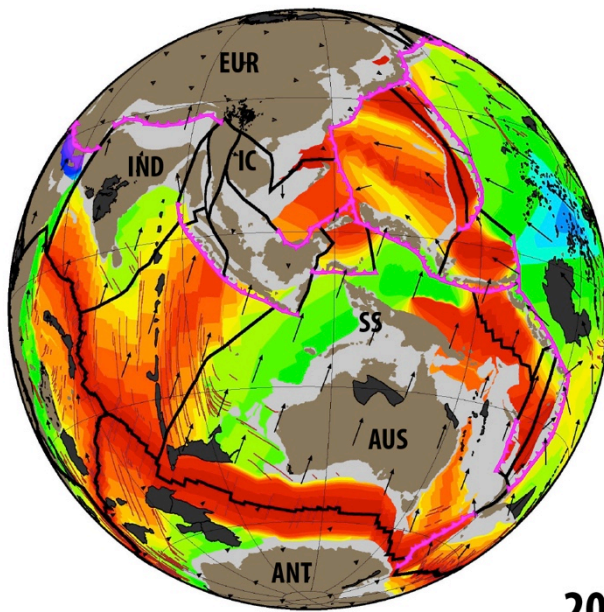


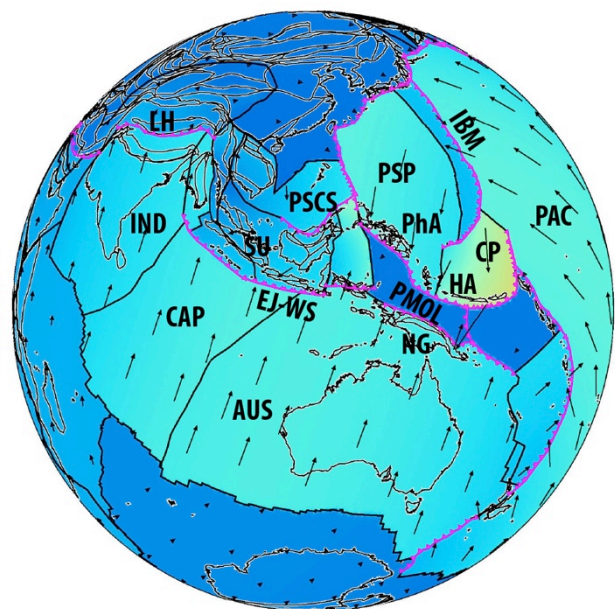
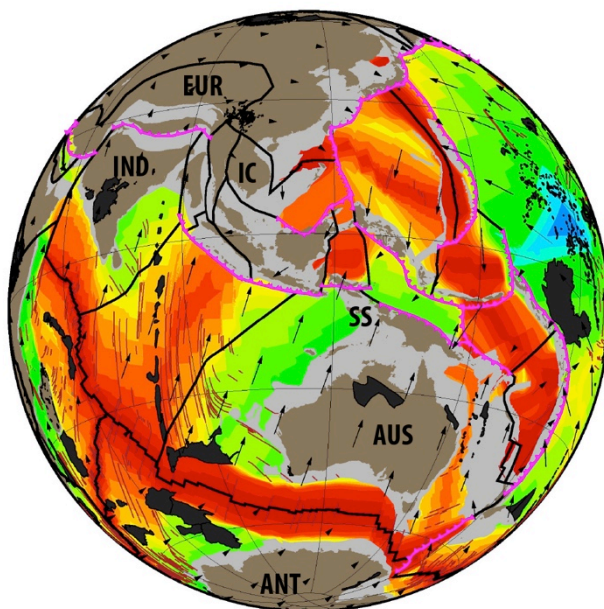
Fig. 18. India's continued, although slowed, northward advance results in the clockwise rotation and lateral extrusion of Indochina (IC), leading to the first stages of oroclinal bending in western Sundaland. The Sepik Terrane docks with the New Guinea margin, and the Sula Spur (SS) continental promontory on the northern Australian margin approaches Sundaland. CP – Caroline Plate, PSP – Philippine Sea Plate.

Gibbons et al. (2015)



20 Ma

This Study



1209

1210 **Fig. 19.** The extrusion of Indochina due to India's northward motion, together with the collision
 1211 between Sula Spur and West Sulawesi results in the oroclinal bending of Sundaland, resulting in
 1212 major counterclockwise rotation of Borneo relative to Sumatra and the Malay Peninsula. South-
 1213 dipping subduction initiates by ~20 Ma to account for the Maramuni Arc volcanics on New Guinea,
 1214 with coeval north-dipping subduction of the Proto Molucca Plate (PMOL) accommodating southward
 1215 motion of the Caroline Plate (CP) and the Halmahera Arc (HA).

1216

1217

1218 3.4.2 *Northern Sundaland collisions*

1219

1220 The geological record on the Sundaland continental promontory captures the geodynamic
1221 interaction between the Tethyan and proto-Pacific oceanic domains, and holds clues as to how the
1222 present-day complexity of plate boundaries developed. Most notably, an ongoing topic of interest
1223 relates to how the east Asian margin transitioned from purely Andean-style subduction (Fig. 20) in
1224 the Late Cretaceous (Shi and Li, 2012), to one that is presently dominated by a labyrinthine network
1225 of intra-oceanic active margins connected by splayed transforms, ridge segments and diffuse plate
1226 boundaries (Bird, 2003). Although much of the proto-Pacific plates have been recycled into the
1227 mantle, the preserved flanks of the seafloor spreading history have been used to restore the lost plates,
1228 assuming seafloor spreading symmetry (Seton et al., 2012). However, the location and evolution of
1229 subduction zones is difficult to constrain, with the only clues coming from paleomagnetic constraints,
1230 arc volcanics and present-day mantle structure (Hall and Spakman, 2002; Miller et al., 2006; Queano
1231 et al., 2007; Zhao et al., 2007).

1232 Although a key component of the intra-oceanic system is the Philippine Sea Plate, which is
1233 discussed in Section 3.5.1, the transition from Andean-style to intra-oceanic subduction north of
1234 Sundaland is most likely controlled by back-arc basin opening processes in the Late Cretaceous
1235 (Morley, 2012a). In the model proposed in Zahirovic et al. (2014), and adopted here, the emplacement
1236 of the Fukien-Reinan massif (Fig. 20) from Andean-style subduction ceases in the Late Cretaceous
1237 (Jahn et al., 1976), and was replaced with extension and back-arc basin opening (Li, 2000) due to
1238 rollback of the Izanagi slab (Figs. 13-14, 16). Such a scenario is consistent with the onset of Late
1239 Cretaceous tectonic subsidence in East Asian basins (Yang et al., 2004), as well as the crustal and
1240 biogeographic affinity between continental fragments wedged in northern Borneo and the Philippine
1241 Archipelago, namely the Semitau and Mindoro blocks, and their likely origin on the South China
1242 continental margin (Fig. 20) in the Late Cretaceous (Zahirovic et al., 2014). The rollback induced
1243 extension in the overriding plate (Schellart and Lister, 2005) likely progressed to back-arc basin

1244 opening, following the analogue of the Tyrrhenian back-arc system in the Mediterranean that
 1245 detached and carried continental blocks to eventually collide as allochthons with a distant margin
 1246 (Doglioni, 1991; Jolivet et al., 1999; Rehault et al., 1987). In the case of the Proto South China Sea,
 1247 the Semitau and Mindoro fragments were likely detached from the East Asian margin by ~65 Ma,
 1248 based on the onset of tectonic subsidence (Yang et al., 2004) and the ~59 Ma emplacement of supra-
 1249 subduction zone ophiolites on Mindoro (Yumul et al., 2009). The continued rollback transferred
 1250 Semitau and Mindoro southward, resulting in an Eocene collision with the northern Borneo margin
 1251 to produce the Sarawak Orogeny (Cullen, 2010; Fyhn et al., 2010; Hutchison, 1996; Hutchison,
 1252 2004), after which southward subduction consumed the Proto South China Sea to emplace widespread
 1253 volcanism on northern Borneo (Soeria-Atmadja et al., 1999).

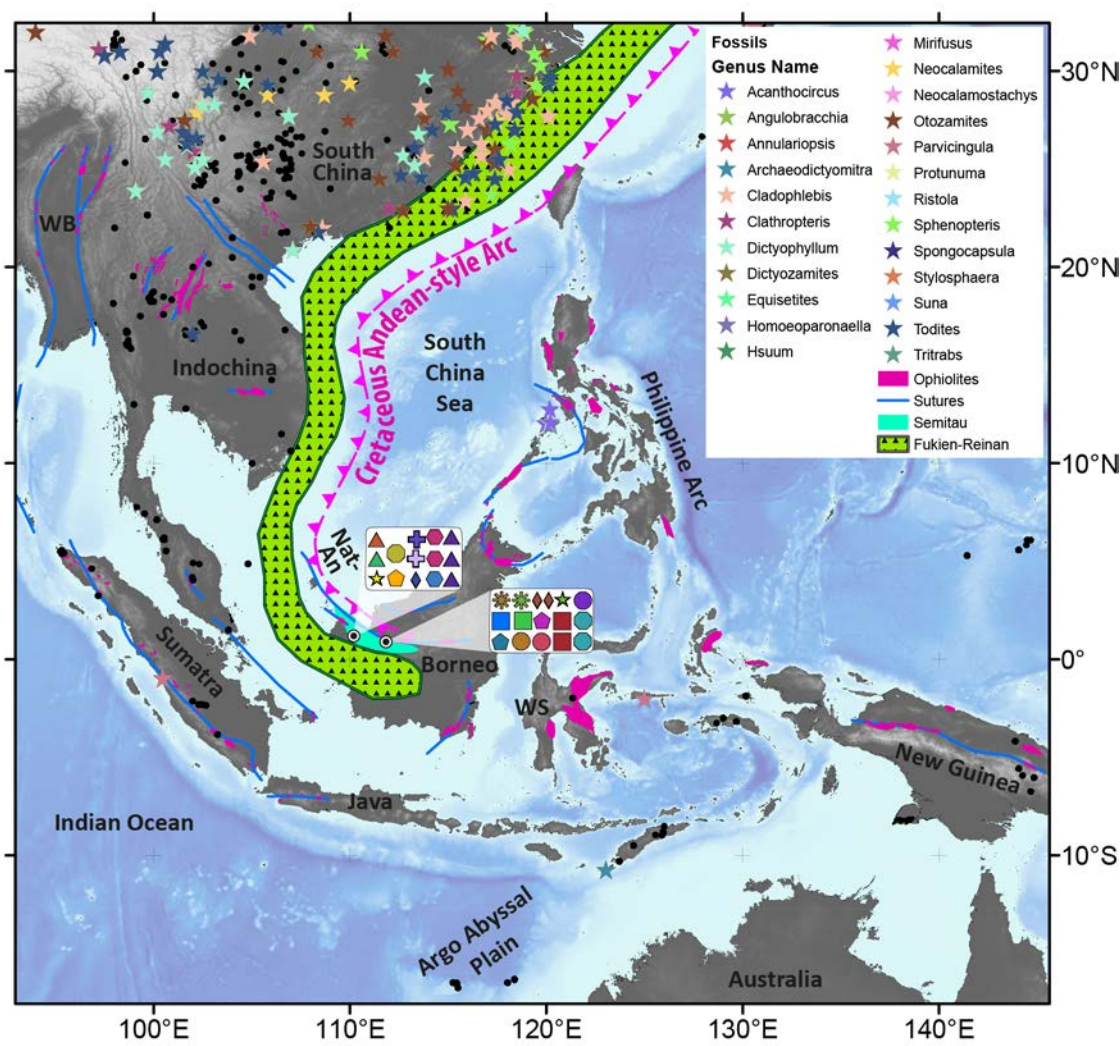


Fig. 20. Triassic and Jurassic fossil occurrences from the global Paleobiology Database (now Fossilworks) from Semitau (northern Borneo), represented by coloured symbols. The same fossils are also found elsewhere in Asia, with the strongest biogeographic affinity with mainland South China. The curved Fukien-Reinan massif (green hatched region) represents the Cretaceous Andean-style east Asian margin, which was replaced with an intra-oceanic setting in the Late Cretaceous. The curvature of the Andean-style magmatic arc also supports strong oroclinal bending of Sundaland in post-Cretaceous times. Nat-An – Natuna–Anambas Arc, WB – West Burma, WS – West Sulawesi. Figure adapted from Zahirovic et al. (2014).

The slab pull from south-dipping Proto South China Sea subduction along northern Borneo, along with the clockwise (CW) extrusion of Indochina resulting from the India-Eurasia collision (Fuller et al., 1991; Tapponnier et al., 1982), may have led to significant adjustments in the plate boundary forces acting on Sundaland. The ~32 Ma onset of seafloor spreading along the South China margin (Fig. 18) detached the Dangerous Grounds-Reed Bank continental blocks to open the South China Sea (Lee and Lawver, 1994; Lee and Lawver, 1995), with collision of the continental fragments with northern Borneo and South Palawan at ~15 Ma resulting in ophiolite obduction and the Sabah Orogeny (Hutchison, 2004; Hutchison et al., 2000), as well as choking the north Borneo subduction system and shutting down seafloor spreading in the South China Sea (Briais et al., 1993). This southward collision was wedged between the India-Eurasia collision from ~47 Ma (see Section 3.2) and the collision of the Australian northern margin with eastern Sundaland from ~25 Ma (Bergman et al., 1996; Hall, 2002). This arrangement of plate boundaries, and the driving forces, presumably had significant consequences for the rotational history of Borneo and the deformation of Sundaland.

1280 3.4.3 *Sundaland oroclinal bending*

1281

1282 The large counterclockwise (CCW) rotation of Borneo, relative to stable Sundaland, in the
1283 Cenozoic has drawn a range of interpretations and led to a number of competing models (see
1284 discussion in Zahirovic et al. (2014)). Each model of Borneo rotation has consequences for the
1285 deformation history on Sundaland (in particular, the basins of the Sunda Shelf and Java Sea), as well
1286 as understanding the mechanism that led to the 90° CCW rotation of Borneo relative to Sundaland in
1287 the Mesozoic, including up to 50° CCW rotation since 25 Ma (Fuller et al., 1999). In the absence of
1288 large transform faults, such as the Red River Fault bounding northern Indochina, within the Java Sea
1289 or the Sunda Shelf, Hutchison (2010) proposed a model of oroclinal bending for the rotation of
1290 Borneo as a mechanism to explain the deformation of the Sundaland continental promontory.

1291 Hutchison (2010) synthesised the paleomagnetic evidence, as well as observations of curved
1292 lineaments observed in the gravity anomalies of Sundaland and the curvature of the Natuna and
1293 Anambas Cretaceous paleo-arc (Fig. 20) to infer that wholesale bending of Sundaland accommodated
1294 the CW rotation of Indochina and the CCW rotation of Borneo (Fuller et al., 1999; Fuller et al., 1991).
1295 The curved lineaments (Fig. 21) are most likely to be successive generations of ancient volcanic arcs
1296 (Hutchison, 2010), with the most obvious example being the curved arc belonging to the Middle to
1297 Late Triassic tin belt granites on Bangka and Billiton islands, as well as the previously-mentioned
1298 Natuna-Anambas Cretaceous Arc. Zahirovic et al. (2014) expanded on the work of Hutchison (2010)
1299 and used filtered Bouguer anomalies (Balmino et al., 2012) to extract geometrical constraints on the
1300 oroclinal bending (Fig. 21), and constructed a kinematic oroclinal bending model that accounts up to
1301 ~78° CCW rotation of Borneo since ~50 Ma.

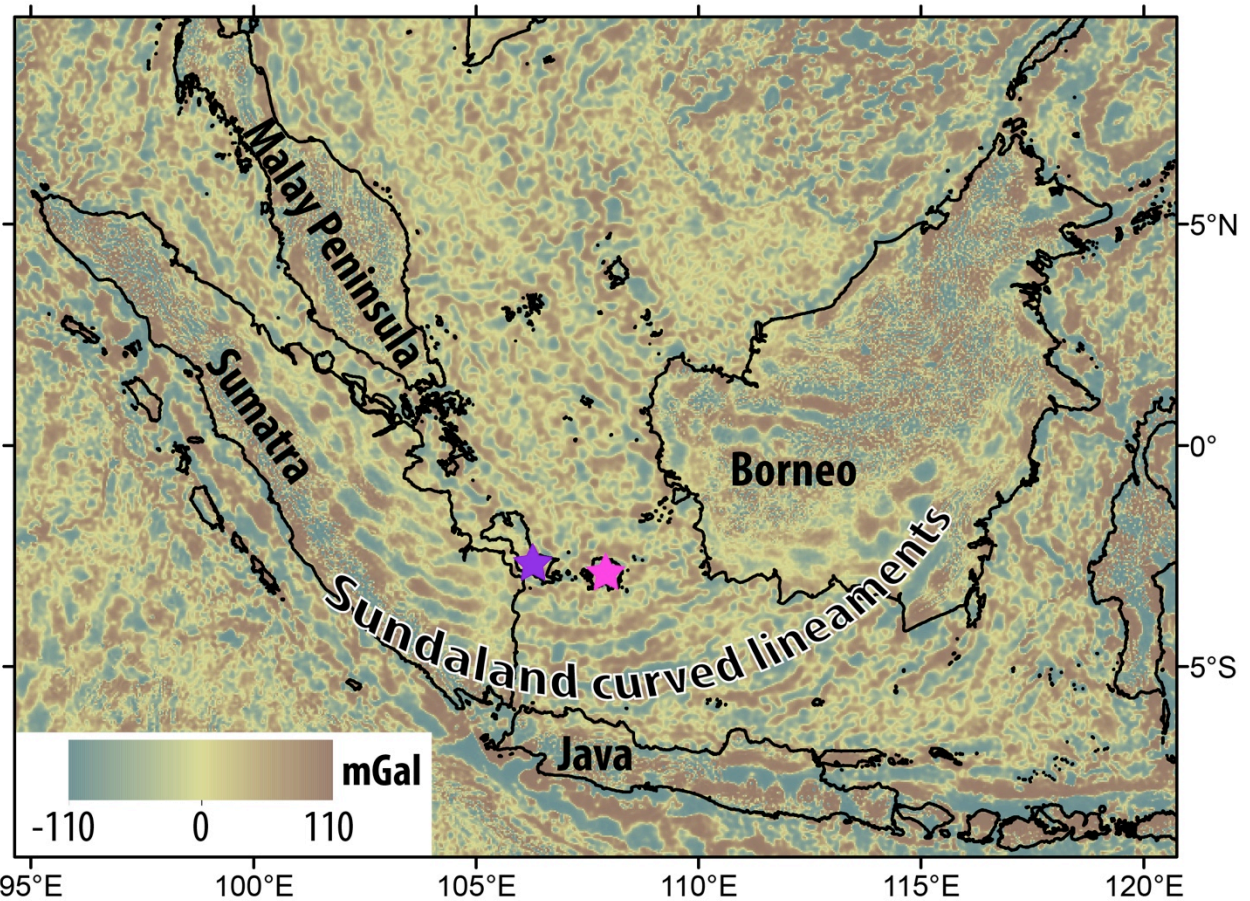


Fig. 21. The band-pass-filtered (150 to 10 km) Bouguer gravity anomalies from the 1 min World Gravity Map (Balmino et al., 2012) highlights the large-scale structures and the curved lineaments on Sundaland, resulting from oroclinal bending as proposed by Hutchison (2010). Bangka Island – purple, Belitung (Billiton) Island – pink.

One important distinction between the oroclinal bending of Sundaland and classical models of oroclinal bending largely relates to the tightness of the oroclinal folds and the deformation experienced by the continental crust (Carey, 1955; Eldredge et al., 1985). In the case of Sundaland, the hinge of the orocline is likely to be in the Sunda Shelf west of Borneo, with a wide region of bending rather than tight oroclinal bends that are typically reported for Kazakhstan (Abrajevitch et al., 2008) and the Mediterranean (Rosenbaum, 2014). Although the boundaries of the Sundaland continental promontory experienced compression during oroclinal bending, the Java Sea and Sunda Shelf were dominated by extension from Eocene times to the mid Miocene, after which a major phase

1316 of basin inversion dominated the tectonic regime of Sundaland to the present (Doust and Sumner,
1317 2007; Pubellier and Morley, 2014).

1318

1319 **3.5 New Guinea and the Philippines**

1320

1321 **3.5.1 *Origin and evolution of the Philippine Archipelago***

1322

1323 Tectonic reconstructions of the transfer of Gondwana-derived terranes following the breakup
1324 of Pangea are limited by the lack of preserved seafloor, but are typically supplemented with high-
1325 quality and well-constrained onshore geological data that helps reconstruct the synthetic seafloor
1326 spreading histories. However, the region east of Sundaland, which includes the Philippines and New
1327 Guinea are considerably more complicated, as they straddle the Tethyan and (proto-) Pacific tectonic
1328 domains, resulting in a complex interaction dominated by back-arc basin formation processes and
1329 multiple phases of collision, obduction and subduction that consumed them.

1330 One early synthesis of the tectonic evolution of the post-Eocene West Pacific was carried out
1331 by Jolivet et al. (1989), who modelled the plate motions in six stages (56, 43, 32, 20, 12 and 3 Ma),
1332 and importantly, provided finite rotation poles that define their time-dependent plate circuit. In the
1333 reconstructions of Jolivet et al. (1989), and subsequent models (Hall et al., 1995a; Lee and Lawver,
1334 1995; Pubellier et al., 2003; Queano et al., 2007; Zahirovic et al., 2014), the Philippine Sea Plate
1335 develops in near-equatorial southern latitudes during the Eocene (Hall et al., 1995a; Hall et al., 1995b;
1336 Richter and Ali, 2015), and is isolated from the surrounding plate circuits by a network of plate
1337 boundaries (including subduction zones and transforms) for much of the time. This tectonic isolation,
1338 and lack of preserved seafloor spreading linking the Philippine Sea Plate directly to the Pacific,
1339 Eurasian or Australian plates leads to difficulties in reconstructing the absolute and relative plate
1340 motions of this region that links the Pacific with the Indian oceans. However, the seafloor spreading
1341 history within the Philippine Sea Plate itself has been well-documented, including the opening of the

1342 West Philippine Basin between ~55 and 33 Ma (see Hilde and Chao-Shing (1984), Deschamps and
1343 Lallemant (2002), and references therein) and the back-arc opening of the Shikoku and Parece Vela
1344 back-arc basins between ~29 and 15 Ma from Philippine Sea Plate rotation (Sdrolias et al., 2004) and
1345 Izu-Bonin-Mariana trench rollback (Kobayashi, 2004).

1346 Although the seafloor spreading history of the Philippine Sea Plate is confined to post-Eocene
1347 times, the Philippine Arc has recorded a much longer history of subduction, with the earliest supra-
1348 subduction zone (SSZ) rocks from the Late Jurassic. The SSZ ophiolites from the Philippine Arc have
1349 ages of 156.3 ± 2.0 Ma and 150.9 ± 3.3 Ma (Lagonoy Ophiolite), and 142 ± 4 Ma (Gag Island,
1350 Halmahera) from the synthesis of Encarnación (2004). They are discussed at length in Zahirovic et
1351 al. (2014). Recent work by Deng et al. (2015) reported mid-Cretaceous, 126 ± 3 Ma and 119 ± 2 Ma
1352 (U-Pb), SSZ volcanics from Cebu Island. These ages are consistent with the minimum 99.9 ± 7.0 Ma
1353 (Ar-Ar) age of the Calaguas Ophiolite (Geary et al., 1988; Geary and Kay, 1989), and the 100 ± 4 Ma
1354 arc rocks reported from Obi Island on Halmahera (Hall et al., 1995b), suggesting continuous Early
1355 Cretaceous subduction along the Philippine Arc. To reconcile the likely southern hemisphere origin
1356 of the Philippine Arc and the Late Jurassic-Early Cretaceous temporal similarity with north
1357 Gondwana rifting events, Zahirovic et al. (2014) proposed a SSZ origin in the vicinity of New Guinea,
1358 recently independently suggested by Deng et al. (2015). The multiple generations of ophiolites may
1359 suggest a tectonic scenario similar to the current multi-generation opening of back-arcs along the Izu-
1360 Bonin-Mariana system, and may explain the origin of the Daito and Oki-Daito ridges as paleo-arc
1361 features in the north West Philippine Basin.

1362

1363 ***3.5.2 Nature of the New Guinea margin since the Late Jurassic***

1364

1365 To accommodate the northern Gondwana rifting episode in the Late Jurassic, Zahirovic et al.
1366 (2014) placed the East Java-West Sulawesi continental fragments along New Guinea as the simplest
1367 end-member of transferring blocks north towards Sundaland, but acknowledged that an Argo Abyssal

1368 Plain origin (NW Australian shelf) would also be possible due to the lack of preserved seafloor
1369 spreading histories to constrain a pre-drift fit. In this study, we implement the Argo origin end-
1370 member scenario, which is consistent with the zircon age spectra linking East Java to the NW
1371 Australian shelf (Sevastjanova et al., 2015; Smyth et al., 2007). The 158-137 Ma ages of mafic rocks,
1372 some of which are associated with pillow basalts, on West Sulawesi (Polvé et al., 1997) are consistent
1373 with the oldest oceanic crust (155 ± 3.4 Ma) in the Argo Abyssal Plain on the NW Australian Shelf
1374 (Gradstein and Ludden, 1992). By shifting these continental fragments west along northern
1375 Gondwana, the New Guinea margin can accommodate the source of the Philippine Archipelago to
1376 have formed along its margin. The benefit of such a scenario is that it accounts for the origin of
1377 (likely) Jurassic age SSZ ophiolites within the Central Ophiolite Belt in New Guinea (Monnier et al.,
1378 2000). However, the Late Jurassic-Early Cretaceous ($\sim 157 \pm 16$ Ma) and Late Cretaceous (66 ± 1.6
1379 Ma) are unpublished ages from Permana (1998), reported in Pubellier et al. (2003), and require further
1380 corroboration. What is known is that at least part of the New Guinea margin was an active margin in
1381 Early Cretaceous times, as indicated by the Early Cretaceous volcanism and the Kondaku Tuffs (Dow,
1382 1977; Rickwood, 1954), and likely represents the continuation of the long-lived east Gondwana active
1383 margin.

1384 To what extent the Late Jurassic-Early Cretaceous active margin extended west into the
1385 Indonesian portion of New Guinea remains poorly constrained. In the east, the protolith of the Bena
1386 Bena metamorphics is partly Late Triassic (221 Ma) in age, and is intruded by Jurassic granite of 172
1387 Ma in age (Davies, 2012). In the west, the Bird's Head region experienced granitoid emplacement in
1388 the Early Jurassic with one sample yielding an age of 197 ± 3 Ma (K-Ar) (Pieters et al., 1983) and
1389 the 210 ± 25 Ma Mangole Volcanics on Banggai-Sula (Charlton, 2001), with a similar age of $205 \pm$
1390 5 Ma reported further east in the P'nyang-1 exploration well in Papua New Guinea (Valenti, 1993).
1391 These results suggest that the trench along western New Guinea may have undergone rollback by the
1392 Late Jurassic to explain Early Cretaceous volcanics confined only to eastern New Guinea. Such a
1393 scenario is also consistent with the sedimentary history that records syn-rift sedimentation in the

1394 Early-Middle Jurassic, followed by a post-breakup unconformity and the formation of a diachronous
1395 passive margin along much of New Guinea (Pigram and Panggabean, 1984), with the exception of
1396 continued Early Cretaceous arc volcanism in the east.

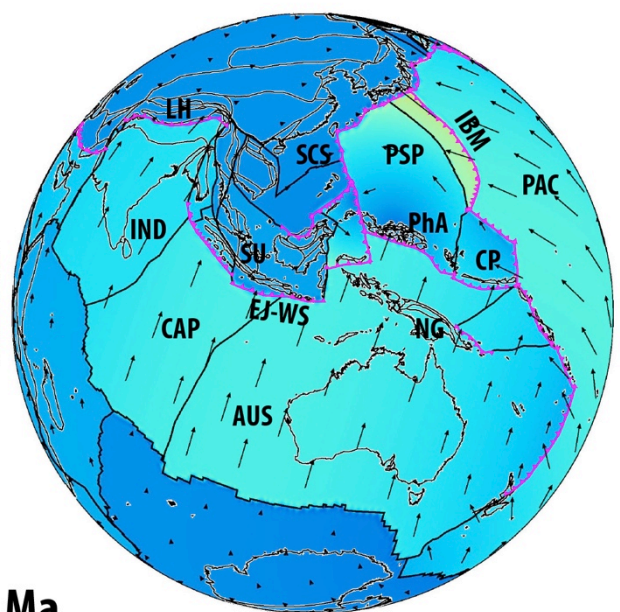
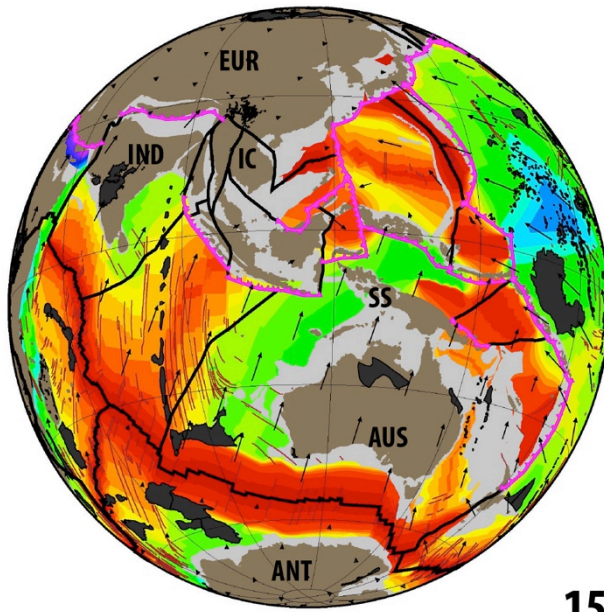
1397 Although the Early-Middle Jurassic rift-drift sequence is well preserved on New Guinea, few
1398 constraints exist to identify which (if any) continental terranes rifted from this margin (Hill and Hall,
1399 2003; Pigram and Symonds, 1991). Apart from the East Java and West Sulawesi blocks (Zahirovic
1400 et al., 2014), parts of the Sepik Terrane may represent a para-allochthon that detached from the margin
1401 in the Jurassic, as invoked in this study, to open a somewhat-narrow oceanic basin and form the Late
1402 Jurassic SSZ ophiolites (Permana, 1998; Pubellier et al., 2003) exposed along the Central Ophiolite
1403 Belt in New Guinea (Fig. 3). Even though the Sepik Terrane is the largest accreted block on the New
1404 Guinea margin, the composite nature of the Sepik crust – with both continental and intra-oceanic arc
1405 fragments (Klootwijk et al., 2003) – leads to an enigmatic tectonic evolution. The New Guinea margin
1406 experienced at least two collisional phases; one in the late Eocene (Hall, 2002) to mid Oligocene
1407 (Crowhurst et al., 1996; Pigram and Symonds, 1991), and another major collision responsible for
1408 compressional deformation in the Mobile Belt during the late Miocene (Hall, 2002; Hill and Hall,
1409 2003; Hill and Raza, 1999). However, the collisional history of the Sepik Terrane remains
1410 controversial in terms of whether the terrane first collided with one or more intra-oceanic arcs and
1411 subsequently welded to New Guinea, or whether the converse is true.

1412 Although the size of the oceanic basin that separated the Sepik Terrane from mainland New
1413 Guinea remains uncertain, the longevity of the oceanic basin can be inferred from subduction-related
1414 metamorphics that are distributed along the Central (Irian) Ophiolite Belt (Fig. 3), and eastward into
1415 the April Ultramafics and the Marum Ophiolite. The ~68 Ma high-temperature metabasites and
1416 ~44 Ma blueschists in the West Papuan Ophiolite (Weyland Overthrust) indicate that subduction of
1417 the Sepik oceanic basin was underway (Davies, 2012), which is consistent with ~45 to 40 Ma
1418 glaucophane (K-Ar) and 28 to 25 Ma (K-Ar) phengite ages (Baldwin et al., 2012) in the April
1419 Ultramafics. The Balantak Ophiolite on the East and Southeast Sulawesi Arm records ages of ~96-

1420 32 Ma (Monnier et al., 1995), with a paleo-latitudinal constraint of $17 \pm 4^\circ\text{S}$ at 80 Ma (Mubroto et
1421 al., 1994) suggesting that these ophiolites formed somewhere between Sundaland and the New
1422 Guinea margin. Such a scenario is consistent with north-dipping subduction of the Sepik oceanic
1423 basin, which may have generated supra-subduction zone ophiolites that were subsequently obducted
1424 onto Sulawesi. The Maastrichtian (~71 to 66 Ma, stratigraphic correlation and dating using
1425 foraminifera) Emo volcanics (Worthing and Crawford, 1996) were likely emplaced in a back-arc
1426 setting from north-dipping subduction along the Sepik Terrane, with final docking likely taking place
1427 by ~30 Ma (Findlay, 2003; Zahirovic et al., 2014), based on the 35 to 31 Ma (Ar-Ar) amphibolite age
1428 of the Emo metamorphics (Worthing and Crawford, 1996) and the cooling histories of exhumed
1429 blocks (Crowhurst et al., 1996).

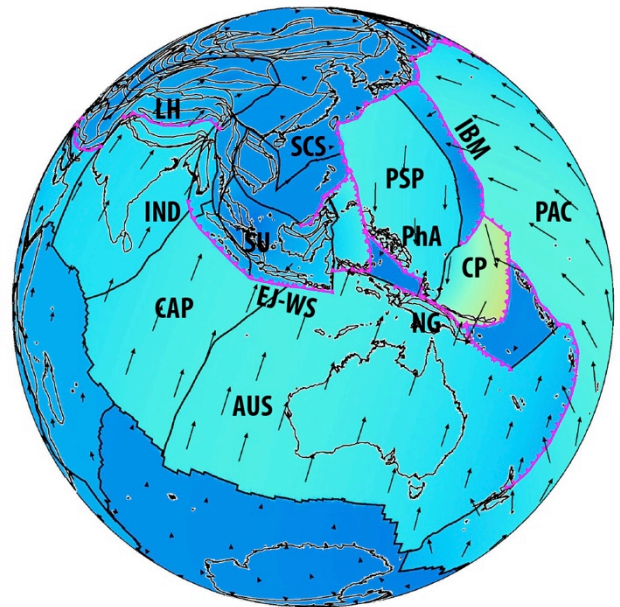
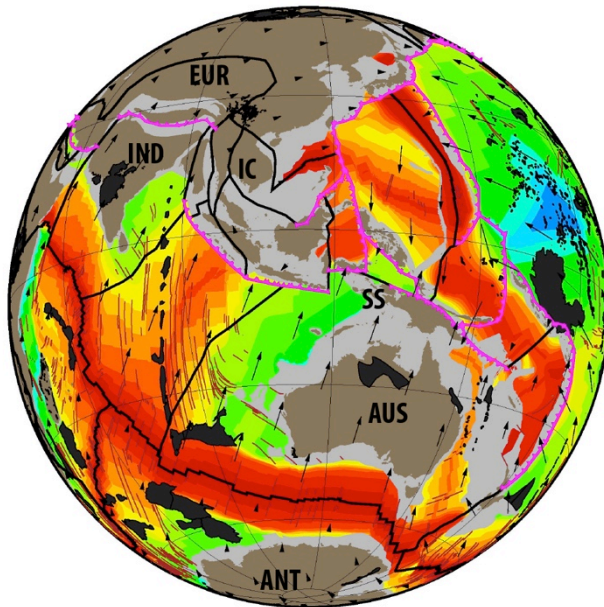
1430 Following the docking of the Sepik composite terrane, south-dipping subduction was likely
1431 established (Figs. 19, 22) to account for the ~18 to 8 Ma Maramuni Arc volcanism (Hill and Hall,
1432 2003; Page, 1976), followed by post-collisional volcanism to at least ~1 Ma (Holm et al., 2014; van
1433 Dongen et al., 2010). The approaching Halmahera Arc, attached to the southern portion of the
1434 Caroline Plate, likely collided with the northern New Guinea margin by ~14 Ma (Figs. 22-23), leading
1435 to a major compressional phase in the Mobile Belt, that has been inferred from apatite fission track
1436 geochronology (Hill and Raza, 1999; Kendrick, 2000). Although the New Guinea margin is a key
1437 component of the Australian, Pacific and Eurasian convergence zone, more work is required to
1438 resolve competing tectonic scenarios for this margin (van Ufford and Cloos, 2005). However,
1439 additional insights can be made from interpretations of mantle structure from seismic tomography, as
1440 well as testing end-member scenarios using coupled plate kinematic and numerical mantle convection
1441 modelling of the New Guinea margin.

Gibbons et al. (2015)



15 Ma

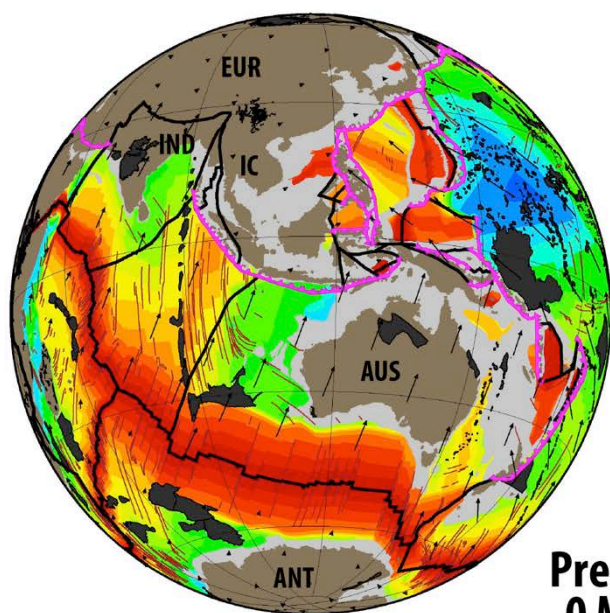
This Study



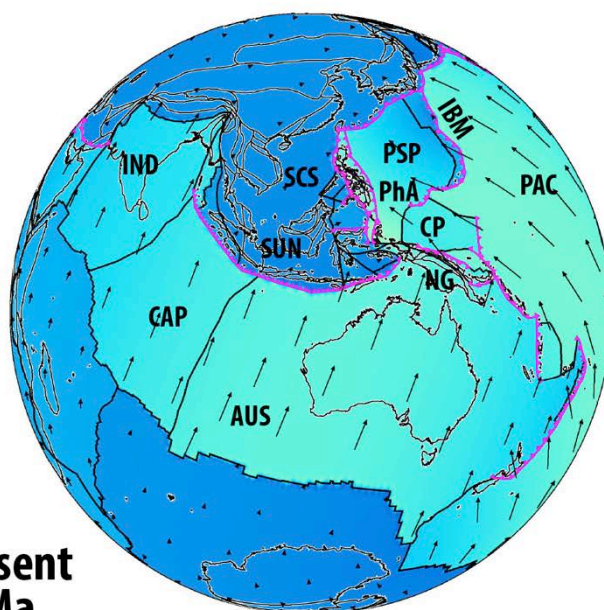
1442

1443 **Fig. 22.** The 15 Ma timestep records the transition to compressional tectonics on Sundaland and New
 1444 Guinea. The arrival of the Dangerous Grounds-Reed Bank continental fragment shuts down Proto
 1445 South China Sea subduction along Borneo, and results in ophiolite obduction in Palawan and
 1446 orogenesis on Borneo. In the refined reconstructions, the Halmahera Arc collides with New Guinea
 1447 at ~15 Ma to result in major compression in the New Guinea Mobile Belt.

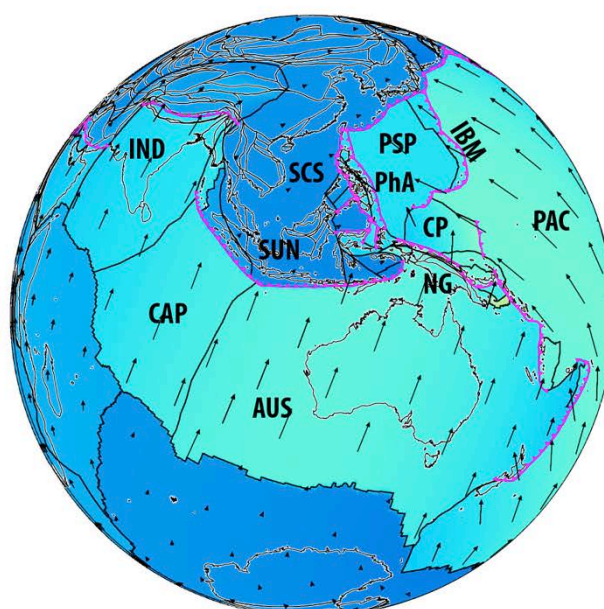
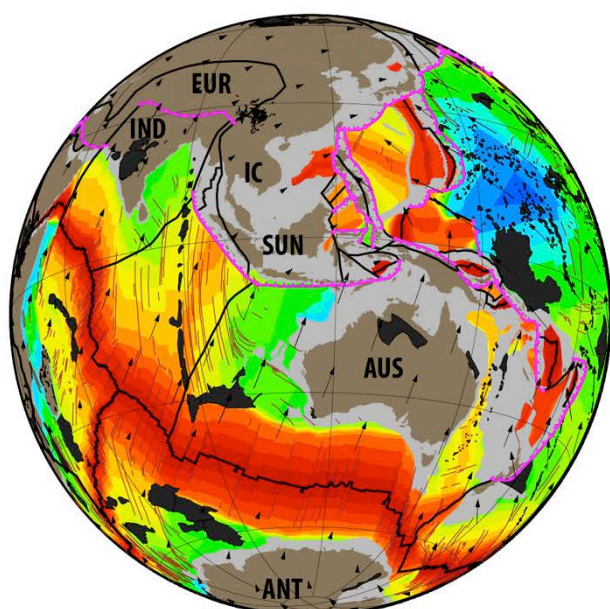
Gibbons et al. (2015)



Present
0 Ma



This Study



1448

1449 **Fig. 23.** The present-day tectonic configuration of Southeast Asia is the result of long-lived Indo-
 1450 Australian, Eurasian and Pacific convergence accommodated by the subduction of Tethyan ocean
 1451 basins and back-arcs. The northward motion of India is significantly slower than in the early Eocene,
 1452 with intra-plate diffuse deformation in the Capricorn (CAP) Plate since ~20 Ma.

1453 4 Insights from age-coded slabs in seismic tomography

1454

1455 In light of the complex tectonic evolution of Southeast Asia and the Tethyan-Pacific oceanic
1456 linkages, we interpret high velocity seismic anomalies from the P-wave model of Li et al. (2008) to
1457 obtain insights into the subduction history (Fig. 24). Although assuming constant and vertical slab
1458 sinking is a simplification, it is arguably a reasonable assumption for the late Cenozoic where large
1459 lateral slab advection would be limited, as indicated by previous estimates of less than ~1-2 cm/yr of
1460 mid-mantle lateral flow in the Tethyan realm (Becker and Faccenna, 2011; Zahirovic et al., 2012).
1461 We compare the plate reconstructions with age-coded depth slices of high velocity seismic anomalies,
1462 applying a sinking rate of 2 cm/yr in the lower mantle, and end-member estimates of 3 and 8 cm/yr
1463 in the upper mantle (see Methods). The proposed lower mantle slab sinking rates for the Tethyan
1464 realm are larger (~2 cm/yr) than estimated global averages (1.2-1.3 cm/yr in Butterworth et al., 2014;
1465 van der Meer et al., 2010), and may reflect the suction exerted by deep slabs in this slab graveyard
1466 area (Conrad and Lithgow - Bertelloni, 2004).

1467 The plate reconstructions in our base model (Zahirovic et al., 2014) were calibrated for the
1468 Philippine Sea Plate and Sundaland using a similar method (assuming sinking rates of 3 and 1.2 cm/yr
1469 in the upper and lower mantle, respectively). However, in the refined reconstructions, we do not
1470 modify the Sundaland oroclinal bending model, but modify the position of the Philippine Sea Plate
1471 since ~30 Ma to ensure collision of the Halmahera Arc with New Guinea at ~15 Ma, to account for
1472 the onset of widespread compression in the New Guinea Mobile Belt (Hill and Hall, 2003).
1473 Consequently, the match between Sundaland subduction zones and age-coded slabs from tomography
1474 is not surprising. Modifications to fit the Philippine Sea Plate to surface geology since ~30 Ma, rather
1475 than seismic tomography, presents a case study to test whether both geological and seismic
1476 tomographic constraints can be accommodated simultaneously.

1477

Upper mantle: 3 cm/yr
Lower mantle: 2 cm/yr

Upper mantle: 8 cm/yr
Lower mantle: 2 cm/yr

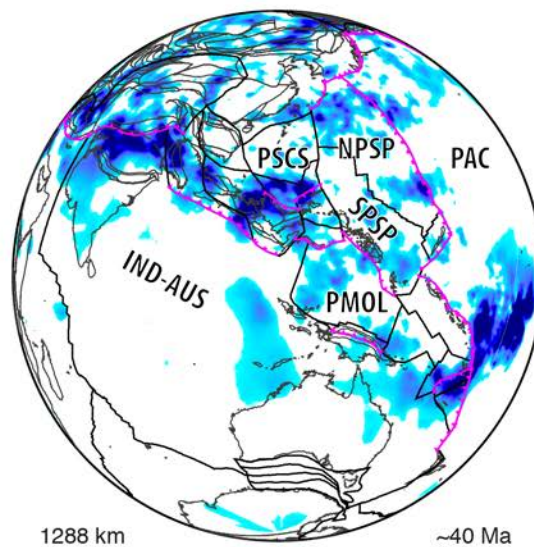
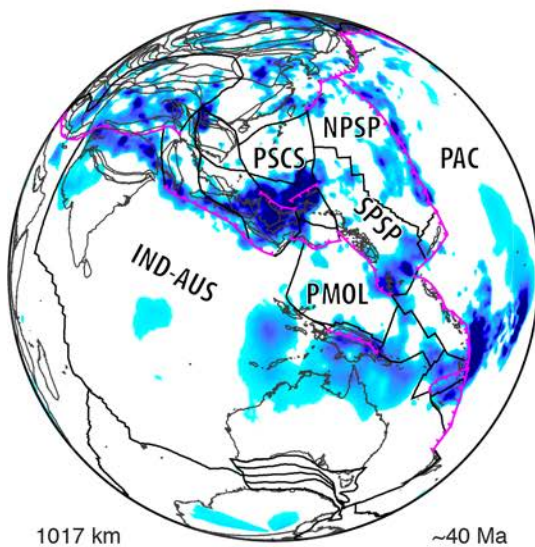
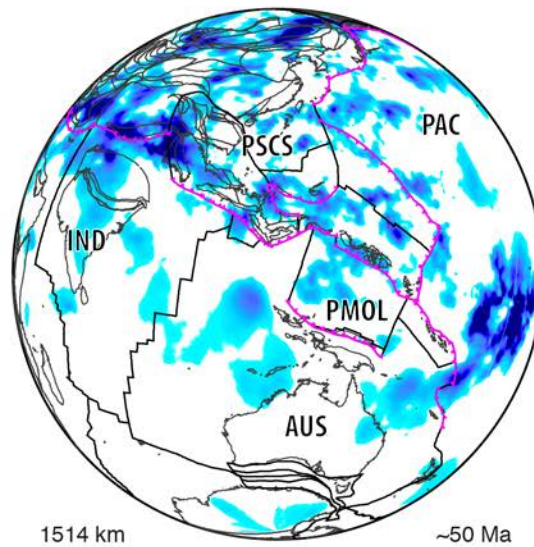
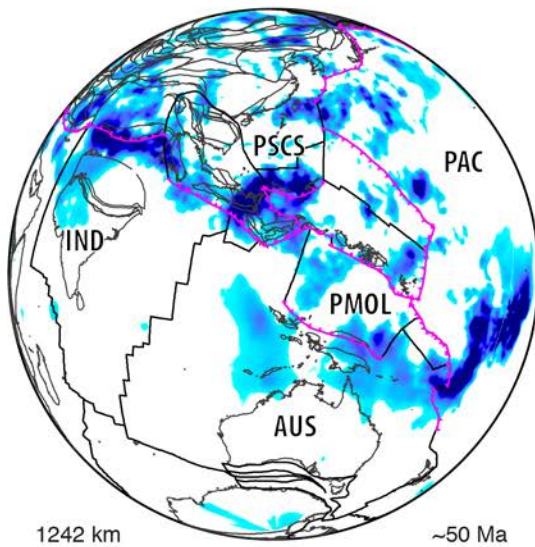
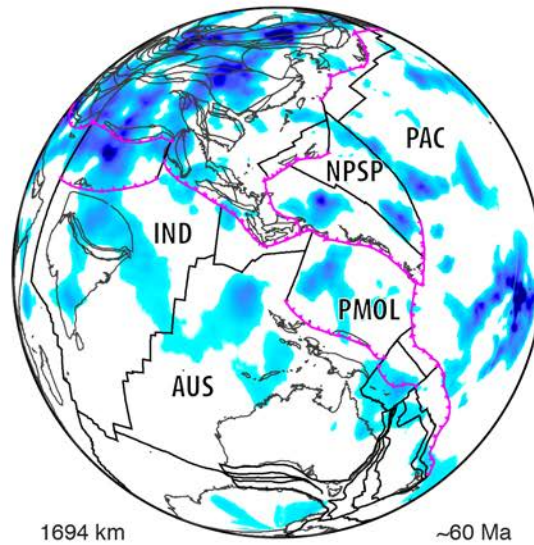
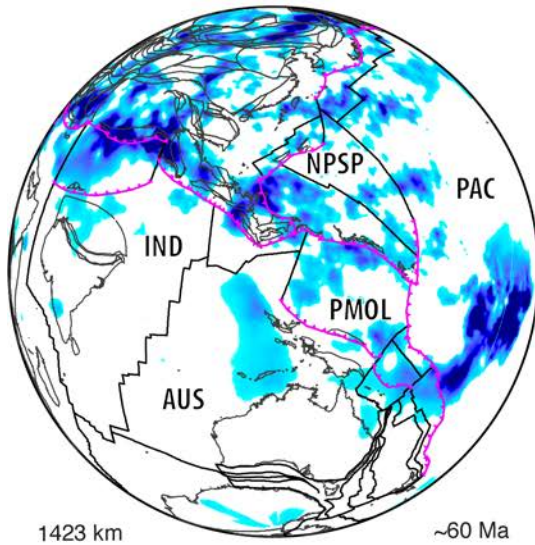
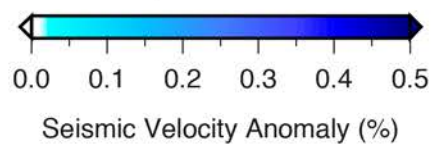
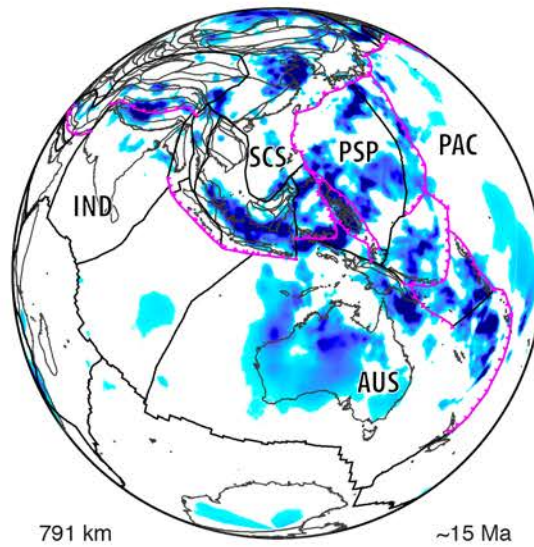
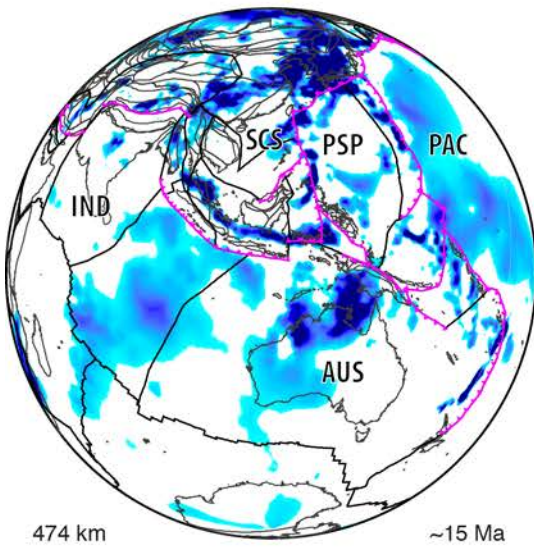
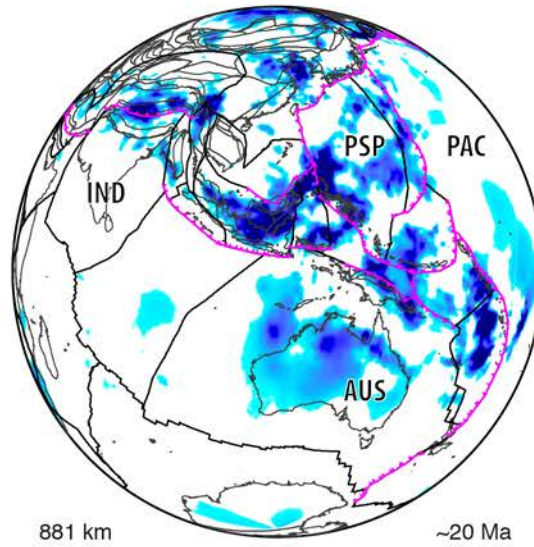
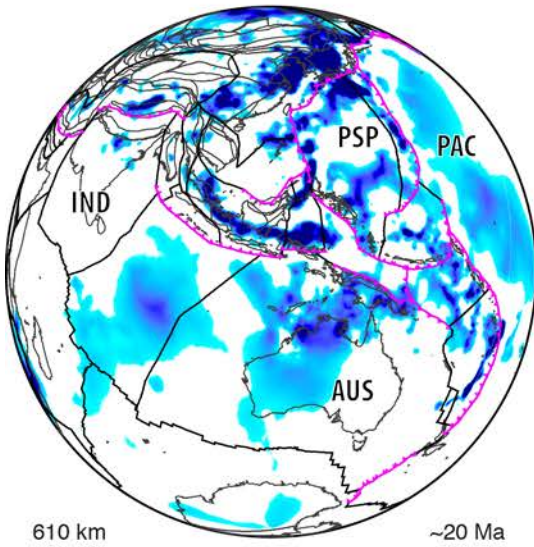
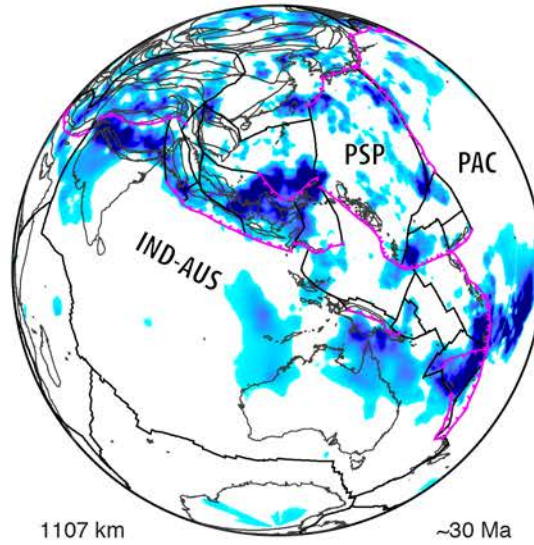
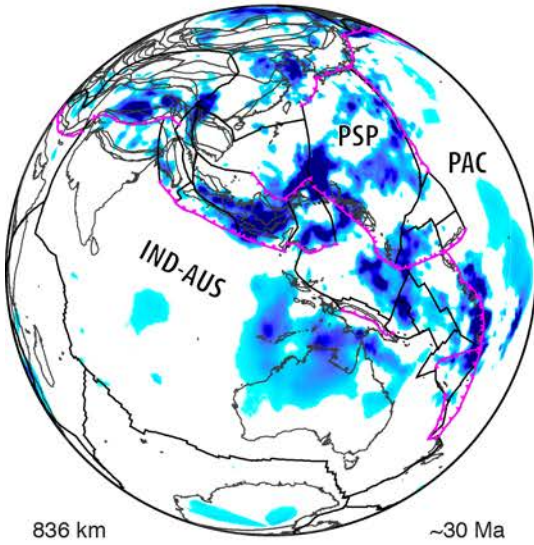


Fig. 24. Fast seismic velocity anomalies from the Li et al. (2008) P-wave seismic tomography model compared to our refined plate reconstructions. Ages are attributed to depths assuming that the average

1481 vertical sinking rate of slabs is ~ 2 cm/yr in the lower mantle, and 3 cm/yr (left) and 8 cm/yr (right) in
1482 the upper mantle. Additional polygons in Australian-Antarctic and Lord Howe-Tasman Sea regions
1483 represent areas of deforming continental crust. See Supplementary Animations 5 and 6.

Upper mantle: 3 cm/yr
Lower mantle: 2 cm/yr

Upper mantle: 8 cm/yr
Lower mantle: 2 cm/yr



1485 **Fig. 24.** (continued)

1486

1487 At ~60 Ma (Fig. 24), the scenario invoking a slower sinking rate in the upper mantle better
1488 reproduces the Sunda slab, as well as the subduction of the Proto Molucca Plate (PMOL) beneath the
1489 Philippine Arc and the rollback-induced opening of the Proto South China Sea. The match with the
1490 Sunda and Philippine slabs is not surprising, as a slower sinking rate was also used to calibrate the
1491 position of these blocks in our base plate motion model (Zahirovic et al., 2014). Interestingly, the gap
1492 in the Sunda slab along Sumatra in both sinking rate end-members, coinciding with the modelled
1493 location of the Wharton Ridge, supports the slab window scenario proposed by Whittaker et al.
1494 (2007). Both slab sinking scenarios reproduce the Andean-style subduction along southern Eurasia
1495 consuming the Kohistan-Ladakh and Woyla back-arc basins, as implemented in the reconstructions
1496 based on the near-equatorial latitudes from paleomagnetic estimates. At ~50 Ma, the slower sinking
1497 rate matches the oroclinal bending of Sundaland and subduction of the Proto South China Sea, which
1498 is again expected due to calibration of the reconstructions with tomography. However, the match to
1499 subduction of the Sepik oceanic basin north of New Guinea is not imposed, and suggests the large E-
1500 W slab presently beneath Australia is likely sourced from this subduction system (Schellart and
1501 Spakman, 2015).

1502 The 40 and 30 Ma timesteps in the age-coded seismic tomography depth slices support waning
1503 subduction in the India-Eurasia segment of the active margin, and active subduction along northern
1504 Borneo (Fig. 24), and. The ~20 and 15 Ma reconstructions (Fig. 19 and 21) highlight the requirement
1505 of south-dipping subduction along New Guinea to account for the Maramuni Volcanics (Fig. 24), as
1506 well as contemporaneous north-dipping subduction along the Halmahera Arc, which is terminated
1507 after ~15 Ma following the arc-continent collision on northern New Guinea. The collision of
1508 Dangerous Grounds-Reed Bank with northern Borneo at ~15 Ma also choked the north Borneo
1509 subduction zone, and likely resulted in Proto South China Sea slab breakoff. The ~15 Ma
1510 reconstruction using the faster sinking rate, and corresponding to a 791 km depth slice, shows a

discrete slab volume along northern Borneo that we interpret as the Proto South China Sea slab (Fig. 24).

The seismic tomographic interpretation highlights that the refinement of the New Guinea margin (namely the Maramuni subduction zone) and the adjustment to the Philippine Sea Plate (namely the position of the Halmahera Arc) since ~30 Ma can accommodate both the geological and the tomographic constraints. Neither sinking rate scenarios produce consistent matches throughout the plate reconstruction timeframe, likely due to the complex time-varying slab sinking rates and regional interactions of slabs in a spherical mantle shell. However, the assumption of vertical sinking of slabs is likely to be an acceptable estimate of trench locations in the Cenozoic for slabs that are still attached to the subducting plate, or slabs that have experienced little stagnation or folding in the mantle transition zone. The numerical computations described in the following section provide a more consistent approach to tracking slabs in the mantle resulting from the complex subduction history in the Tethys, east and Southeast Asia, and New Guinea.

5 Numerical modelling results

5.1 Large-scale post-Jurassic mantle evolution of the Tethyan tectonic domain

We present the first synthesis of post-Jurassic Tethyan plate reconstructions and geodynamics in a 4D (space and time) global context. We ran five cases of coupled plate kinematic and geodynamic numerical experiments, mainly to test end-member plate reconstructions, and present 3D snapshots of two experiments that compare the Zahirovic et al. (2014) model with refinements for the Neo-Tethys, Philippine Sea Plate and New Guinea presented in this study (Fig. 25). Although the mantle convection models are initiated at 230 Ma during the time of Pangea stability, we present only the post ~160 Ma timeframe applicable to the refined plate reconstructions. At ~160 Ma, the dominant feature of the mantle is the circum-Pangea subduction girdle, as well as the southern Eurasian active

margin consuming Meso-Tethyan oceanic lithosphere (Fig. 25a). The tectonic scenario presented invokes the northward continuation of East Gondwana subduction along New Guinea and connecting to the East Asian subduction of the Izanagi Plate. By ~140 Ma the rollback of the Lhasa trench opens the Kohistan-Ladakh back-arc basin, with a slower opening and southward position of ~10°N in our base model by 100 Ma (Zahirovic et al., 2014), compared with the equatorial position implemented in this study following Burg (2011) and Gibbons et al. (2015).

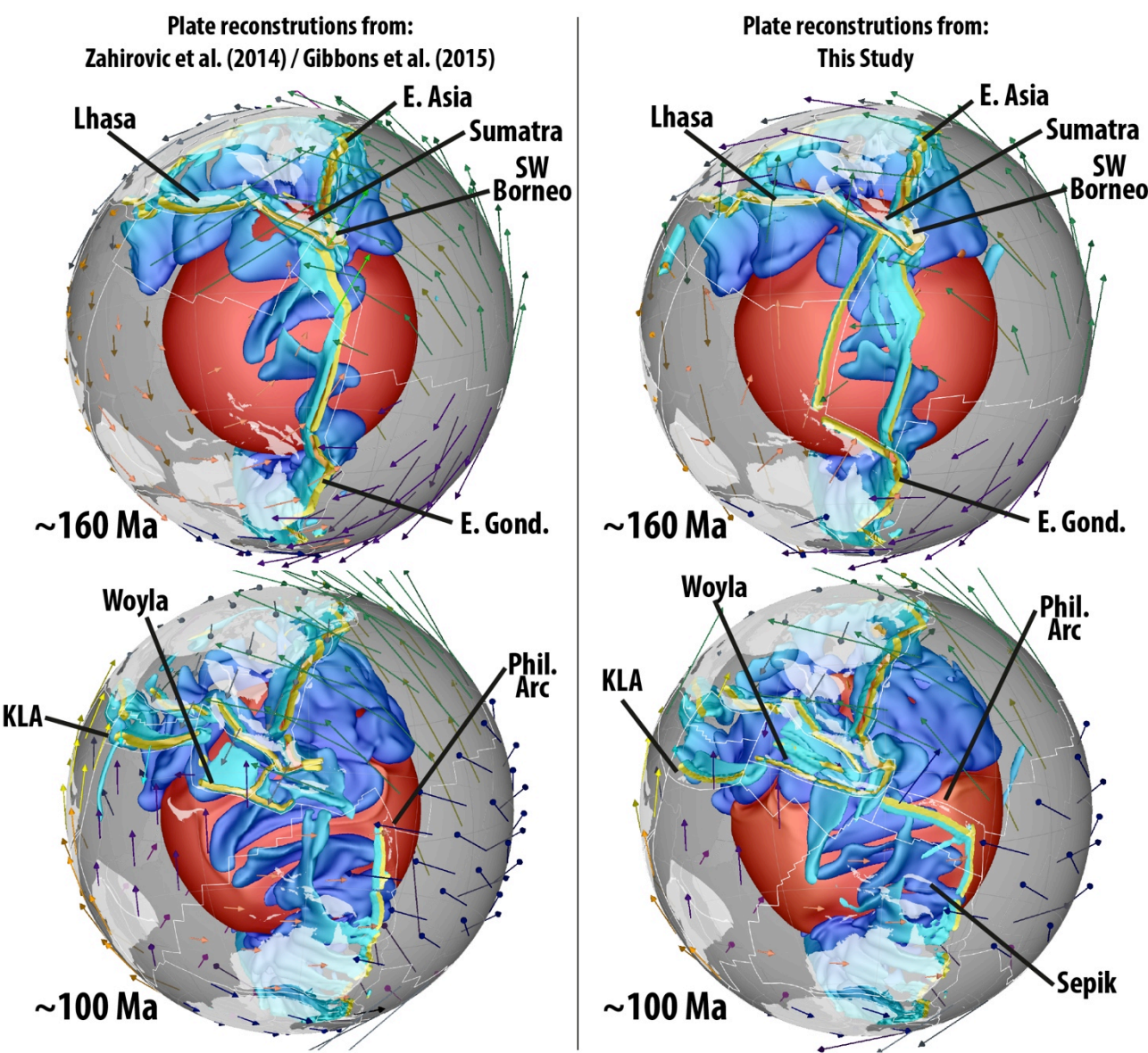


Fig. 25a. Snapshots of mantle structure including sinking slab volumes (blue) and thermochemical upwellings (red) from the core-mantle boundary are visualised in GPlates using the mantle temperature predictions from the CitcomS numerical experiments of mantle flow depicting Case 4 (left) and 5 (right). The snapshots compare the large-scale mantle evolution in the latest Jurassic and

1547 Early Cretaceous from Tethyan subduction along Lhasa and the Kohistan-Ladakh Arc (KLA), as well
1548 as recycling of proto-Pacific lithosphere along the East Asian, East Gondwana and Philippine Arc
1549 subduction zones. Plate boundaries (white), velocities (coloured arrows) and reconstructed present-
1550 day coastlines (translucent white) are plotted. Subduction zones are yellow regions, and slab
1551 colouring is a function of depth from light blue (shallow slabs) to darker blue (deep slabs). These
1552 snapshots highlight the global nature of our numerical experiments, with complex interactions of
1553 slabs as they sink in the mantle shell. The experiments allow us to track the sinking trajectory (vertical
1554 and lateral) of the slabs to identify their source from the present-day mantle prediction, which are
1555 compared to the mantle structure imaged using P- and S-wave seismic tomographic techniques.
1556 Central co-ordinate is 10°S, 115°E.

1557

1558 As our modelling domain is spherical, and because the flow is constrained to follow surface
1559 velocities that include net rotation of the lithosphere, lateral mantle flow may influence the trajectory
1560 of sinking slabs. As subducting slabs sink in the mantle, the core-mantle boundary becomes draped
1561 with older slabs that sweep the hotter material into the large-scale Pacific and African upwellings
1562 (Bower et al., 2013; McNamara and Zhong, 2005) (Fig. 25). In addition, mantle flow advects slabs
1563 laterally, with notable southward (and somewhat westward) translation of the Paleo-Tethyan slabs,
1564 and eastward advection of the east Asian slabs (Fig. 25). India's collision with the Kohistan-Ladakh
1565 Arc ceases intra-oceanic subduction by ~50 Ma in our model, resulting in the Andean-style
1566 subduction of the Kohistan-Ladakh back-arc basin along southern Lhasa (Fig. 25b). The ~47 Ma
1567 continent-continent collision temporarily shuts down subduction, causing a slab break-off event,
1568 followed by ongoing subduction of the Greater Indian mantle lithosphere (Capitanio et al., 2010).
1569 Australia's northward motion results in the northern margin, including New Guinea, overriding the
1570 Southeast Asian slab graveyard from ~30 Ma following the docking of Sepik, and the initiation of
1571 south-dipping Maramuni subduction from ~20 Ma.

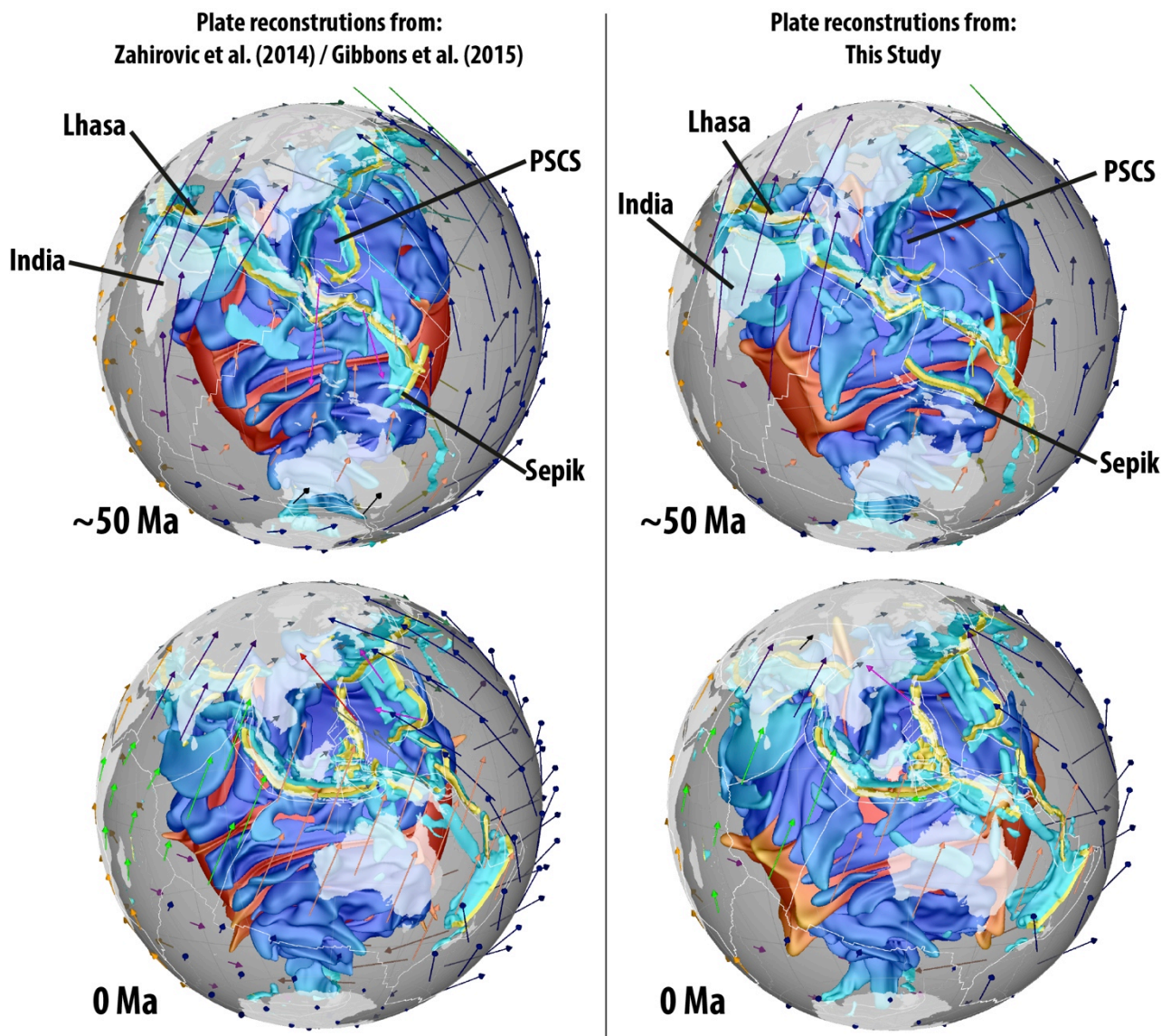


Fig. 25b. Coupled plate reconstructions and mantle flow models in the Eocene and present-day, highlighting the draping of subducted slabs along the core-mantle boundary and the self-organisation of the African and Pacific large-scale upwellings as a result of post-Pangea subduction. These models are interrogated regionally using vertical profiles in Figs. 26-29. Centre co-ordinate is 10°S, 115°E. See Supplementary Animation 7 consistent with right panels.

The large-scale evolution of slab sinking and lateral advection, as well as the evolution of the large-scale upwellings, can be depicted in 3D hemispherical views of the mantle, while regional cross-sections of the numerical experiments provide a more detailed approach to interrogating the

1582 spatio-temporal geodynamic evolution of key subduction zones from post-Jurassic plate
1583 reconstructions.

1584

1585 **5.2 Regional interpretations of mantle evolution**

1586

1587 To capture the detailed evolution of subduction, vertical cross-sections of the mantle are
1588 presented in a plate frame of reference (i.e., fixed to the overriding plate, Figs. 26-29). Such time-
1589 dependent sections help understand the sinking trajectory of subducted slabs, as well as interpreting
1590 sinking rates and lateral mantle flow resulting from the post-Jurassic plate reconstructions. For the
1591 geological reasoning underpinning the reconstructions, please refer to Section 3 and Table 3.

1592 **5.2.1 India-Eurasia convergence**

1593

1594 The India-Eurasia segment is best represented by a largely north-south profile at present-day
1595 that is reconstructed with Lhasa (Fig. 26). At ~160 Ma, the Paleo-Tethyan slab has detached and is
1596 sinking through mid-mantle depths at ~1.5 cm/yr (Fig. 26a,h), while the Meso-Tethys is being
1597 actively consumed northward beneath Lhasa in both plate reconstruction scenarios. Both tectonic
1598 scenarios include southward slab rollback and the establishment of a Kohistan-Ladakh (Tethyan)
1599 back-arc basin, reaching to ~10°N in the base model (Zahirovic et al., 2014) and the equator at
1600 ~100 Ma in this study (Fig. 26c,j). Using the base reconstructions, the Meso-Tethyan slab only
1601 penetrates the mantle transition zone at ~100 Ma and begins sinking into the lower mantle by ~90 Ma
1602 (Fig. 26, Supplementary Animation 7). In the refined reconstructions the slab enters the mantle
1603 transition zone by ~120 Ma, and enters the lower mantle by ~110 Ma. This reflects greater
1604 convergence rates due to the combined effect of greater slab rollback in the refined reconstructions,
1605 as well as continued seafloor spreading north of India during this timeframe. In the base
1606 reconstructions, the seafloor spreading north of India is abandoned by ~120 Ma, leading to lower
1607 convergence rates across the Kohistan-Ladakh Tethyan trench (Fig. 10). This results in the subduction

1608 of larger volumes of older, and therefore thicker, oceanic lithosphere, while in the refined
1609 reconstructions subducted volumes along the Kohistan-Ladakh Arc system in the Early to mid-
1610 Cretaceous are smaller because the oceanic lithosphere associated with the Neo-Tethyan seafloor
1611 spreading north of India by ~100 Ma is younger and thinner (Fig. 26j). Once the Tethyan slab has
1612 entered the lower mantle, the sinking rate in the refined reconstruction is only ~1.4 cm/yr (between
1613 100 and 89 Ma), while it is ~2.5 cm/yr in the base reconstructions (between 89 and 79 Ma) likely due
1614 to the larger subducted volumes.

1615 The intersection of the Neo-Tethyan mid-oceanic ridge with the Kohistan-Ladakh subduction
1616 zone in the mid-Cretaceous would likely lead to slab breakoff and the formation of a slab window.
1617 However, our model does not capture the complexity of a subduction hiatus that would be associated
1618 with a slab window along Kohistan-Ladakh in the mid-Cretaceous. Perhaps due to the arrival of
1619 buoyant oceanic crust at the intra-oceanic subduction system, north-dipping subduction becomes
1620 established along Lhasa and begins to consume the Kohistan-Ladakh back-arc basin, eventually
1621 resulting in two Late Cretaceous north-dipping subduction zones in the Neo-Tethys (see Section 3.2).
1622 The mid-ocean ridge from the Kohistan-Ladakh back-arc is subducted in the Late Cretaceous in both
1623 reconstruction scenarios, with no interruption in subduction assumed in the base reconstructions. In
1624 the alternative reconstructions we impose a subduction hiatus along Lhasa from 80 to 65 Ma, which
1625 leads to slab breakoff. This slab window may be linked to adakitic volcanism at ~80 Ma (Wen et al.,
1626 2008a), followed by a ~75-60 Ma magmatic gap, in the Gangdese Batholith (Chung et al., 2005; Ji et
1627 al., 2009; Wen et al., 2008b).

1628 In both reconstruction scenarios, Greater India collides with Kohistan-Ladakh by ~50 Ma,
1629 inducing Neo-Tethyan slab break-off at ~5-10°N. Since the Kohistan-Ladakh Arc is at equatorial
1630 latitudes in the refined reconstructions in the mid-Cretaceous, one may expect the collision with India
1631 to occur by ~60 Ma. As the magmatic chemistry change is much later, at 52 Ma (Bouilhol et al.,
1632 2013), the model includes some advance of the intra-oceanic subduction system between ~60 and 52
1633 Ma. In the base reconstructions, the Kohistan-Ladakh Arc is closer to Eurasia at pre-collision times,

1634 meaning that relatively little trench advance is required. However, in both instances, the Tethyan slab
1635 is anchored in the lower mantle, leading to India overriding the sinking slabs. Andean-style
1636 subduction of the Kohistan-Ladakh back-arc along southern Lhasa is temporarily shut off by the ~47-
1637 40 Ma continent-continent collision, after which subduction of Greater India (continental) mantle
1638 lithosphere continues to present-day in the refined reconstructions. The Meso- and Neo-Tethyan slabs
1639 are predicted at present to be approximately at mid-mantle depths (~1000 to 2000 km), with a
1640 latitudinal range of ~0 to 35°N, using the base model plate reconstructions (Fig. 30, IND-EUR). More
1641 generally, the base plate reconstruction in modelled Case 4 reproduces a number of discrete slabs at
1642 mid-mantle depths, with a large latitudinal range, which is consistent with the interpretations of the
1643 mantle structure by van der Voo et al. (1999b) (Fig. 5).

1644 Although the numerical model that uses the refined reconstructions presented in this study has
1645 the same radial viscosity profile, the Meso- and Neo-Tethyan slabs are predicted to be shallower at
1646 ~800 to 1500 km depths, as opposed to ~1000 to 2000 km depths predicted using the base
1647 reconstructions (Fig. 26g,n). This is likely due to the subduction of smaller volumes of younger
1648 Tethyan oceanic lithosphere north of India in the Cretaceous, resulting in less negative buoyancy. In
1649 addition, the required trench advance also results in folding of the Tethyan slab at the mantle transition
1650 zone, leading to generally shallower penetration into the lower mantle. In the post-collision
1651 timeframe, the Tethyan slab sinks at a rate of ~0.65 cm/yr (from 38 to 0 Ma) using the base
1652 reconstructions, and ~0.25 cm/yr (from 39 to 0 Ma) using the refined reconstructions where the slab
1653 is almost stagnant at ~1000 km depth (Supplementary Animation 7). The time-varying sinking rates
1654 in the lower mantle highlight the role active subduction has in adding negatively buoyant slab
1655 volumes into the mantle, and the role of thermal diffusion of slabs in reducing negative buoyancy of
1656 subducted lithosphere. A slightly deeper depth range (~1000 to 2000 km) provides a better match to
1657 the equivalent P- and S-wave tomography slice (Fig. 30, IND-EUR), as is obtained with the base
1658 plate reconstructions (Gibbons et al., 2015; Zahirovic et al., 2014), with the potential that slabs may
1659 extend further south of the equator based on the S-wave model.

Plate reconstructions:
Zahirovic et al. (2014)
Gibbons et al. (2015)

Plate reconstructions:
This Study

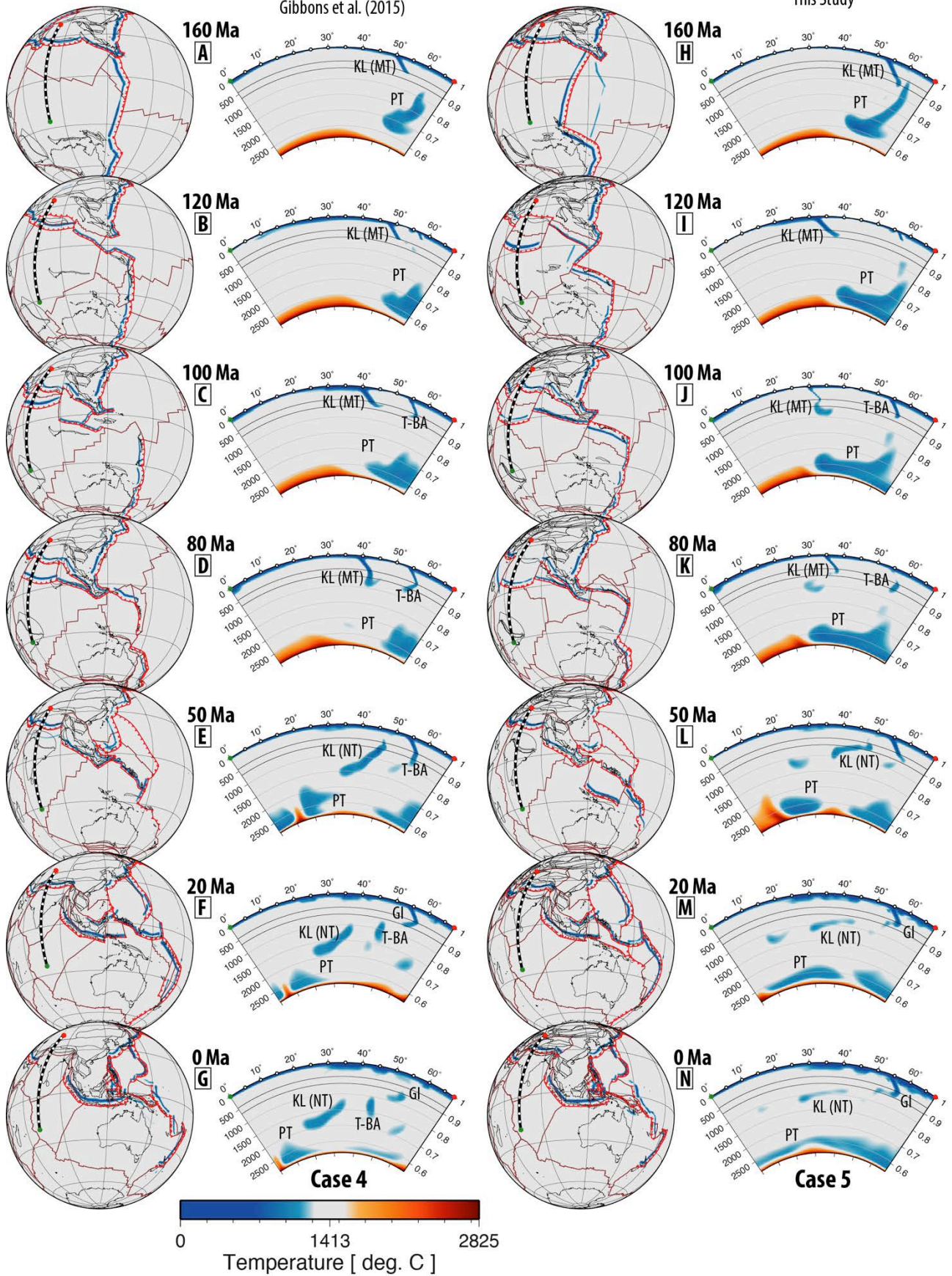


Fig. 26. Time-dependent evolution of the India-Eurasia convergence zone, with a representative vertical slice reconstructed with Lhasa to capture the evolution of the Kohistan-Ladakh (KL) and Tethyan (T-BA) intra-oceanic subduction zones modelled in Zahirovic et al. (2014) and Gibbons et al. (2015) (left), and compared to the subduction histories implied in the revised plate reconstructions presented in this study (right). The cross-sections depict the temperature field from the numerical mantle flow models, and the globes show the position of the vertical slices through time, the plate reconstruction and the predicted mantle temperature field at ~400 km depth. The background mantle temperature is ~1413°C, and the small tick marks on the temperature scale represent temperature intervals of 250°C. Great circle angular distance along the vertical profile is shown on the x-axis. The left y-axis represents depth in kilometres, and on the right represents non-dimensional Earth radius. The plate reconstructions are plotted in an orthographic projection with centre co-ordinate of 15°S, 115°E. GI – Greater India (continental) mantle lithosphere, MT – Meso-Tethys slab, NT – Neo-Tethys slab, PT – Paleo-Tethys slab. See Supplementary Animation 8.

5.2.2 *Woyla and Sumatra active margin evolution*

The Sumatra segment of the Sunda margin accommodates northward subduction of the Meso-Tethys in the Late Jurassic, with rollback of the slab opening the Woyla back-arc to near-equatorial latitudes (Fig. 27), similar to the development of the Kohistan-Ladakh Arc further to the west. In the base reconstructions, the rollback imposed is faster and the maximum southward extent of subduction is ~0-10°S (Fig. 11). This leads to a smaller volume of subducted slabs folded in the mantle transition zone. Although the base reconstruction maintains convergence across the Woyla subduction zone, there is significant trench advance between ~100 and 75 Ma, leading to a similar smearing effect of slabs in the transition zone. Although trench advance occurs at present-day along the Izu-Bonin-Mariana Trench (Becker et al., 2015; Carlson and Mortera-Gutiérrez, 1990; Mathews, 2014), the

1686 modelled values in our base reconstructions are likely excessive, with a more geodynamically
1687 reasonable evolution of trench migration in the refined reconstructions.

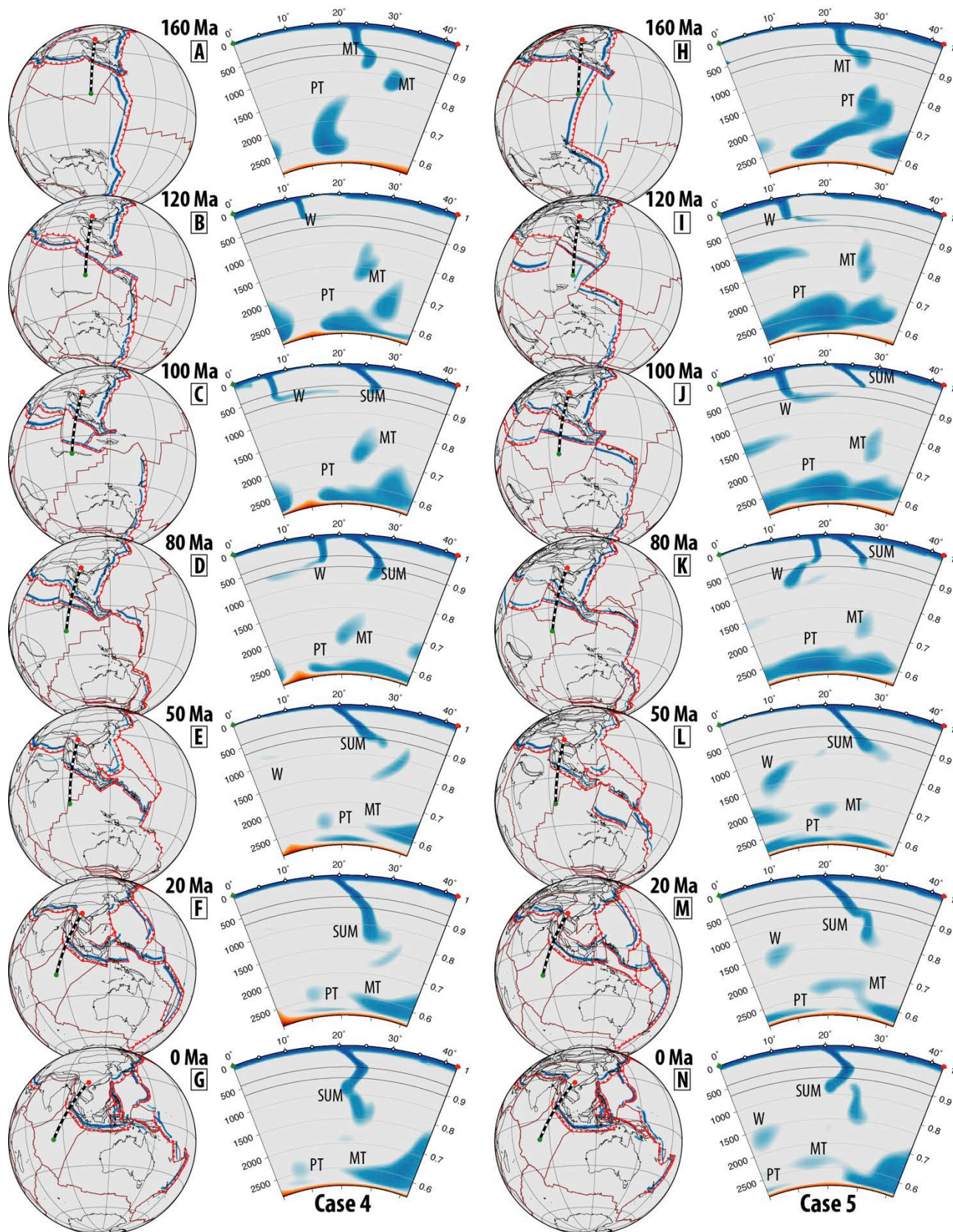
1688

1689 Subduction continues along Sumatra to consume the Woyla back-arc basin, and is interrupted
1690 for ~10 Myr between accretion of the Woyla Arc onto the Sumatran margin between ~75 and 65 Ma
1691 in the base reconstructions. Due to the convergence required between the Tethyan-Indian Ocean and
1692 Eurasia, we impose a shorter ~5 Myr hiatus in subduction between 75 and 70 Ma to induce slab
1693 breakoff that may have occurred due to Woyla Terrane accretion. Our assumption of slab breakoff is
1694 simplistic and based on the magmatic gap, and more realistic slab breakoff timings of 5-10 Myr after
1695 collision (Li et al., 2013; van Hunen and Allen, 2011) will need to be considered in future refinements
1696 of the model in this region.

1697 In both tectonic reconstructions, subduction at the Sunda Trench is initiated at ~70-65 Ma,
1698 and persists to present-day. The slab is predicted to have penetrated the lower mantle by ~50 Ma,
1699 after which the collision of India with Eurasia, and subsequent rotation of Indochina and much of
1700 Sundaland from ~30 Ma leads to a kink in the slab in the mantle transition zone (410 to 660 km, Fig.
1701 27g,n). Although the kink results from the constant slab dip imposed in the slab assimilation, this slab
1702 kink is imaged by the P- and S-wave seismic tomography analysed here, and also recently discussed
1703 in Hall and Spakman (2015). The numerical experiments of mantle flow also reproduce the latitudinal
1704 range of the subducted slab (Fig. 30, SUM), as well as a gap in the slab at depths greater than ~1500
1705 km, consistent with earlier interpretations of the Sunda slab (Widiyantoro and van der Hilst, 1996).
1706 The mantle convection models predict the Woyla/Meso-Tethys slab at ~1500 to 2000 km depths at
1707 ~10°S along the Sumatran vertical slice (Fig. 30, SUM), and ~20°S along the Java-Borneo Sundaland
1708 slice (Fig. 30, SUN), which is likely to be equivalent to fast seismic velocities in P- and S-wave
1709 tomography at ~1500-2000 and ~1200-1600 km depth along the Sumatran and Java-Borneo vertical
1710 slices, respectively.

Plate reconstructions:
Zahirovic et al. (2014)
Gibbons et al. (2015)

Plate reconstructions:
This Study



1711

1712

1713

Fig. 27. Reconstructed vertical profiles across northwest Sumatra highlighting the evolution of the Woyla intra-oceanic and Sunda subduction zones through time, with both numerical experiments

1714 predicting a significant kink in the Sumatran portion of the Sunda slab (SUM) when the slab dip is
1715 held constant during the clockwise rotation and extrusion of Indochina. MT – Meso-Tethys slab, NT
1716 – Neo-Tethys slab, PT – Paleo-Tethys slab, W – Woyla slab. See Supplementary Animation 9.

1717

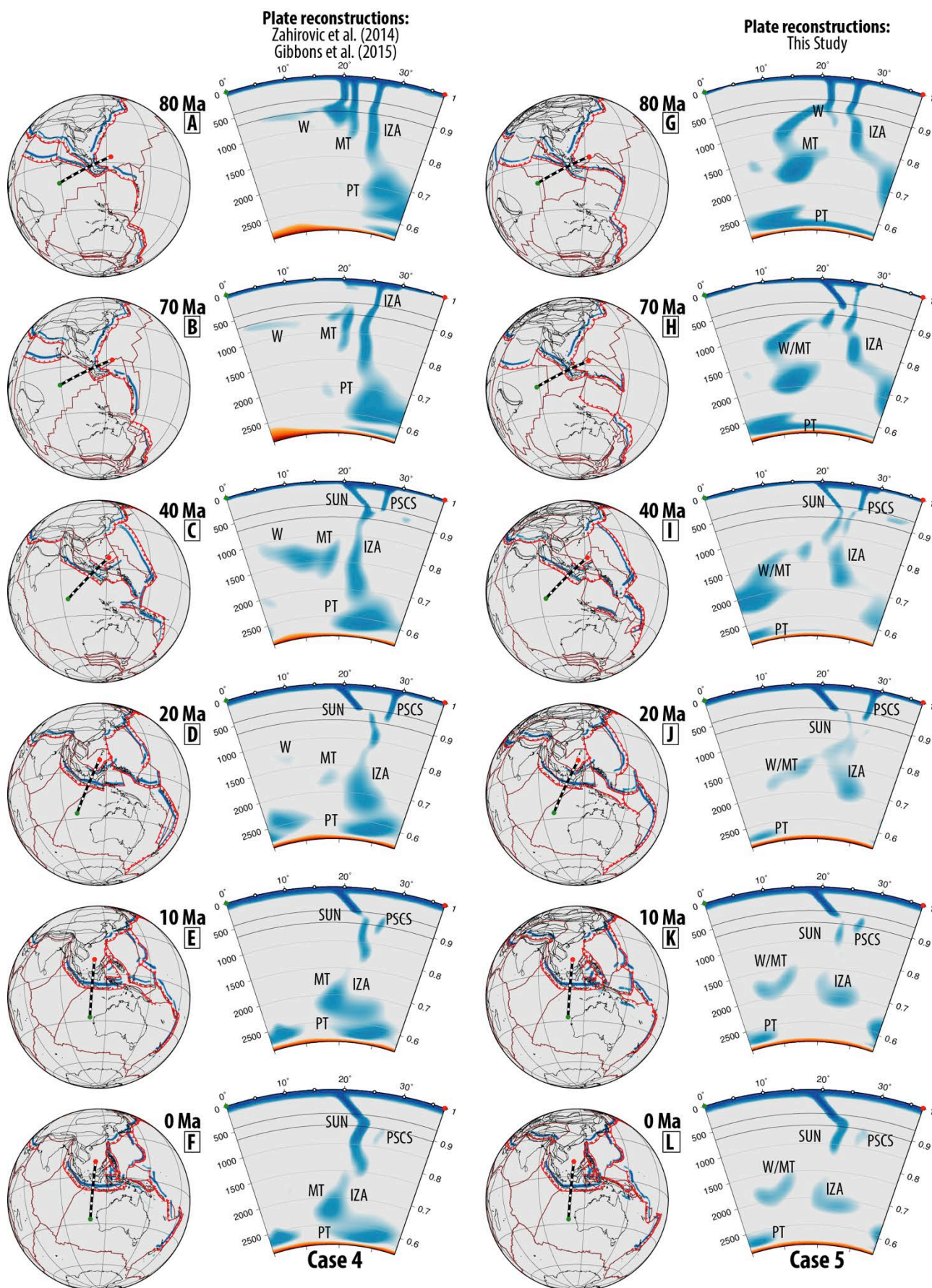
1718 **5.2.3 *Java and Borneo subduction history***

1719

1720 Similar to the Sumatra margin, the Java segment of the Sunda Trench accommodates
1721 subduction of the Meso-Tethys and the Woyla back-arc basin during the Cretaceous (Fig. 28).
1722 However, as this segment represents the Sundaland continental promontory, south-dipping
1723 subduction of the Izanagi Plate is contemporaneous to the Tethyan subduction history. As a result,
1724 the mid- and lower mantle slabs are likely to be a mixture of Pacific- and Tethyan-derived slabs. The
1725 accretion of the Woyla Arc temporarily shuts off subduction in this segment in the Late Cretaceous
1726 at ~70 Ma in the base reconstructions (Fig. 28b,h), followed by the accretion of the Semitau
1727 continental fragment and Proto South China Sea Arc onto northern Borneo at ~45 Ma in both
1728 reconstruction scenarios (Fig. 28c,i). The late Eocene is dominated by renewed north-dipping Sunda
1729 subduction and south-dipping subduction of the Proto South China Sea. Although the Sunda
1730 subduction continues to the present-day, the Proto South China Sea subduction is interrupted at
1731 ~15 Ma with the docking of the Dangerous Grounds-Reed Bank continental fragment along northern
1732 Borneo, which leads to the abandonment of the South China Sea seafloor spreading. The refined
1733 reconstructions imply a longer-lived Meso-Tethyan Plate that is completely consumed by ~45 Ma,
1734 leading to much younger oceanic crust and thinner oceanic lithosphere subducted at the Sunda Trench
1735 than in the base reconstructions. This leads to the subduction of smaller slab volumes between ~60
1736 and 30 Ma for the refined reconstructions that predict a smaller and shallower slab that penetrates to
1737 ~1200 km depth at present. In contrast, the base reconstructions lead to a larger Sunda slab at depths
1738 of ~1500 km (Fig. 30, SUN), which is consistent with the interpretations of P- and S-wave seismic
1739 tomography. The kink in the slab observed in the Sumatra segment (Fig. 30, SUM) is much less

1740 pronounced in the Java region (Fig. 30, SUN), especially when compared to the results using our base
1741 plate reconstruction. A gap in the slab is also reproduced for depths greater than ~1500 km, with older
1742 Tethyan and Izanagi slab fragments reproduced near the core-mantle boundary when comparing to
1743 the S-wave seismic tomography (Fig. 30, SUN). The Proto South China Sea slab is predicted at ~600-
1744 1000 km depths, while P- and S-wave tomographic images indicate a slab stagnating at the base of
1745 the 410-660 km mantle transition zone.

1746



1747

1748 **Fig. 28.** Reconstructed vertical slice through eastern Sundaland, capturing the subduction of the
 1749 Meso- and Neo-Tethyan, as well Indian Ocean, basins. The Sunda slab is predicted to reach a

1750 maximum depth of ~1500 km along southern Sundaland in the base reconstructions, and ~1200 km
1751 in the refined reconstructions, while a small Proto South China Sea slab is predicted just beneath the
1752 660 km upper-lower mantle transition. See Supplementary Animation 10.

1753

1754 **5.2.4 New Guinea margin evolution**

1755

1756 Further east along the New Guinea Tethyan segment, the Early Cretaceous Sepik oceanic
1757 basin is consumed at a north-dipping subduction zone from ~40 Ma (Fig. 29b) in the base model
1758 reconstructions, while in our refined model subduction starts earlier at ~71 Ma (Fig. 29g) to account
1759 for the ~71 to 66 Ma Emo volcanics (Worthing and Crawford, 1996) that likely formed in the back-
1760 arc of this subduction system. North-dipping subduction along the Sepik Terrane is interrupted at ~30
1761 Ma in both plate reconstruction scenarios, based on the timing of docking of the composite terrane at
1762 the New Guinea margin. We impose slab breakoff during the collision, leading to a slab that is
1763 entrained in the upper part of the lower mantle (660-1000 km depths) for both reconstruction
1764 scenarios. In the base model, north-dipping subduction is then accommodated along the Halmahera
1765 Arc, which forms the southern boundary of the Caroline Plate, and is accreted to the New Guinea
1766 margin diachronously from west to east by ~5 Ma. In the refined reconstructions, a south-dipping
1767 subduction zone is implemented (Fig. 29j) to account for the ~18 to 8 Ma Maramuni Arc volcanics
1768 (Hill and Hall, 2003; Page, 1976), as well as simultaneous north-dipping subduction along the
1769 Halmahera Arc. Both subduction zones are abandoned progressively from ~15 Ma, resulting from
1770 the collision of the Halmahera Arc with the New Guinea margin.

1771 The numerical experiments of mantle flow assimilating the base plate motion model predict
1772 two slabs at depths between ~500 and 1000 km (Fig. 30, PNG), with the southernmost slab at ~20°S
1773 belonging to the Sepik oceanic basin, and the northern slab at 0 to 5°S resulting from the subduction
1774 of the Solomon Sea along the Halmahera Arc. With the addition of the Maramuni subduction zone in
1775 the refined plate reconstructions (~20 to 10 Ma, Fig. 29), an additional slab is predicted at slightly

1776 deeper depths of ~900 to 1500 km at ~15°S. The Sepik oceanic basin slab is predicted to be further
1777 south in the refined plate reconstruction scenario, at depths of ~700 to 1000 km and latitude of ~30°S
1778 (Fig. 30, PNG). This difference in latitude is largely due to the earlier onset of Sepik oceanic gateway
1779 subduction at ~71 Ma in the refined reconstructions, leading to the slab entering the lower mantle at
1780 more southerly latitudes, as opposed to the younger age of ~40 Ma subduction onset using the base
1781 reconstructions (Fig. 29b). The refined plate reconstructions result in a much better fit with the mantle
1782 structure than the base model, with the ~30°S position of the Sepik oceanic gateway slab
1783 corresponding to the fast seismic anomaly interpreted beneath Lake Eyre in eastern Australia, recently
1784 interpreted in Schellart and Spakman (2015). However, a slab at ~1300 to 1800 km depths at present-
1785 day (PNG, Fig. 30), and latitudes between ~10°S and the equator, is not accounted for in either model
1786 of mantle flow – suggesting the Cretaceous plate reconstruction needs additional refinement.

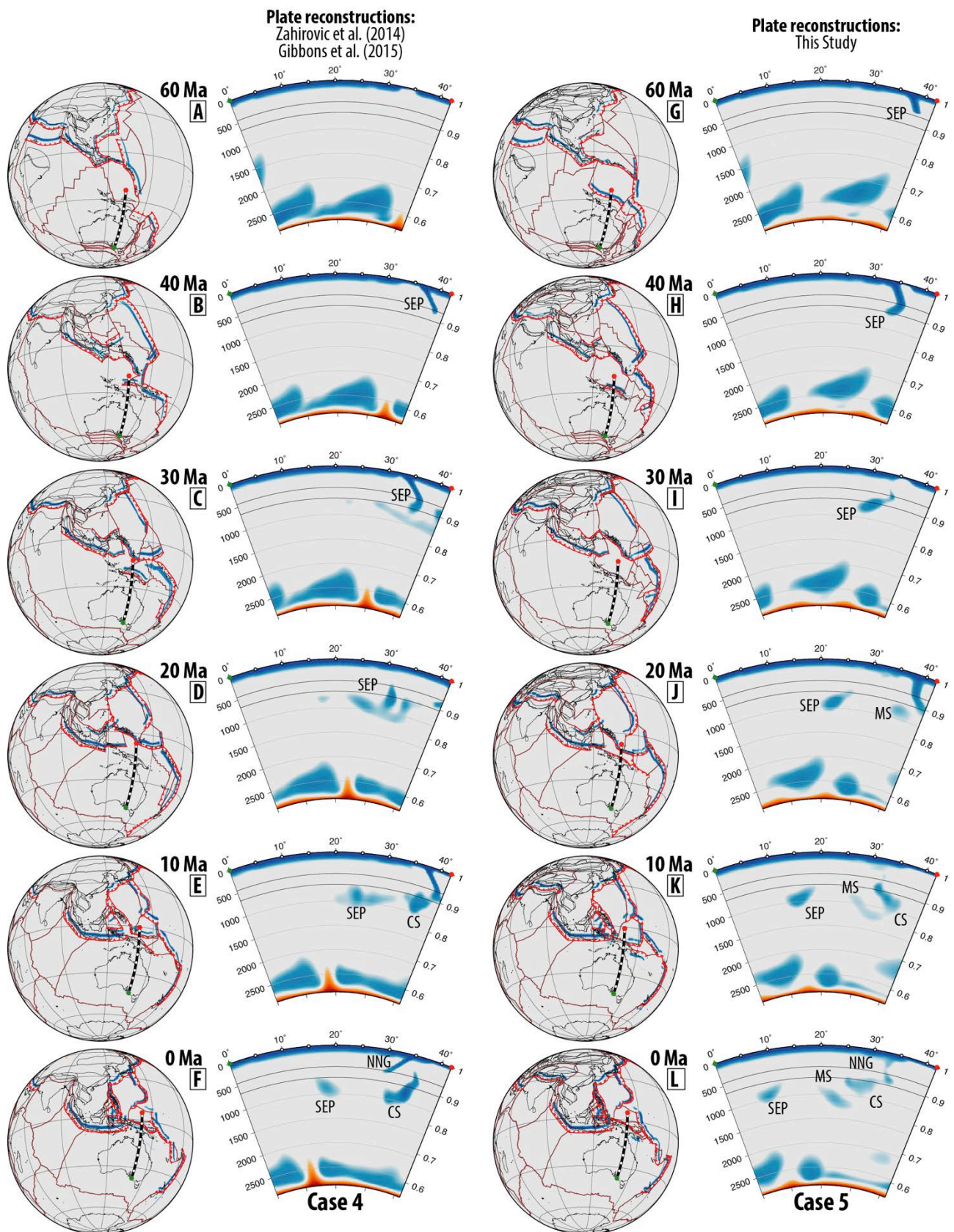
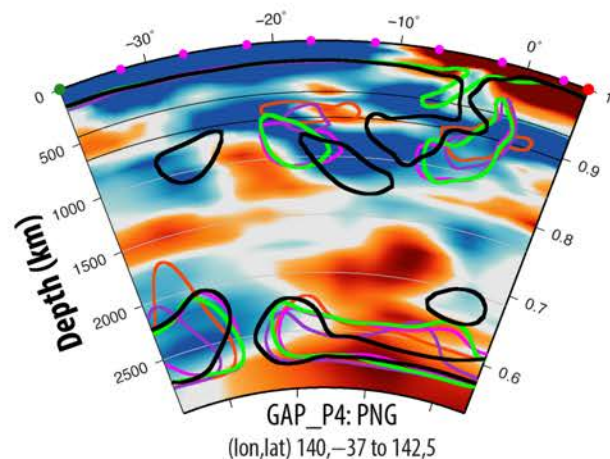
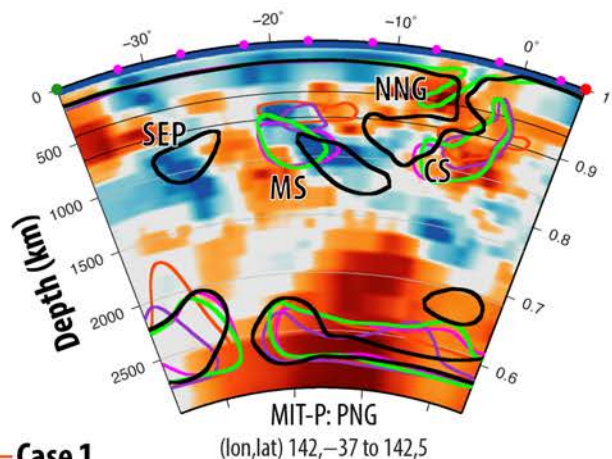
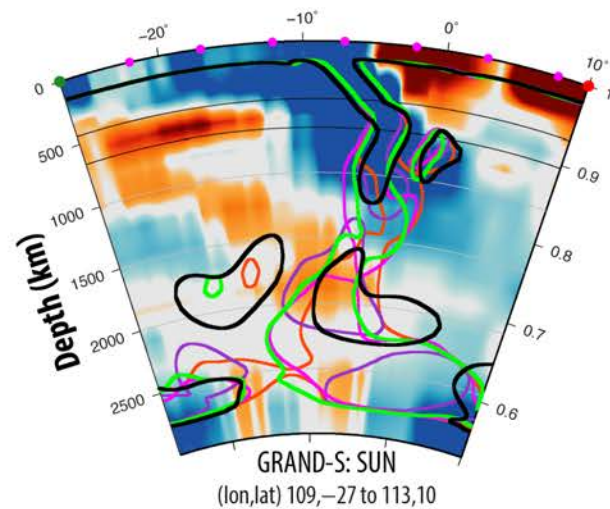
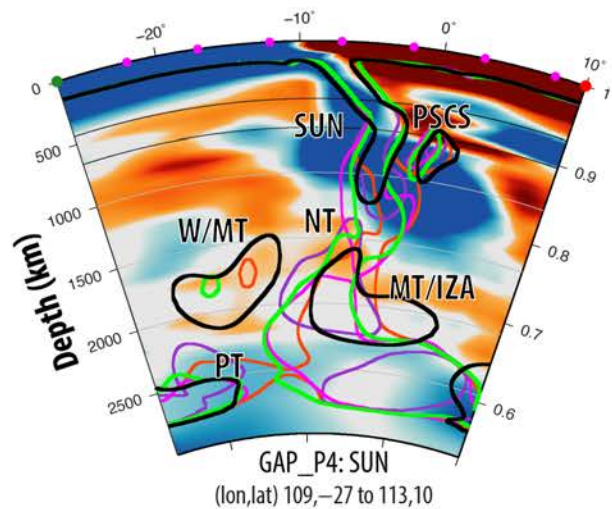
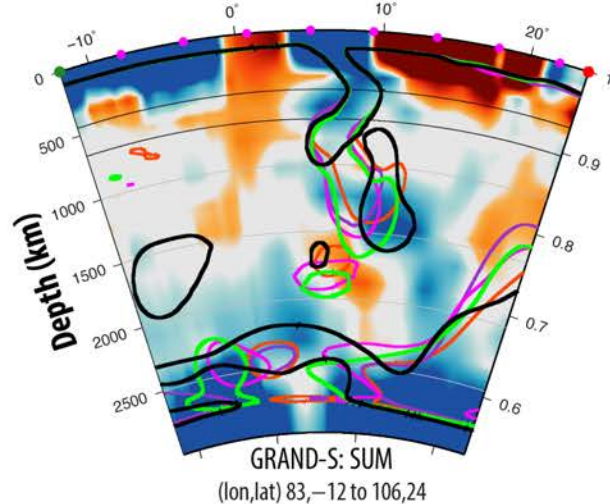
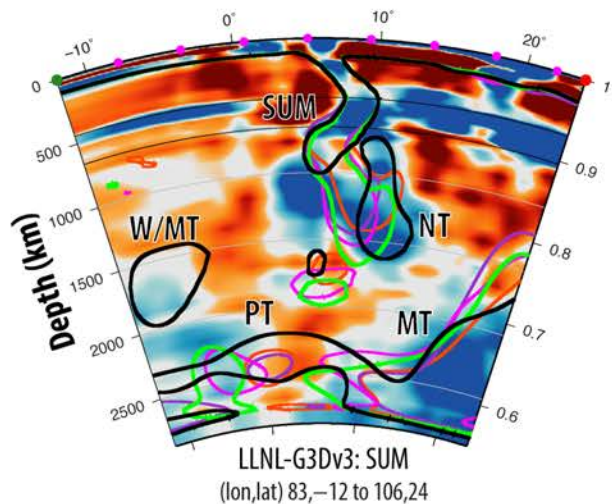
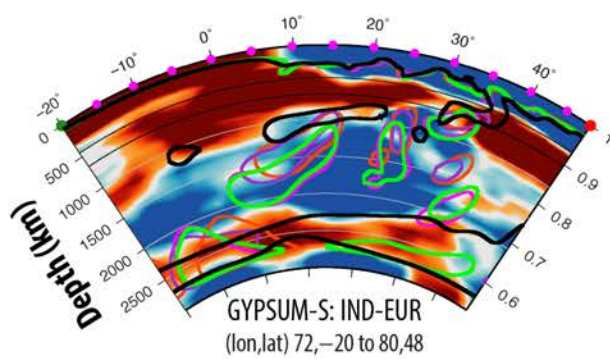
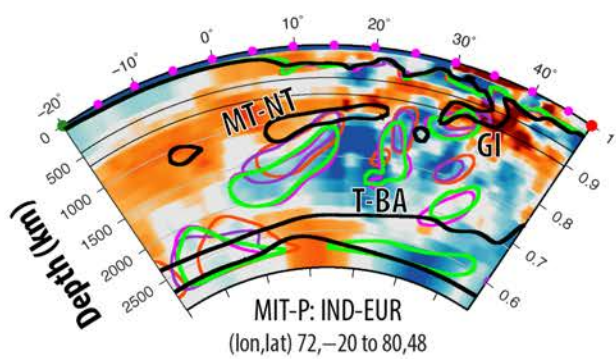


Fig. 29. Reconstructed representative profile through Australia and New Guinea, highlighting that the revised plate reconstructions account for additional slab volumes above mid-mantle depths. The southernmost slab is related to the subduction of the Sepik oceanic gateway (SEP) between ~71 and

1791 30 Ma, while Maramuni subduction (MS) has taken place since ~20 Ma, coeval with north-dipping
1792 subduction along the Halmahera Arc to produce the Caroline/Proto Molucca slab (CS). See
1793 Supplementary Animation 11.

1794

1795



- Case 1
- Case 2
- Case 3
- Case 4
- Case 5

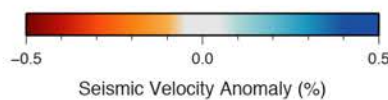


Fig. 30. Present-day mantle structure along vertical slices through India (IND-EUR), northwest Sumatra (SUM), eastern Sundaland (SUN) and Australia-New Guinea (PNG) using P- and S-wave seismic tomography models, superimposed with the predicted slabs (coloured lines) from five computations of mantle flow. Case 1 to 4 uses the Zahirovic et al. (2014) plate reconstruction, but varies the radial viscosity profile of the mantle. Case 5 uses the plate reconstruction presented in this study, and the preferred viscosity structure used in Case 4. Slabs from the numerical models are defined as regions 10% colder than the background mantle temperature. The P-wave seismic tomographic models used are the MIT-P (Li et al., 2008), GAP_P4 (Obayashi et al., 2013) and LLNL-G3Dv3 (Simmons et al., 2015). Both P- and S-wave models from Simmons et al. (2010) are used, as well as the S-wave model from Grand (2002). The x-axis of the vertical section represents latitude. Table 4 lists the differences between Cases 1 to 5. The start and end coordinates for each profile are included on each cross-section, and plotted geographically in Figs. 26-29 and Supplementary Fig. 2.

6 Discussion

We have demonstrated the strength of using coupled plate tectonic reconstructions and numerical models of mantle flow to test competing kinematic scenarios in the absence of preserved seafloor spreading histories. In addition, the global nature of the models removes the edge effects associated with Cartesian box models of mantle convection, and allows us to track the origin and trajectory of sinking slabs, and therefore their sinking rates, which can then be compared to the mantle structure interpreted from P- and S-wave seismic tomography (Fig. 30).

6.1 Intra-oceanic subduction in the Meso- and Neo-Tethys

In the India-Eurasia segment of the Tethyan margin, a number of important geodynamic implications arise from the Neo-Tethyan seafloor spreading history and the evolution of intra-oceanic

1822 subduction zones along southern Eurasia. Although early plate reconstructions of the Tethys
1823 incorporated intra-oceanic subduction and an initial collision between Greater India and the Kohistan-
1824 Ladakh Arc at or before ~53 Ma (Patriat and Achache, 1984), this two-stage India-Eurasia collision
1825 scenario was abandoned based on subsequent work that argued that Kohistan and Ladakh first
1826 collided with Eurasia in the Late Cretaceous along the Shyok Suture Zone (Clift et al., 2002; Debon
1827 et al., 1987; Treloar et al., 1996). However, recent work requires near-equatorial position of the
1828 Kohistan-Ladakh Arc in the Late Cretaceous (Burg, 2011; Chatterjee et al., 2013; Zaman et al., 2013;
1829 Zaman and Torii, 1999), and an initial arc-continent collision between Greater India and the Neo-
1830 Tethyan intra-oceanic arc sometime between ~60 and 50 Ma (Aitchison et al., 2007; Bouilhol et al.,
1831 2013; Khan et al., 2009). Our results favour a ~60 Ma arc-continent collision if the near-equatorial
1832 paleo-latitudes of Kohistan-Ladakh are robust, as a younger collision requires more significant
1833 advance of the Kohistan-Ladakh intra-oceanic trench before Greater India enters the subduction zone,
1834 terminating the subduction of oceanic lithosphere. The Kohistan-Ladakh back-arc basin was then
1835 subducted along southern Lhasa at an Andean-style margin, with final Shyok suturing occurring by
1836 40 Ma (Bouilhol et al., 2013; Gibbons et al., 2015; Zahirovic et al., 2014).

1837 The geodynamic implications of a well-established intra-oceanic system in the Neo-Tethys,
1838 suggest a scenario that is much like the present-day Izu-Bonin-Mariana Arc in the west Pacific. The
1839 paleo-latitudinal position of the intra-oceanic arc largely determines the timing of Neo-Tethyan ridge
1840 subduction, as well as the plate driving forces acting on the Indian Plate. In our reconstruction, the
1841 Neo-Tethyan mid-oceanic ridge is consumed at the Kohistan-Ladakh subduction zone from ~105 Ma
1842 (Figs. 11 and 26c,j). Subduction of the southern Neo-Tethyan flank of the spreading system from
1843 ~100 Ma would have been associated with progressively strengthening northward slab pull, to which
1844 we attribute the change towards largely northward convergence with Eurasia that is best represented
1845 by the ~110-90 Ma fracture zone bends in the Wharton Basin (Gibbons et al., 2015; Matthews et al.,
1846 2011; Matthews et al., 2012).

1847 The role of two coeval north-dipping subduction zones in the Neo-Tethys (Fig. 26) were
1848 suggested to have contributed to the ~80 Ma acceleration of India in Gibbons et al. (2015), which has
1849 recently been proposed as a mechanism for India's rapid northward advance using numerical
1850 techniques quantifying plate driving forces in Jagoutz et al. (2015). Although the arrival of the
1851 Reunion Plume head south of India at ~65 Ma possibly played a role in India's acceleration (Cande
1852 and Stegman, 2011; van Hinsbergen et al., 2011), the effects were likely short-lived (~5-10 Myr), and
1853 post-date by 15 Myr the initial acceleration of India from ~80 Ma. India's northward acceleration
1854 resulting from greater slab pull (and slab suction) may have induced stronger large-scale mantle return
1855 flow, possibly triggering the ascent of the Reunion Plume from the margin of the lower mantle
1856 African super-swell (Fig. 25). The recent data compilations of the surface geology, as well as new
1857 plate reconstructions and numerical approaches, suggest that a two-stage collision between India and
1858 Eurasia is more likely than a single continent-continent collision, and that the Tethyan tectonic
1859 evolution was punctuated by generations of back-arc basins and intra-oceanic subduction systems
1860 more similar to the present-day West Pacific, than a simpler long-lived Andean-style margin.

1861

1862 **6.2 Southeast Asia and New Guinea**

1863

1864 Southeast Asia, and in particular Sundaland and New Guinea, played an important role in the
1865 convergence history of Australia, Eurasia and the Pacific. In this study we have shown that our plate
1866 reconstructions are compatible, at least to the first-order, with fast seismic anomalies imaged by
1867 seismic tomography. In particular, the numerical methods suggest that the extrusion and clockwise
1868 rotation of Indochina from ~30 Ma is likely responsible for the Sunda slab kink beneath west Sumatra.
1869 The models reproduce the depth of the Sunda slab beneath Sumatra and Borneo, which supports
1870 subduction initiation from ~65 Ma, rather than from ~45 Ma (Hall, 2012). If the 1600 km deep Sunda
1871 slab represents subduction since 45 Ma (Hall and Spakman, 2015), then an average whole-mantle
1872 sinking rate of 3.5 cm/yr is required, while our post-65 Ma subduction history would require average

sinking rates of 2.5 cm/yr, which is more consistent with previous studies of sinking rates in numerical models (Butterworth et al., 2014; Steinberger et al., 2012). The constraints from the subduction-related volcanic history of Sumatra (McCourt et al., 1996) result in a predicted slab that is consistent with P- and S-wave tomography. This highlights that segmentation of the Neo-Tethyan and Indian Ocean plates across pre-existing structural fabric (Hall, 2012) is not required to account for the subduction history recorded on the Sumatra-Java Sundaland margin. Although Hall and Spakman (2015) invoke a leaky transform in the Neo-Tethys at $\sim 90^\circ\text{E}$ (Fig. 4c) to explain a possible $\sim 90\text{-}45$ Ma subduction hiatus, the mantle discontinuity linked to this interpretation is much further east at 110°E . There is a clearer discontinuity in slab structure east of $\sim 120^\circ\text{E}$ (Fig. 24), which represents the complex subduction history of New Guinea that is possibly linked to the evolution of the Philippine Sea Plate and the Pacific, rather than Sundaland.

The relatively small slabs predicted at ~ 600 to 1000 km depth beneath northern Borneo in our models roughly correspond to the interpreted Proto South China Sea slab (Zahirovic et al., 2014) imaged in seismic tomography at shallower depths in the mantle transition zone (~ 410 to 660 km). This suggests that Proto South China Sea subduction along northern Borneo may have started later than 45 Ma, which would be consistent with a shallower slab, and perhaps linked to a ~ 32 Ma onset in seafloor spreading of the South China Sea (Briais et al., 1993). However, a major phase of volcanism along northern Borneo from ~ 50 Ma (Soeria-Atmadja et al., 1999) might instead indicate earlier subduction initiation. In this case, stagnation of the Proto South China Sea slab in the mantle transition zone could play an important role in the depth mismatch between our numerical experiments and the seismic tomographic constraints. Recent backward-advection modelling by Yang et al. (2016) suggests that the large volume of subducted slab beneath Sundaland stagnated in the mantle transition zone before ~ 30 Ma, and entered the lower mantle as a slab avalanche in the Miocene from ~ 20 Ma. This work highlights the time-varying slab sinking rates in the region, but more importantly, demonstrates that a slab avalanche resulted in dynamic subsidence of Sundaland and flooding (Yang et al., 2016) that was asynchronous with global eustasy (Haq et al., 1987). In

1899 addition, the slab avalanche was likely responsible for Miocene basin inversions (Doust and Sumner,
1900 2007) by propagating stresses acting on the lithosphere. Since Proto South China Sea subduction
1901 ceased at ~15 Ma, recorded by cessation of seafloor spreading in the South China Sea (Briais et al.,
1902 1993), it is therefore likely that the Proto South China Sea slab is in the upper mantle or transition
1903 zone when considering the role of slab stagnation in this region. This interpretation is in contrast with
1904 that of Hall and Spakman (2015) who argued for a lower mantle (~1200 km deep) position of the
1905 Proto South China Sea slab.

1906 Further east on New Guinea, the complexity of the surface geology has led to competing plate
1907 tectonic reconstruction scenarios (van Ufford and Cloos, 2005), some of which are discussed in this
1908 study. Our plate reconstructions and numerical experiments of mantle flow require Sepik oceanic
1909 gateway subduction in the Late Cretaceous, likely from ~70 Ma, which accounts for the present-day
1910 slab at mid-mantle depths at ~30°S beneath Lake Eyre in northern South Australia, consistent with
1911 recent interpretations (Schellart and Spakman, 2015). However, the slab our mantle flow model
1912 predicts is smaller, which raises the possibility that the Sepik oceanic basin was larger than modelled
1913 in our plate reconstructions. The refinement to the plate reconstructions and inclusion of south-
1914 dipping Maramuni Arc subduction along New Guinea from ~20 to 6 Ma, with coeval north-dipping
1915 subduction along the Halmahera Arc, improves the fit between predicted slab distributions and the
1916 mantle structure inferred from seismic tomography. We interpret the presently-inactive Trobriand
1917 Trough as the Maramuni Arc subduction zone (active ~18 to 8 Ma). The Maramuni subduction may
1918 have caused the dynamic subsidence and progressive flooding inferred for the northern Australian
1919 shelf since the Oligocene (DiCaprio et al., 2009; DiCaprio et al., 2011; Sandiford, 2007; Spasojevic
1920 and Gurnis, 2012). Although our results reproduce the Sepik and Maramuni slabs, more work is
1921 required to account for a consistently-imaged near-equatorial slab at ~1500 km depths that is not
1922 reproduced by either of the plate reconstruction scenarios presented in this study. Further work using
1923 numerical techniques is required to improve the understanding of the complex tectonic linkage
1924 between Southeast Asia and the Pacific through New Guinea.

1925

1926 **6.3 Relevance to global plate reconstructions and geodynamics**

1927

1928 Our coupled plate kinematic and numerical geodynamic approach has wider implications for
1929 understanding the long-term evolution of the plate-mantle system. One important outcome is that
1930 numerical models testing alternative plate reconstruction scenarios that are compared to mantle
1931 structure from seismic tomography should consider the regional and global plate tectonic evolution.
1932 The evolution of Neo-Tethyan intra-oceanic subduction along the Kohistan-Ladakh and Woyla arc
1933 systems also has wider geodynamic implications. Although we implemented subduction initiation at
1934 the passive margin of the back-arc systems, a more complicated geodynamic mechanism may be
1935 required, such as the inversion of a mid-oceanic ridge to become a subduction zone in order to
1936 accommodate convergence and explain ophiolite obduction (Hébert et al., 2012; Shemenda, 1993).
1937 Due to the paucity of data constraining the nature and location of subduction initiation of the Woyla
1938 back-arc basin, a south-dipping subduction zone as proposed by Morley (2012a) will also require
1939 testing in future work. However, India’s Late Cretaceous northward acceleration from two coeval
1940 and coupled north-dipping subduction zones (Jagoutz et al., 2015) may also require two north-dipping
1941 subduction zones in the Woyla segment of the Neo-Tethyan active margin, which highlights the
1942 prevalence of intra-oceanic subduction in the Neo-Tethys.

1943 **7 Conclusions**

1944

1945 This study shows the power of considering the coupled plate-mantle system to study the
1946 geodynamics of the Tethyan tectonic domain that is dominated by long-term Eurasian, Indo-
1947 Australian and Pacific convergence following Pangea breakup. The reconstructions, used as boundary
1948 conditions in mantle flow simulations, consider intra-oceanic subduction along the entire south
1949 Eurasian active margin from ~160 Ma in the Neo-Tethys. We suggest that the Neo-Tethyan ridge was

likely consumed along the Kohistan-Ladakh intra-oceanic arc from ~105 Ma, followed by northward subduction of the Indian Plate that significantly modified India's plate motion direction. For Sundaland, a tectonic scenario with Woyla Arc accretion at ~75-70 Ma, followed by a ~10 Myr subduction hiatus, and renewed subduction along the south Sundaland margin by ~60 Ma places the Sunda slab at the same depth as in P- and S-wave seismic tomography. In addition, our results suggest that a slab beneath northern Borneo, which is likely stagnant in the mantle transition zone, could be a remnant of the Proto South China Sea. Further east along New Guinea, the plate reconstructions coupled to geodynamic experiments are consistent with north-dipping subduction along the Halmahera Arc coeval with the ~20 Ma onset of south-dipping Maramuni subduction along New Guinea. The Late Cretaceous (~71 Ma) onset of Sepik oceanic basin subduction, followed by the docking of the Sepik composite terrane to southern New Guinea by ~30 Ma, produces a mid-mantle slab imaged in tomography beneath Lake Eyre in Australia, as discussed in Schellart and Spakman (2015), due to the combination of southward mantle flow and Australia's northward advance towards the Southeast Asian slab burial grounds.

We present testable and reproducible plate reconstructions with regional refinements and improvements to the understanding of post-Jurassic eastern Tethyan geodynamics. The reconstructions may form the basis of future work to better understand the tectonics of the Tethyan domain, and could also be used to study oceanic circulation, long-term climate change and biogeographic dispersal pathways. In addition, our work highlights the need for testing competing plate reconstruction scenarios using numerical modelling approaches in a global and geodynamic framework.

Acknowledgements

N.F. and R.D.M. were supported by ARC grants DP130101946 and Statoil ASA through ARCIH130200012, S.Z. by ARC grant IH130200012, M.S. by ARC grant FT130101564, K.J.M. by ARC grant DP130101946. M.G. was supported by Statoil ASA and by the NSF through EAR-

1161046 and EAR-1247022. K.C.H. was supported by Oil Search Limited. This research was undertaken with the assistance of resources from the National Computational Infrastructure (NCI), which is supported by the Australian Government. We are grateful to John Cannon, Michael Chin, Robin Watson, Mark Turner, James Boyden and James Clark for their help in developing the open-source community plate reconstruction software GPLates, as well as relevant workflows. We thank Michael G. Tetley for providing technical support and workflow enhancement that improved the management of seafloor isochrons and other GPLates-related geometries, and Tobias Pfaffelmoser for help with implementing the GPLates 3D functionality. We are also grateful to Luke Mahoney for helpful discussions that improved the manuscript. We thank the Editor, Robert Holm and Bernhard Steinberger for constructive reviews. This work was conducted within the industry linkage and collaborative framework of the Basin GENeSIS Industrial Transformation Research Hub. The full supplement can be downloaded from ftp://ftp.earthbyte.org/Data_Collections/Zahirovic_etal_ESR_EasternTethys_Supplement.zip.

References

Abrajevitch, A., van der Voo, R., Bazhenov, M.L., Levashova, N.M. and McCausland, P.J.A., 2008. The role of the Kazakhstan orocline in the late Paleozoic amalgamation of Eurasia. *Tectonophysics*, 455(1): 61-76.

Acharyya, S.K., 1998. Break-up of the greater Indo-Australian continent and accretion of blocks framing south and east Asia. *Journal of Geodynamics*, 26(1): 149-170.

Aitchison, J.C., Ali, J.R. and Davis, A.M., 2007. When and where did India and Asia collide? *Journal of Geophysical Research*, 112(B05423): 1-19.

Aitchison, J.C., Davis, A.M., Liu, J., Luo, H., Malpas, J.G., McDermid, I.R.C., Wu, H., Ziabrev, S.V. and Zhou, M., 2000. Remnants of a Cretaceous intra-oceanic subduction system within the Yarlung-Zangbo suture (southern Tibet). *Earth and Planetary Science Letters*, 183(1-2): 231-244.

Alisic, L., Gurnis, M., Stadler, G., Burstedde, C. and Ghattas, O., 2012. Multi - scale dynamics and rheology of mantle flow with plates. *Journal of Geophysical Research: Solid Earth* 117(B10).

Alisic, L., Gurnis, M., Stadler, G., Burstedde, C., Wilcox, L.C. and Ghattas, O., 2010. Slab stress and strain rate as constraints on global mantle flow. *Geophysical Research Letters*, 37(22).

Amante, C., Eakins, B.W. and Boulder, C., 2009. ETOPO1 1 arc-minute global relief model: Procedures, data sources and analysis. NOAA Technical Memorandum.

Audley-Charles, M.G., 1966. Mesozoic palaeogeography of Australasia. *Palaeogeography, Palaeoclimatology, Palaeoecology*, 2: 1-25.

- 2012 Audley-Charles, M.G., 1988. Evolution of the southern margin of Tethys (North Australian region)
2013 from early Permian to late Cretaceous. Geological Society, London, Special Publications,
2014 37(1): 79-100.
- 2015 Audley-Charles, M.G., Ballantyne, P.D. and Hall, R., 1988. Mesozoic-Cenozoic Rift-Drift
2016 Sequence of Asian Fragments from Gondwanaland. Tectonophysics, 155(1-4): 317-330.
- 2017 Baldwin, S.L., Fitzgerald, P.G. and Webb, E.W., 2012. Tectonics of the New Guinea Region. Annu.
2018 Rev. Earth Planet. Sci., 40: 495-520.
- 2019 Balmino, G., Vales, N., Bonvalot, S. and Briais, A., 2012. Spherical harmonic modelling to ultra-
2020 high degree of Bouguer and isostatic anomalies. Journal of Geodesy, 86(7): 499-520.
- 2021 Barber, A.J. and Crow, M.J., 2003. An evaluation of plate tectonic models for the development of
2022 Sumatra. Gondwana Research, 6(1): 1-28.
- 2023 Baumann, T.S. and Kaus, B.J.P., 2015. Geodynamic inversion to constrain the non-linear rheology
2024 of the lithosphere. Geophysical Journal International, 202(2): 1289-1316.
- 2025 Baxter, A.T., Aitchison, J.C., Ziyabrev, S.V. and Ali, J.R., 2011. Upper Jurassic radiolarians from
2026 the Naga ophiolite, Nagaland, northeast India. Gondwana Research, 20(2): 638-644.
- 2027 Becker, T., Schaeffer, A., Lebedev, S. and Conrad, C., 2015. Toward a generalized plate motion
2028 reference frame. Geophysical Research Letters, 42(9): 3188-3196.
- 2029 Becker, T.W., 2006. On the effect of temperature and strain-rate dependent viscosity on global
2030 mantle flow, net rotation, and plate-driving forces. Geophysical Journal International,
2031 167(2): 943-957.
- 2032 Becker, T.W. and Faccenna, C., 2011. Mantle conveyor beneath the Tethyan collisional belt. Earth
2033 and Planetary Science Letters, 310(3, Åì4): 453-461.
- 2034 Bergman, S.C., Coffield, D.Q., Talbot, J.P. and Garrard, R.A., 1996. Tertiary tectonic and
2035 magmatic evolution of western Sulawesi and the Makassar Strait, Indonesia: evidence for a
2036 Miocene continent-continent collision. Geological Society, London, Special Publications,
2037 106(1): 391-429.
- 2038 Besse, J. and Courtillot, V., 1988. Paleogeographic maps of the continents bordering the Indian
2039 Ocean since the Early Jurassic. Journal of Geophysical Research: Solid Earth (1978–2012),
2040 93(B10): 11791-11808.
- 2041 Bijwaard, H. and Spakman, W., 2000. Non-linear global P-wave tomography by iterated linearized
2042 inversion. Geophysical Journal International, 141(1): 71-82.
- 2043 Bijwaard, H., Spakman, W. and Engdahl, E., 1998. Closing the gap between regional and global
2044 travel time tomography. Journal of Geophysical Research, 103(B12): 30055.
- 2045 Bird, P., 2003. An updated digital model of plate boundaries. Geochemistry, Geophysics,
2046 Geosystems, 4(3): 1-52.
- 2047 Bouilhol, P., Jagoutz, O., Hanchar, J.M. and Dudas, F.O., 2013. Dating the India–Eurasia collision
2048 through arc magmatic records. Earth and Planetary Science Letters, 366: 163-175.
- 2049 Bouilhol, P., Schaltegger, U., Chiaradia, M., Ovtcharova, M., Stracke, A., Burg, J.-P. and Dawood,
2050 H., 2011. Timing of juvenile arc crust formation and evolution in the Sapat Complex
2051 (Kohistan–Pakistan). Chemical Geology, 280(3): 243-256.
- 2052 Bower, D., Gurnis, M. and Seton, M., 2013. Lower mantle structure from paleogeographically
2053 constrained dynamic Earth models. Geochemistry, Geophysics, Geosystems, 14(1): 44-63.
- 2054 Bower, D.J., Gurnis, M. and Flament, N., 2015. Assimilating lithosphere and slab history in 4-D
2055 dynamic Earth models. Physics of the Earth and Planetary Interiors, 238: 8-22.
- 2056 Boyden, J., Müller, R., Gurnis, M., Torsvik, T., Clark, J., Turner, M., Ivey-Law, H., Watson, R. and
2057 Cannon, J., 2011. Next-generation plate-tectonic reconstructions using GPlates. In: G.
2058 Keller and C. Barz (Editors), Geoinformatics: Cyberinfrastructure for the Solid Earth
2059 Sciences. Cambridge University Press, Cambridge, UK, pp. 95-114.
- 2060 Briais, A., Patriat, P. and Tapponnier, P., 1993. Updated interpretation of magnetic anomalies and
2061 seafloor spreading stages in the South China Sea: implications for the Tertiary tectonics of
2062 Southeast Asia. Journal of Geophysical Research, 98(B4): 6299-6328.

- 2063 Brown, G.F., 1951. Geologic reconnaissance of the mineral deposits of Thailand. US Government
2064 Printing Office.
- 2065 Bunge, H.-P., Hagelberg, C. and Travis, B., 2003. Mantle circulation models with variational data
2066 assimilation: inferring past mantle flow and structure from plate motion histories and
2067 seismic tomography. *Geophysical Journal International*, 152(2): 280-301.
- 2068 Bunge, H.-P., Richards, M. and Baumgardner, J., 2002. Mantle–circulation models with sequential
2069 data assimilation: inferring present–day mantle structure from plate–motion histories.
2070 *Philosophical Transactions of the Royal Society of London A: Mathematical, Physical and*
2071 *Engineering Sciences*, 360(1800): 2545-2567.
- 2072 Burg, J.P., 2011. The Asia–Kohistan–India Collision: Review and Discussion. In: D. Brown and P.
2073 Ryan (Editors), *Arc-Continent Collision. Frontiers in Earth Sciences*. Springer-Verlag
2074 Berlin, pp. 279-309.
- 2075 Burg, J.P., Jagoutz, O., Dawood, H. and Hussain, S.S., 2006. Precollision tilt of crustal blocks in
2076 rifted island arcs: structural evidence from the Kohistan Arc. *Tectonics*, 25(5).
- 2077 Burke, K. and Dewey, J., 1973. Plume-generated triple junctions: key indicators in applying plate
2078 tectonics to old rocks. *The Journal of Geology*: 406-433.
- 2079 Burrett, C., Duhid, N., Berry, R. and Varne, R., 1991. Asian and south-western Pacific continental
2080 terranes derived from Gondwana, and their biogeographic significance. *Australian*
2081 *Systematic Botany*, 4(1): 13-24.
- 2082 Butterworth, N., Talsma, A., Müller, R., Seton, M., Bunge, H.-P., Schuberth, B., Shephard, G. and
2083 Heine, C., 2014. Geological, tomographic, kinematic and geodynamic constraints on the
2084 dynamics of sinking slabs. *Journal of Geodynamics*, 73: 1-13.
- 2085 Cameron, N.R., Clarke, M.C.G., Aldiss, D.T., Aspden, J.A. and Djunuddin, A., 1980. The
2086 geological evolution of northern Sumatra.
- 2087 Cande, S.C. and Patriat, P., 2015. The anticorrelated velocities of Africa and India in the Late
2088 Cretaceous and early Cenozoic. *Geophysical Journal International*, 200(1): 227-243.
- 2089 Cande, S.C., Patriat, P. and Dymant, J., 2010. Motion between the Indian, Antarctic and African
2090 plates in the early Cenozoic. *Geophysical Journal International*(183): 127-149.
- 2091 Cande, S.C. and Stegman, D.R., 2011. Indian and African plate motions driven by the push force of
2092 the Reunion plume head. *Nature*, 475(7354): 47-52.
- 2093 Capitanio, F.A., Morra, G., Goes, S., Weinberg, R.F. and Moresi, L., 2010. India–Asia convergence
2094 driven by the subduction of the Greater Indian continent. *Nature Geoscience*, 3(2): 136-139.
- 2095 Carey, S.W., 1955. The orocline concept in geotectonics-Part I, Papers and proceedings of the
2096 Royal Society of Tasmania, pp. 255-288.
- 2097 Carlson, R. and Mortera-Gutiérrez, C., 1990. Subduction hinge migration along the Izu-Bonin-
2098 Mariana arc. *Tectonophysics*, 181(1-4): 331-344.
- 2099 Charlton, T.R., 2001. Permo-Triassic evolution of Gondwanan eastern Indonesia, and the final
2100 Mesozoic separation of SE Asia from Australia. *Journal of Asian Earth Sciences*, 19(5):
2101 595-617.
- 2102 Chatterjee, S., Goswami, A. and Scotese, C.R., 2013. The longest voyage: tectonic, magmatic, and
2103 paleoclimatic evolution of the Indian plate during its northward flight from Gondwana to
2104 Asia. *Gondwana Research*, 23(1): 238-267.
- 2105 Chung, S.L., Chu, M.F., Zhang, Y., Xie, Y., Lo, C.H., Lee, T.Y., Lan, C.Y., Li, X., Zhang, Q. and
2106 Wang, Y., 2005. Tibetan tectonic evolution inferred from spatial and temporal variations in
2107 post-collisional magmatism. *Earth-Science Reviews*, 68(3-4): 173-196.
- 2108 Clements, B., Burgess, P.M., Hall, R. and Cottam, M.A., 2011. Subsidence and uplift by slab-
2109 related mantle dynamics: a driving mechanism for the Late Cretaceous and Cenozoic
2110 evolution of continental SE Asia? *Geological Society, London, Special Publications*, 355(1):
2111 37-51.
- 2112 Clements, B. and Hall, R., 2007. Cretaceous to Late Miocene stratigraphic and tectonic evolution of
2113 West Java. *Indonesian Petroleum Association Proceedings*, 31(IPA07-G-037): 1-18.

- 2114 Clements, B. and Hall, R., 2011. A record of continental collision and regional sediment flux for the
2115 Cretaceous and Palaeogene core of SE Asia: implications for early Cenozoic
2116 palaeogeography. *Journal of the Geological Society*, 168: 1187-1200.
- 2117 Clift, P.D., Hannigan, R., Blusztajn, J. and Draut, A.E., 2002. Geochemical evolution of the Dras–
2118 Kohistan Arc during collision with Eurasia: evidence from the Ladakh Himalaya, India.
2119 *Island Arc*, 11(4): 255-273.
- 2120 Conrad, C.P. and Gurnis, M., 2003. Seismic tomography, surface uplift, and the breakup of
2121 Gondwanaland: Integrating mantle convection backwards in time. *Geochemistry*,
2122 *Geophysics, Geosystems*, 4(3).
- 2123 Conrad, C.P. and Lithgow - Bertelloni, C., 2004. The temporal evolution of plate driving forces:
2124 Importance of “slab suction” versus “slab pull” during the Cenozoic. *Journal of*
2125 *Geophysical Research: Solid Earth*, 109(B10).
- 2126 Crowhurst, P.V., Hill, K.C., Foster, D.A. and Bennett, A., 1996. Thermochronological and
2127 geochemical constraints on the tectonic evolution of northern Papua New Guinea.
2128 *Geological Society Special Publications*, 106(Tectonic Evolution of Southeast Asia): 525-
2129 537.
- 2130 Cullen, A.B., 2010. Transverse segmentation of the Baram-Balabac Basin, NW Borneo: refining the
2131 model of Borneo's tectonic evolution. *Petroleum Geoscience*, 16(1): 3-29.
- 2132 Daly, M.C., Cooper, M.A., Wilson, I., Smith, D.G. and Hooper, B.G.D., 1991. Cenozoic plate
2133 tectonics and basin evolution in Indonesia. *Marine and Petroleum Geology*, 8(1): 2-21.
- 2134 Davies, H.L., 2012. The geology of New Guinea-the cordilleran margin of the Australian continent.
2135 *Episodes*, 35(1): 87-102.
- 2136 de Bruyn, M., Stelbrink, B., Morley, R.J., Hall, R., Carvalho, G.R., Cannon, C.H., van den Bergh,
2137 G., Meijaard, E., Metcalfe, I. and Boitani, L., 2014. Borneo and Indochina are major
2138 evolutionary hotspots for Southeast Asian biodiversity. *Systematic biology*, 63(6): 879-901.
- 2139 Debayle, E. and Ricard, Y., 2013. Seismic observations of large-scale deformation at the bottom of
2140 fast-moving plates. *Earth and Planetary Science Letters*, 376: 165-177.
- 2141 Debon, F., Le Fort, P., Dautel, D., Sonet, J. and Zimmermann, J.L., 1987. Granites of western
2142 Karakorum and northern Kohistan (Pakistan): a composite Mid-Cretaceous to upper
2143 Cenozoic magmatism. *Lithos*, 20(1): 19-40.
- 2144 Deng, J., Yang, X., Zhang, Z.-F. and Santosh, M., 2015. Early Cretaceous arc volcanic suite in
2145 Cebu Island, Central Philippines and its implications on paleo-Pacific plate subduction:
2146 Constraints from geochemistry, zircon U–Pb geochronology and Lu–Hf isotopes. *Lithos*,
2147 230: 166-179.
- 2148 Deschamps, A. and Lallemand, S., 2002. The West Philippine Basin: An Eocene to early Oligocene
2149 back arc basin opened between two opposed subduction zones. *Journal of Geophysical*
2150 *Research: Solid Earth* (1978–2012), 107(B12): EPM 1-1-EPM 1-24.
- 2151 DiCaprio, L., Gurnis, M. and Müller, R.D., 2009. Long-wavelength tilting of the Australian
2152 continent since the Late Cretaceous. *Earth and Planetary Science Letters*, 278(3-4): 175-185.
- 2153 DiCaprio, L., Gurnis, M., Müller, R.D. and Tan, E., 2011. Mantle dynamics of continentwide
2154 Cenozoic subsidence and tilting of Australia. *Lithosphere*: L140. 1v1.
- 2155 Doglioni, C., 1991. A proposal for the kinematic modelling of W - dipping subductions - possible
2156 applications to the Tyrrhenian - Apennines system. *Terra Nova*, 3(4): 423-434.
- 2157 Domeier, M. and Torsvik, T.H., 2014. Plate tectonics in the late Paleozoic. *Geoscience Frontiers*,
2158 5(3): 303-350.
- 2159 Doust, H. and Sumner, H.S., 2007. Petroleum systems in rift basins—a collective approach
2160 in Southeast Asian basins. *Petroleum Geoscience*, 13(2): 127-144.
- 2161 Dow, D.B., 1977. A geological synthesis of Papua New Guinea, 201. Bureau of Mineral Resources,
2162 Australian Government Publishing Service.
- 2163 Elburg, M., van Leeuwen, T. and Foden, J., 2003. Spatial and temporal isotopic domains of
2164 contrasting igneous suites in Western and Northern Sulawesi, Indonesia. *Chemical Geology*,
2165 199(3): 243-276.

- 2166 Eldredge, S., Bachtadse, V. and van der Voo, R., 1985. Paleomagnetism and the orocline
2167 hypothesis. *Tectonophysics*, 119(1): 153-179.
- 2168 Encarnación, J., 2004. Multiple ophiolite generation preserved in the northern Philippines and the
2169 growth of an island arc complex. *Tectonophysics*, 392(1): 103-130.
- 2170 Faccenna, C., Becker, T.W., Lallemand, S. and Steinberger, B., 2012. On the role of slab pull in the
2171 Cenozoic motion of the Pacific plate. *Geophysical Research Letters*, 39(3).
- 2172 Fairbridge, R.W., 1963. The Indian Ocean and the status of Gondwanaland. *Progress in*
2173 *Oceanography*, 3: 83-136.
- 2174 Findlay, R.H., 2003. Collision tectonics of northern Papua New Guinea: key field relationships
2175 demand a new model. *Geological Society of America Special Papers*, 372: 291-307.
- 2176 Fitch, T.J., 1972. Plate convergence, transcurrent faults, and internal deformation adjacent to
2177 southeast Asia and the western Pacific. *Journal of Geophysical Research*, 77(23): 4432-
2178 4460.
- 2179 Fjeldskaar, W., Lindholm, C., Dehls, J.F. and Fjeldskaar, I., 2000. Postglacial uplift, neotectonics
2180 and seismicity in Fennoscandia. *Quaternary Science Reviews*, 19(14-15): 1413-1422.
- 2181 Flament, N., Gurnis, M., Müller, R.D., Bower, D.J. and Husson, L., 2015. Influence of subduction
2182 history on South American topography. *Earth and Planetary Science Letters*, 430: 9-18.
- 2183 Flament, N., Gurnis, M., Williams, S., Seton, M., Skogseid, J., Heine, C. and Müller, R.D., 2014.
2184 Topographic asymmetry of the South Atlantic from global models of mantle flow and
2185 lithospheric stretching. *Earth and Planetary Science Letters*, 387: 107-119.
- 2186 Flower, M.F.J. and Dilek, Y., 2003. Arc-trench rollback and forearc accretion: 1. A collision-
2187 induced mantle flow model for Tethyan ophiolites. *Geological Society, London, Special*
2188 *Publications*, 218(1): 21-41.
- 2189 Forsyth, D. and Uyeda, S., 1975. On the relative importance of the driving forces of plate motion.
2190 *Geophysical Journal International*, 43(1): 163-200.
- 2191 Forte, A.M. and Mitrovica, J.X., 1996. New inferences of mantle viscosity from joint inversion of
2192 long - wavelength mantle convection and post - glacial rebound data. *Geophysical Research*
2193 *Letters*, 23(10): 1147-1150.
- 2194 Foulger, G.R., Panza, G.F., Artemieva, I.M., Bastow, I.D., Cammarano, F., Evans, J.R., Hamilton,
2195 W.B., Julian, B.R., Lustrino, M. and Thybo, H., 2013. Caveats on tomographic images.
2196 *Terra Nova*, 25(4): 259-281.
- 2197 Fuller, M., Ali, J.R., Moss, S.J., Frost, G.M., Richter, B. and Mahfi, A., 1999. Paleomagnetism of
2198 Borneo. *Journal of Asian Earth Sciences*, 17(1-2): 3-24.
- 2199 Fuller, M., Haston, R., Lin, J.-L., Richter, B., Schmidtke, E. and Almasco, J., 1991. Tertiary
2200 paleomagnetism of regions around the South China Sea. *Journal of Southeast Asian Earth*
2201 *Sciences*, 6(3): 161-184.
- 2202 Fyhn, M.B.W., Pedersen, S.A.S., Boldreel, L.O., Nielsen, L.H., Green, P.F., Dien, P.T., Huyen,
2203 L.T. and Frei, D., 2010. Palaeocene–early Eocene inversion of the Phuquoc–Kampot Som
2204 Basin: SE Asian deformation associated with the suturing of Luconia. *Journal of the*
2205 *Geological Society*, 167(2): 281-295.
- 2206 Gaina, C. and Müller, R.D., 2007. Cenozoic tectonic and depth/age evolution of the Indonesian
2207 gateway and associated back-arc basins. *Earth-Science Reviews*, 83(3-4): 177-203.
- 2208 Gasperini, P. and Sabadini, R., 1989. Lateral heterogeneities in mantle viscosity and post glacial
2209 rebound. *Geophysical Journal International*, 98(3): 413-428.
- 2210 Geary, E.E., Harrison, T.M. and Heizler, M., 1988. Diverse ages and origins of basement
2211 complexes, Luzon, Philippines. *Geology*, 16(4): 341-344.
- 2212 Geary, E.E. and Kay, R.W., 1989. Identification of an Early Cretaceous ophiolite in the Camarines
2213 Norte-Calaguas Islands basement complex, eastern Luzon, Philippines. *Tectonophysics*,
2214 168(1): 109-126.
- 2215 Gee, J.S. and Kent, D.V., 2007. Source of oceanic magnetic anomalies and the geomagnetic
2216 polarity time scale. *Treatise on Geophysics*, Vol. 5: Geomagnetism: 455-507.

- 2217 Ghose, R., Yoshioka, S. and Oike, K., 1990. Three-dimensional numerical simulation of the
2218 subduction dynamics in the Sunda arc region, Southeast Asia. *Tectonophysics*, 181(1): 223-
2219 255.
- 2220 Gibbons, A., Zahirovic, S., Müller, R.D., Whittaker, J. and Yatheesh, V., 2015. A tectonic model
2221 reconciling evidence for the collisions between India, Eurasia and intra-oceanic arcs of the
2222 central-eastern Tethys. *Gondwana Research FOCUS*, 28(2): 451-492.
- 2223 Gibbons, A.D., Barckhausen, U., van den Bogaard, P., Hoernle, K., Werner, R., Whittaker, J.M. and
2224 Müller, R.D., 2012. Constraining the Jurassic extent of Greater India: Tectonic evolution of
2225 the West Australian margin. *Geochemistry Geophysics Geosystems*, 13(5): 25.
- 2226 Gibbons, A.D., Whittaker, J.M. and Müller, R.D., 2013. The breakup of East Gondwana:
2227 Assimilating constraints from Cretaceous ocean basins around India into a best - fit tectonic
2228 model. *Journal of Geophysical Research: Solid Earth*, 13(5).
- 2229 Glišović, P. and Forte, A.M., 2014. Reconstructing the Cenozoic evolution of the mantle:
2230 Implications for mantle plume dynamics under the Pacific and Indian plates. *Earth and
2231 Planetary Science Letters*, 390: 146-156.
- 2232 Goldfarb, R.J., Taylor, R.D., Collins, G.S., Goryachev, N.A. and Orlandini, O.F., 2014.
2233 Phanerozoic continental growth and gold metallogeny of Asia. *Gondwana Research*, 25(1):
2234 48-102.
- 2235 Görür, N. and Sengör, A.M.C., 1992. Paleogeography and tectonic evolution of the eastern
2236 Tethysides: implications for the northwest Australian margin breakup history, *Proceedings
2237 of the Ocean Drilling Program, Scientific Results*, pp. 83-106.
- 2238 Gurlan, A.T., Meynadier, L. and Allègre, C.J., 2008. Tectonically driven changes in the Indian
2239 Ocean circulation over the last 25 Ma: Neodymium isotope evidence. *Earth and Planetary
2240 Science Letters*, 267(1): 353-364.
- 2241 Gradstein, F.M. and Ludden, J.N., 1992. Radiometric age determinations for basement from Sites
2242 765 and 766, Argo Abyssal Plain and northwestern Australian margin, *Proceedings of the
2243 ocean drilling program, Scientific Results*, pp. 557-559.
- 2244 Grand, S.P., 2002. Mantle shear-wave tomography and the fate of subducted slabs. *Philosophical
2245 Transactions of the Royal Society of London. Series A: Mathematical, Physical and
2246 Engineering Sciences*, 360(1800): 2475.
- 2247 Guillaume, B., Martinod, J., Husson, L., Roddaz, M. and Riquelme, R., 2009. Neogene uplift of
2248 central eastern Patagonia: Dynamic response to active spreading ridge subduction?
2249 *Tectonics*, 28(2).
- 2250 Guntoro, A., 1999. The formation of the Makassar Strait and the separation between SE Kalimantan
2251 and SW Sulawesi. *Journal of Asian Earth Sciences* 17: 79-98.
- 2252 Gurnis, M., Hall, C. and Lavie, L., 2004. Evolving force balance during incipient subduction.
2253 *Geochemistry, Geophysics, Geosystems*, 5: -.
- 2254 Gurnis, M., Turner, M., Zahirovic, S., DiCaprio, L., Spasojevic, S., Müller, R.D., Boyden, J., Seton,
2255 M., Manea, V.C. and Bower, D.J., 2012. Plate Tectonic Reconstructions with Continuously
2256 Closing Plates. *Computers & Geosciences*, 38(1): 35-42.
- 2257 Hafkenscheid, E., Wortel, M.J.R. and Spakman, W., 2006. Subduction history of the Tethyan
2258 region derived from seismic tomography and tectonic reconstructions. *Journal of
2259 Geophysical Research-Solid Earth*, 111(B8): B08401.
- 2260 Hager, B.H., 1984. Subducted slabs and the geoid: constraints on mantle rheology and flow. *Journal
2261 of Geophysical Research*, 89(B7): 6003-6015.
- 2262 Hager, B.H. and O'Connell, R.J., 1981. A simple global model of plate dynamics and mantle
2263 convection. *Journal of Geophysical Research: Solid Earth* (1978–2012), 86(B6): 4843-4867.
- 2264 Haile, N.S., 1979. Palaeomagnetic evidence for rotation and northward drift of Sumatra. *Journal of
2265 the Geological Society*, 136(5): 541-546.
- 2266 Haile, N.S., McElhinny, M.W. and McDougall, I., 1977. Palaeomagnetic data and radiometric ages
2267 from the Cretaceous of West Kalimantan (Borneo), and their significance in interpreting
2268 regional structure. *Journal of the Geological Society*, 133(2): 133-144.

- 2269 Halbouty, M.T., King, R.E., Klemme, H.D., Dott, S., R H and Meyerhoff, A.A., 1970. World's
2270 Giant Oil and Gas Fields, Geologic Factors Affecting Their Formation, and Basin
2271 Classification: Part II: Factors Affecting Formation of Giant Oil and Gas Fields, and Basin
2272 Classification, M 14: Geology of Giant Petroleum Fields, pp. 528-555.
- 2273 Hall, C.E., Gurnis, M., Sdrolias, M., Lavier, L.L. and Müller, R.D., 2003. Catastrophic initiation of
2274 subduction following forced convergence across fracture zones. *Earth and Planetary Science*
2275 *Letters*, 212(1): 15-30.
- 2276 Hall, R., 1996. Reconstructing Cenozoic SE Asia. Geological Society, London, Special
2277 Publications, 106(1): 153-184.
- 2278 Hall, R., 2002. Cenozoic geological and plate tectonic evolution of SE Asia and the SW Pacific:
2279 computer-based reconstructions, model and animations. *Journal of Asian Earth Sciences*,
2280 20(4): 353-431.
- 2281 Hall, R., 2011. Australia–SE Asia collision: plate tectonics and crustal flow. Geological Society,
2282 London, Special Publications, 355(1): 75-109.
- 2283 Hall, R., 2012. Late Jurassic–Cenozoic reconstructions of the Indonesian region and the Indian
2284 Ocean. *Tectonophysics*, 570-571: 1-41.
- 2285 Hall, R., Ali, J.R. and Anderson, C.D., 1995a. Cenozoic Motion of the Philippine Sea Plate -
2286 Paleomagnetic Evidence from Eastern Indonesia. *Tectonics*, 14(5): 1117-1132.
- 2287 Hall, R., Ali, J.R., Anderson, C.D. and Baker, S.J., 1995b. Origin and motion history of the
2288 Philippine Sea Plate. *Tectonophysics*, 251(1): 229-250.
- 2289 Hall, R. and Spakman, W., 2002. Subducted slabs beneath the eastern Indonesia-Tonga region:
2290 insights from tomography. *Earth and Planetary Science Letters*, 201(2): 321-336.
- 2291 Hall, R. and Spakman, W., 2003. Mantle structure and tectonic evolution of the region north and
2292 east of Australia. *Geological Society of America Special Papers*, 372: 361-381.
- 2293 Hall, R. and Spakman, W., 2015. Mantle structure and tectonic history of SE Asia. *Tectonophysics*,
2294 658: 14-45.
- 2295 Hamilton, W.B., 1979. Tectonics of the Indonesian region. US Govt. Print. Off.
- 2296 Haq, B.U., Hardenbol, J. and Vail, P.R., 1987. Chronology of fluctuating sea levels since the
2297 Triassic. *Science*, 235(4793): 1156-1167.
- 2298 Hébert, R., Bezard, R., Guilmette, C., Dostal, J., Wang, C.S. and Liu, Z.F., 2012. The Indus–
2299 Yarlung Zangbo ophiolites from Nanga Parbat to Namche Barwa syntaxes, southern Tibet:
2300 First synthesis of petrology, geochemistry, and geochronology with incidences on
2301 geodynamic reconstructions of Neo-Tethys. *Gondwana Research*, 22(2): 377-397.
- 2302 Heine, C. and Müller, R.D., 2005. Late Jurassic rifting along the Australian North West Shelf:
2303 margin geometry and spreading ridge configuration. *Australian Journal of Earth Sciences*,
2304 52(1): 27-39.
- 2305 Heine, C., Müller, R.D. and Gaina, C., 2004. Reconstructing the lost eastern Tethys ocean basin:
2306 convergence history of the SE Asian margin and marine gateways. *Continent-Ocean*
2307 *Interactions Within East Asian Marginal Seas*, Geophys. Monogr. Ser, 149: 37-54.
- 2308 Hellinger, S.J., 1981. The uncertainties of finite rotations in plate tectonics. *Journal of Geophysical*
2309 *Research: Solid Earth* (1978–2012), 86(B10): 9312-9318.
- 2310 Herold, N., Buzan, J., Seton, M., Goldner, A., Green, J.A.M., Müller, R.D., Markwick, P. and
2311 Huber, M., 2014. A suite of early Eocene (~ 55 Ma) climate model boundary conditions.
2312 *Geoscientific Model Development*, 7(5): 2077-2090.
- 2313 Hilde, T.W.C. and Chao-Shing, L., 1984. Origin and evolution of the West Philippine Basin: a new
2314 interpretation. *Tectonophysics*, 102(1): 85-104.
- 2315 Hill, K.C. and Hall, R., 2003. Mesozoic–Cenozoic evolution of Australia's New Guinea margin in a
2316 west Pacific context. *Geological Society of Australia Special Publications*, 22: 265-289.
- 2317 Hill, K.C. and Raza, A., 1999. Arc - continent collision in Papua Guinea: Constraints from fission
2318 track thermochronology. *Tectonics*, 18(6): 950-966.
- 2319 Holm, R.J., Spandler, C. and Richards, S.W., 2014. Continental collision, orogenesis and arc
2320 magmatism of the Miocene Maramuni arc, Papua New Guinea. *Gondwana Research*.

- 2321 Hopper, J.R., Mutter, J.C., Larson, R.L. and Mutter, C.Z., 1992. Magmatism and rift margin
2322 evolution: Evidence from northwest Australia. *Geology*, 20(9): 853-857.
- 2323 Hu, X., Garzanti, E., Moore, T. and Raffi, I., 2015. Direct stratigraphic dating of India-Asia
2324 collision onset at the Selandian (middle Paleocene, 59±1 Ma). *Geology*, 43(10): 859-862.
- 2325 Huber, M. and Goldner, A., 2012. Eocene monsoons. *Journal of Asian Earth Sciences*, 44: 3-23.
- 2326 Hutchison, C.S., 1975. Ophiolite in Southeast Asia. *Geological Society of America Bulletin*, 86(6):
2327 797-806.
- 2328 Hutchison, C.S., 1996. The 'Rajang accretionary prism' and 'Lupar Line' problem of Borneo.
2329 Geological Society, London, Special Publications, 106(1): 247-261.
- 2330 Hutchison, C.S., 2004. Marginal basin evolution: the southern South China Sea. *Marine and*
2331 *Petroleum Geology*, 21(9): 1129-1148.
- 2332 Hutchison, C.S., 2010. Oroclines and paleomagnetism in Borneo and South-East Asia.
2333 *Tectonophysics*, 496(1): 53-67.
- 2334 Hutchison, C.S., Bergman, S.C., Swauger, D.A. and Graves, J.E., 2000. A Miocene collisional belt
2335 in north Borneo: uplift mechanism and isostatic adjustment quantified by thermochronology.
2336 *Journal of the Geological Society*, 157(4): 783-793.
- 2337 Jagoutz, O., Macdonald, F.A. and Royden, L., 2016. Low-latitude arc-continent collision as a
2338 driver for global cooling. *Proceedings of the National Academy of Sciences*, 113(18): 4935-
2339 4940.
- 2340 Jagoutz, O., Royden, L., Holt, A.F. and Becker, T.W., 2015. Anomalously fast convergence of
2341 India and Eurasia caused by double subduction. *Nature Geoscience*, 8(6): 475-478.
- 2342 Jagoutz, O. and Schmidt, M.W., 2012. The formation and bulk composition of modern juvenile
2343 continental crust: the Kohistan arc. *Chemical Geology*, 298: 79-96.
- 2344 Jahn, B.-M., Chen, P.Y. and Yen, T.P., 1976. Rb-Sr ages of granitic rocks in southeastern China
2345 and their tectonic significance. *Geological Society of America Bulletin*, 87(5): 763-776.
- 2346 Jarvis, G.T. and Lowman, J.P., 2005. Sinking slabs below fossil subduction zones. *Physics of The*
2347 *Earth and Planetary Interiors*, 152(1-2): 103-115.
- 2348 Jarvis, G.T. and Lowman, J.P., 2007. Survival times of subducted slab remnants in numerical
2349 models of mantle flow. *Earth and Planetary Science Letters*, 260(1-2): 23-36.
- 2350 Ji, W.-Q., Wu, F.-Y., Chung, S.-L., Li, J.-X. and Liu, C.-Z., 2009. Zircon U-Pb geochronology and
2351 Hf isotopic constraints on petrogenesis of the Gangdese batholith, southern Tibet. *Chemical*
2352 *Geology*, 262(3): 229-245.
- 2353 Jolivet, L., Faccenna, C., D'Agostino, N., Fournier, M. and Worrall, D., 1999. The kinematics of
2354 back-arc basins, examples from the Tyrrhenian, Aegean and Japan Seas. Geological Society,
2355 London, Special Publications, 164(1): 21-53.
- 2356 Jolivet, L., Huchon, P. and Rangin, C., 1989. Tectonic setting of Western Pacific marginal basins.
2357 *Tectonophysics*, 160(1): 23-47.
- 2358 Katili, J.A., 1971. A review of the geotectonic theories and tectonic maps of Indonesia. *Earth-*
2359 *Science Reviews*, 7(3): 143-163.
- 2360 Katili, J.A., 1975. Volcanism and plate tectonics in the Indonesian island arcs. *Tectonophysics*,
2361 26(3): 165-188.
- 2362 Kendrick, R.D., 2000. Structure, tectonics and thermochronology of the Irian Jaya Fold Belt, Irian
2363 Jaya, Indonesia, La Trobe University.
- 2364 Khan, S.D., Walker, D.J., Hall, S.A., Burke, K.C., Shah, M.T. and Stockli, L., 2009. Did the
2365 Kohistan-Ladakh island arc collide first with India? *Geological Society of America Bulletin*,
2366 121(3-4): 366.
- 2367 Klootwijk, C., Giddings, J., Pigram, C.J., Loxton, C., Davies, H., Rogerson, R. and Falvey, D.,
2368 2003. North Sepik region of Papua New Guinea: palaeomagnetic constraints on arc
2369 accretion and deformation. *Tectonophysics*, 362: 273-301.
- 2370 Kobayashi, K., 2004. Origin of the Palau and Yap trench-arc systems. *Geophysical Journal*
2371 *International*, 157(3): 1303-1315.

- 2372 Lambeck, K., Smither, C. and Johnston, P., 1998. Sea level change, glacial rebound and mantle
2373 viscosity for northern Europe. *Geophysical Journal International*, 134(1): 102-144.
- 2374 Le Pichon, X., 1968. Sea-floor spreading and continental drift. *Journal of Geophysical Research*,
2375 73(12): 3661-3697.
- 2376 Lee, C.-T.A., Shen, B., Slotnick, B.S., Liao, K., Dickens, G.R., Yokoyama, Y., Lenardic, A.,
2377 Dasgupta, R., Jellinek, M. and Lackey, J.S., 2013. Continental arc–island arc fluctuations,
2378 growth of crustal carbonates, and long-term climate change. *Geosphere*, 9(1): 21-36.
- 2379 Lee, T.Y. and Lawver, L.A., 1994. Cenozoic plate reconstruction of the South China Sea region.
2380 *Tectonophysics*, 235(1-2): 149-180.
- 2381 Lee, T.Y. and Lawver, L.A., 1995. Cenozoic plate reconstruction of Southeast Asia.
2382 *Tectonophysics*, 251(1-4): 85-138.
- 2383 Leith, C., 1926. The mineral resources of the Far East. *Foreign Affairs*, 4(3): 433-442.
- 2384 Leng, W. and Gurnis, M., 2015. Subduction initiation at relic arcs. *Geophysical Research Letters*,
2385 42.
- 2386 Li, C., van der Hilst, R.D., Engdahl, E.R. and Burdick, S., 2008. A new global model for P wave
2387 speed variations in Earth's mantle. *Geochemistry, Geophysics, Geosystems*, 9(5): 21.
- 2388 Li, X., 2000. Cretaceous magmatism and lithospheric extension in Southeast China. *Journal of*
2389 *Asian Earth Sciences*, 18(3): 293-305.
- 2390 Li, Z.-H., Xu, Z., Gerya, T. and Burg, J.-P., 2013. Collision of continental corner from 3-D
2391 numerical modeling. *Earth and Planetary Science Letters*, 380: 98-111.
- 2392 Lithgow - Bertelloni, C. and Richards, M.A., 1998. The dynamics of Cenozoic and Mesozoic plate
2393 motions. *Reviews of Geophysics*, 36(1): 27-78.
- 2394 Liu, L. and Gurnis, M., 2008. Simultaneous inversion of mantle properties and initial conditions
2395 using an adjoint of mantle convection. *Journal of Geophysical Research B*, 113(B08405):
2396 17.
- 2397 Lohman, D.J., de Bruyn, M., Page, T., von Rintelen, K., Hall, R., Ng, P.K., Shih, H.-T., Carvalho,
2398 G.R. and von Rintelen, T., 2011. Biogeography of the Indo-Australian archipelago. *Annual*
2399 *Review of Ecology, Evolution, and Systematics*, 42: 205-226.
- 2400 Mathews, D.C., 2014. The Absolute Motion of Trenches and Age of the Subducting Slab. Master's
2401 Thesis, Department of Earth Science. Rice University: 49.
- 2402 Matthews, D., 1990. Serendipity or economics? Tin and the theory of mineral discovery and
2403 development, 1800–1920. *Business History*, 32(3): 15-48.
- 2404 Matthews, K.J., Müller, R.D. and Sandwell, D.T., 2016. Oceanic microplate formation records the
2405 onset of India–Eurasia collision. *Earth and Planetary Science Letters*, 433: 204-214.
- 2406 Matthews, K.J., Müller, R.D., Wessel, P. and Whittaker, J.M., 2011. The tectonic fabric of the
2407 ocean basins. *Journal of Geophysical Research*, 116(B12): B12109.
- 2408 Matthews, K.J., Seton, M. and Müller, R.D., 2012. A global-scale plate reorganization event at
2409 105– 100 Ma. *Earth and Planetary Science Letters*, 355: 283-298.
- 2410 McCourt, W.J., Crow, M.J., Cobbing, E.J. and Amin, T.C., 1996. Mesozoic and Cenozoic plutonic
2411 evolution of SE Asia: evidence from Sumatra, Indonesia. *Geological Society, London,*
2412 *Special Publications*, 106(1): 321-335.
- 2413 McDermid, I.R.C., Aitchison, J.C., Davis, A.M., Harrison, T.M. and Grove, M., 2002. The Zedong
2414 terrane: a Late Jurassic intra-oceanic magmatic arc within the Yarlung–Tsangpo suture
2415 zone, southeastern Tibet. *Chemical Geology*, 187(3): 267-277.
- 2416 McElhinny, M.W., Embleton, B.J.J., Ma, X.H. and Zhang, Z.K., 1981. Fragmentation of Asia in the
2417 Permian. *Nature*, 293(5829): 212-214.
- 2418 McKenzie, D.P., 1969. Speculations on the consequences and causes of plate motions. *Geophysical*
2419 *Journal International*, 18(1): 1-32.
- 2420 McKenzie, D.P. and Parker, R.L., 1967. The North Pacific: an example of tectonics on a sphere.
2421 *Nature*, 216: 1276-1280.
- 2422 McNamara, A.K. and Zhong, S., 2005. Thermochemical structures beneath Africa and the Pacific
2423 Ocean. *Nature*, 437(7062): 1136-1139.

- 2424 Metcalfe, I., 1988. Origin and assembly of south-east Asian continental terranes. Geological
2425 Society, London, Special Publications, 37(1): 101-118.
- 2426 Metcalfe, I., 1994. Gondwanaland origin, dispersion, and accretion of East and Southeast Asian
2427 continental terranes. *Journal of South American Earth Sciences*, 7(3): 333-347.
- 2428 Metcalfe, I., 1999. Gondwana dispersion and Asian accretion: an overview. In: I. Metcalfe (Editor),
2429 Gondwana dispersion and Asian Accretion. A.A. Balkema, Rotterdam, pp. 9-28.
- 2430 Metcalfe, I., 2002. Permian tectonic framework and palaeogeography of SE Asia. *Journal of Asian
2431 Earth Sciences*, 20(6): 551-566.
- 2432 Metcalfe, I., 2006. Palaeozoic and Mesozoic tectonic evolution and palaeogeography of East Asian
2433 crustal fragments: The Korean Peninsula in context. *Gondwana Research*, 9(1-2): 24-46.
- 2434 Metcalfe, I., 2009. Late Palaeozoic and Mesozoic tectonic and palaeogeographical evolution of SE
2435 Asia. Geological Society, London, Special Publications, 315(1): 7-23.
- 2436 Metcalfe, I., 2011. Tectonic framework and Phanerozoic evolution of Sundaland. *Gondwana
2437 Research*, 19(1): 3-21.
- 2438 Metcalfe, I. and Irving, E., 1990. Allochthonous Terrane Processes in Southeast Asia [and
2439 Discussion]. *Philosophical Transactions of the Royal Society of London A: Mathematical,
2440 Physical and Engineering Sciences*, 331(1620): 625-640.
- 2441 Miller, M.S., Kennett, B.L.N. and Toy, V.G., 2006. Spatial and temporal evolution of the
2442 subducting Pacific plate structure along the western Pacific margin. *Journal of Geophysical
2443 Research: Solid Earth*, 111(B2).
- 2444 Milsom, J., 2000. Stratigraphic constraints on suture models for eastern Indonesia. *Journal of Asian
2445 Earth Sciences*, 18(6): 761-779.
- 2446 Mitchell, A., Chung, S.-L., Oo, T., Lin, T.-H. and Hung, C.-H., 2012. Zircon U–Pb ages in
2447 Myanmar: Magmatic–metamorphic events and the closure of a neo-Tethys ocean? *Journal
2448 of Asian Earth Sciences*, 56: 1-23.
- 2449 Monnier, C., Girardeau, J., Maury, R.C. and Cotten, J., 1995. Back-arc basin origin for the East
2450 Sulawesi ophiolite (eastern Indonesia). *Geology*, 23(9): 851-854.
- 2451 Monnier, C., Girardeau, J., Pubellier, M. and Permana, H., 2000. The central ophiolite belt of Irian
2452 Jaya (Indonesia): petrological and geochemical evidence for a back-arc basin origin.
2453 *Comptes Rendus de l'Academie des Sciences Series IIA Earth and Planetary Science*,
2454 331(11): 691-699.
- 2455 Monod, L. and Prendini, L., 2015. Evidence for Eurogondwana: the roles of dispersal, extinction
2456 and vicariance in the evolution and biogeography of Indo - Pacific Hormuridae (Scorpiones:
2457 Scorpionoidea). *Cladistics*, 31(1): 71-111.
- 2458 Montelli, R., Nolet, G., Dahlen, F.A. and Masters, G., 2006. A catalogue of deep mantle plumes:
2459 new results from finite-frequency tomography. *Geochemistry, Geophysics, Geosystems*,
2460 7(11): Q11007.
- 2461 Morley, C.K., 2012a. Late Cretaceous-early Palaeogene tectonic development of SE Asia. *Earth-
2462 Science Reviews*, 115(1-2): 37-75.
- 2463 Morley, R.J., 2012b. A review of the Cenozoic palaeoclimate history of Southeast Asia. Biotic
2464 evolution and environmental change in Southeast Asia. *The Systematics Association
2465 Special*, 82: 79-114.
- 2466 Morra, G., Seton, M., Quevedo, L. and Müller, R.D., 2013. Organization of the tectonic plates in
2467 the last 200 Myr. *Earth and Planetary Science Letters*, 373: 93-101.
- 2468 Mubroto, B., Briden, J.C., McClelland, E. and Hall, R., 1994. Palaeomagnetism of the Balantak
2469 ophiolite, Sulawesi. *Earth and Planetary Science Letters*, 125(1): 193-209.
- 2470 Müller, R.D., Royer, J.Y. and Lawver, L.A., 1993. Revised plate motions relative to the hotspots
2471 from combined Atlantic and Indian Ocean hotspot tracks. *Geology*, 21(3): 275.
- 2472 Müller, R.D., Sdrolias, M., Gaina, C., Steinberger, B. and Heine, C., 2008. Long-term sea-level
2473 fluctuations driven by ocean basin dynamics. *Science*, 319(5868): 1357.
- 2474 Müller, R.D., Seton, M., Zahirovic, S., Williams, S.E., Matthews, K.J., Wright, N.M., Shephard, G.,
2475 Maloney, K.T., Barnett-Moore, N., Hosseinpour, M., Bower, D.J. and Cannon, J., 2016.

2476 Ocean basin evolution and global-scale plate reorganization events since Pangea breakup.
 2477 Annual Review of Earth and Planetary Sciences, 44.
 2478 Norton, I.O., 1999. Global plate reconstruction model. ExxonMobil Exploration.
 2479 Obayashi, M., Yoshimitsu, J., Nolet, G., Fukao, Y., Shiobara, H., Sugioka, H., Miyamachi, H. and
 2480 Gao, Y., 2013. Finite frequency whole mantle P wave tomography: Improvement of
 2481 subducted slab images. *Geophysical Research Letters*, 40(21): 5652-5657.
 2482 Page, R.W., 1976. Geochronology of igneous and metamorphic rocks in the New Guinea
 2483 Highlands. Australian Government Publ. Service.
 2484 Parkinson, C.D., Miyazaki, K., Wakita, K., Barber, A.J. and Carswell, D.A., 1998. An overview
 2485 and tectonic synthesis of the pre - Tertiary very - high - pressure metamorphic and
 2486 associated rocks of Java, Sulawesi and Kalimantan, Indonesia. *Island Arc*, 7(1 - 2): 184-
 2487 200.
 2488 Patriat, P. and Achache, J., 1984. India-Eurasia collision chronology has implications for crustal
 2489 shortening and driving mechanism of plates. *Nature*, 311: 615-621.
 2490 Paulson, A., Zhong, S. and Wahr, J., 2007. Inference of mantle viscosity from GRACE and relative
 2491 sea level data. *Geophysical Journal International*, 171(2): 497-508.
 2492 Pedersen, R.B., Searle, M.P., Carter, A. and Bandopadhyay, P.C., 2010. U-Pb zircon age of the
 2493 Andaman ophiolite: implications for the beginning of subduction beneath the Andaman-
 2494 Sumatra arc. *Journal of the Geological Society*, 167(6): 1105-1112.
 2495 Penrose, R., 1903. The tin deposits of the Malay Peninsula with special reference to those of the
 2496 Kinta district. *The Journal of Geology*, 11(2): 135-154.
 2497 Permana, H., 1998. Dynamique de la mise en place des ophiolites d'Irian Jaya (Indonesie), PhD
 2498 thesis of the Universite de Nantes, 314 pp.
 2499 Petterson, M.G., 2010. A review of the geology and tectonics of the Kohistan island arc, north
 2500 Pakistan. *Geological Society, London, Special Publications*, 338(1): 287-327.
 2501 Petterson, M.G. and Windley, B.F., 1985. Rb Sr dating of the Kohistan arc-batholith in the Trans-
 2502 Himalaya of north Pakistan, and tectonic implications. *Earth and Planetary Science Letters*,
 2503 74(1): 45-57.
 2504 Pieters, P.E., Pigram, C.J., Trail, D.S., Dow, D.B., Ratman, N. and Sukanto, R., 1983. The
 2505 stratigraphy of western Irian Jaya.
 2506 Pigram, C.J. and Panggabean, H., 1984. Rifting of the northern margin of the Australian continent
 2507 and the origin of some microcontinents in eastern Indonesia. *Tectonophysics*, 107(3): 331-
 2508 353.
 2509 Pigram, C.J. and Symonds, P.A., 1991. A review of the timing of the major tectonic events in the
 2510 New Guinea Orogen. *Journal of Southeast Asian Earth Sciences*, 6(3): 307-318.
 2511 Polvé, M., Maury, R.C., Bellon, H., Rangin, C., Priadi, B., Yuwono, S., Joron, J.L. and Atmadja,
 2512 R.S., 1997. Magmatic evolution of Sulawesi (Indonesia): constraints on the Cenozoic
 2513 geodynamic history of the Sundaland active margin. *Tectonophysics*, 272(1): 69-92.
 2514 Pubellier, M., Ali, J. and Monnier, C., 2003. Cenozoic Plate interaction of the Australia and
 2515 Philippine Sea Plates: "hit-and-run" tectonics. *Tectonophysics*, 363(3): 181-199.
 2516 Pubellier, M., Monnier, C., Maury, R. and Tamayo, R., 2004. Plate kinematics, origin and tectonic
 2517 emplacement of supra-subduction ophiolites in SE Asia. *Tectonophysics*, 392(1): 9-36.
 2518 Pubellier, M. and Morley, C.K., 2014. The basins of Sundaland (SE Asia): Evolution and boundary
 2519 conditions. *Marine and Petroleum Geology*, 58: 555-578.
 2520 Pudsey, C.J., 1986. The Northern Suture, Pakistan: margin of a Cretaceous island arc. *Geological*
 2521 *Magazine*, 123(04): 405-423.
 2522 Pudsey, C.J., Schroeder, R. and Skelton, P.W., 1985. Cretaceous (Aptian/Albian) Age for Island-
 2523 Arc Volcanics, Kohistan, N Pakistan. In: V. Gupta (Editor), *Geology of Western Himalayas*.
 2524 Hindustan Publishing Corporation, pp. 150-168.
 2525 Pusok, A.E. and Kaus, B.J.P., 2015. Development of topography in 3 - D continental - collision
 2526 models. *Geochemistry, Geophysics, Geosystems*.

2527 Queano, K.L., Ali, J.R., Milsom, J., Aitchison, J.C. and Pubellier, M., 2007. North Luzon and the
 2528 Philippine Sea Plate motion model: Insights following paleomagnetic, structural, and age-
 2529 dating investigations. *Journal of Geophysical Research*, 112(B5): B05101.
 2530 Rangin, C., Jolivet, L. and Pubellier, M., 1990. A simple model for the tectonic evolution of
 2531 southeast Asia and Indonesia region for the past 43 my. *Bulletin de la Société géologique de*
 2532 *France*, 6(6): 889-905.
 2533 Ratnaswamy, V., Stadler, G. and Gurnis, M., 2015. Adjoint-based estimation of plate coupling in a
 2534 non-linear mantle flow model: theory and examples. *Geophysical Journal International*,
 2535 202(2): 768-786.
 2536 Rehault, J.P., Moussat, E. and Fabbri, A., 1987. Structural evolution of the Tyrrhenian back-arc
 2537 basin. *Marine Geology*, 74(1): 123-150.
 2538 Rehman, H.U.R., Seno, T., Yamamoto, H. and Khan, T., 2011. Timing of collision of the Kohistan-
 2539 Ladakh Arc with India and Asia: Debate. *Island Arc*, 20(3): 308-328.
 2540 Replumaz, A., Karason, H., van der Hilst, R.D., Besse, J. and Tapponnier, P., 2004. 4-D evolution
 2541 of SE Asia's mantle from geological reconstructions and seismic tomography. *Earth and*
 2542 *Planetary Science Letters*, 221(1-4): 103-115.
 2543 Richards, M.A., Bunge, H.P. and Lithgow - Bertelloni, C., 2000. Mantle convection and plate
 2544 motion history: toward general circulation models. *The history and dynamics of global plate*
 2545 *motions*: 289-307.
 2546 Richter, C. and Ali, J.R., 2015. Philippine Sea Plate motion history: Eocene-Recent record from
 2547 ODP Site 1201, central West Philippine Basin. *Earth and Planetary Science Letters*, 410:
 2548 165-173.
 2549 Rickwood, F.K., 1954. The geology of the western highlands of New Guinea. *Journal of the*
 2550 *Geological Society of Australia*, 2(1): 63-82.
 2551 Rock, N.M.S., Aldiss, D.T., Aspden, J.A., Clarke, M.C.G., Djunuddin, A., Miswar, W.K.,
 2552 Thompson, S.J. and Whandoyo, R., 1983. The Geology of the Lubuksikaping Quadrangle,
 2553 Sumatra. *Geol. Survey of Indonesia*, Bandung.
 2554 Rohrman, M., 2015. Delineating the Exmouth mantle plume (NW Australia) from denudation and
 2555 magmatic addition estimates. *Lithosphere*, 7(4): L445. 1.
 2556 Rolland, J., Condamine, F.L., Beeravolu, C.R., Jiguet, F. and Morlon, H., 2015. Dispersal is a major
 2557 driver of the latitudinal diversity gradient of Carnivora. *Global Ecology and Biogeography*,
 2558 24(9): 1059-1071.
 2559 Romanowicz, B., 2008. Using seismic waves to image Earth's internal structure. *Nature*, 451(7176):
 2560 266-268.
 2561 Rosenbaum, G., 2014. Geodynamics of oroclinal bending: Insights from the Mediterranean. *Journal*
 2562 *of Geodynamics*, 82: 5-15.
 2563 Royer, J.Y. and Chang, T., 1991. Evidence for relative motions between the Indian and Australian
 2564 plates during the last 20 my from plate tectonic reconstructions: implications for the
 2565 deformation of the Indo-Australian plate. *Journal of Geophysical Research*, 96(B7): 11779-
 2566 11,802.
 2567 Ryan, W.B., Carbotte, S.M., Coplan, J.O., O'Hara, S., Melkonian, A., Arko, R., Weissel, R.A.,
 2568 Ferrini, V., Goodwillie, A. and Nitsche, F., 2009. Global Multi - Resolution Topography
 2569 synthesis. *Geochemistry, Geophysics, Geosystems*, 10(3).
 2570 Sandiford, M., 2007. The tilting continent: a new constraint on the dynamic topographic field from
 2571 Australia. *Earth and Planetary Science Letters*, 261(1): 152-163.
 2572 Schaltegger, U., Frank, M. and Burg, J.-P., 2003. A 120 million years record of magmatism and
 2573 crustal melting in the Kohistan Batholith, EGS-AGU-EUG Joint Assembly, pp. 6816.
 2574 Schärer, U., Hamet, J. and Allègre, C.J., 1984. The Transhimalaya (Gangdese) plutonism in the
 2575 Ladakh region: a U Pb and Rb Sr study. *Earth and Planetary Science Letters*, 67(3): 327-
 2576 339.

2577 Schellart, W. and Lister, G., 2005. The role of the East Asian active margin in widespread
2578 extensional and strike-slip deformation in East Asia. *Journal of the Geological Society*,
2579 162(6): 959-972.

2580 Schellart, W.P. and Spakman, W., 2015. Australian plate motion and topography linked to fossil
2581 New Guinea slab below Lake Eyre. *Earth and Planetary Science Letters*, 421: 107-116.

2582 Scotese, C., Boucot, A. and McKerrow, W., 1999. Gondwanan palaeogeography and pal
2583 oclimatology. *Journal of African Earth Sciences*, 28(1): 99-114.

2584 Scotese, C.R., Gahagan, L.M. and Larson, R.L., 1988. Plate tectonic reconstructions of the
2585 Cretaceous and Cenozoic ocean basins. *Tectonophysics*, 155(1): 27-48.

2586 Sdrolias, M. and Müller, R.D., 2006. Controls on back - arc basin formation. *Geochemistry*,
2587 *Geophysics, Geosystems*, 7(4).

2588 Sdrolias, M., Roest, W.R. and Müller, R.D., 2004. An expression of Philippine Sea plate rotation:
2589 the Parece Vela and Shikoku basins. *Tectonophysics*, 394(1): 69-86.

2590 Searle, M.P., Whitehouse, M.J., Robb, L.J., Ghani, A.A., Hutchison, C.S., Sone, M., Ng, S.W.P.,
2591 Roselee, M.H., Chung, S.-L. and Oliver, G.J.H., 2012. Tectonic evolution of the Sibumasu-
2592 Indochina terrane collision zone in Thailand and Malaysia: constraints from new U-Pb
2593 zircon chronology of SE Asian tin granitoids. *Journal of the Geological Society*, 169: 489.

2594 Şengör, A.M.C., Altın, D., Cin, A., Ustaömer, T. and Hsü, K.J., 1988. Origin and assembly of the
2595 Tethyside orogenic collage at the expense of Gondwana Land. *Geological Society, London*,
2596 *Special Publications*, 37(1): 119-181.

2597 Şengör, A.M.C. and Natal'in, B.A., 1996. Paleotectonics of Asia: Fragments of a synthesis. In: A.
2598 Yin and T.M. Harrison (Editors), *The Tectonic Evolution of Asia*. Cambridge Univ. Press
2599 New York, pp. 486-640.

2600 Seton, M., Gaina, C., Müller, R.D. and Heine, C., 2009. Mid-Cretaceous seafloor spreading pulse:
2601 Fact or fiction? *Geology*, 37(8): 687-690.

2602 Seton, M., Müller, R.D., Zahirovic, S., Gaina, C., Torsvik, T.H., Shephard, G., Talsma, A., Gurnis,
2603 M., Turner, M., Maus, S. and Chandler, M., 2012. Global continental and ocean basin
2604 reconstructions since 200 Ma. *Earth-Science Reviews*, 113(3-4): 212-270.

2605 Seton, M., Whittaker, J.M., Wessel, P., Müller, R.D., DeMets, C., Merkouriev, S., Cande, S., Gaina,
2606 C., Eagles, G. and Granot, R., 2014. Community infrastructure and repository for marine
2607 magnetic identifications. *Geochemistry, Geophysics, Geosystems*, 15(4): 1629-1641.

2608 Sevastjanova, I., Hall, R., Rittner, M., Paw, S.M.T.L., Naing, T.T., Alderton, D.H. and Comfort, G.,
2609 2015. Myanmar and Asia united, Australia left behind long ago. *Gondwana Research*.

2610 Shemenda, A.I., 1993. Subduction of the lithosphere and back arc dynamics: Insights from physical
2611 modeling. *Journal of Geophysical Research*, 98(B9): 16167-16185.

2612 Shi, G., Cui, W., Cao, S., Jiang, N., Jian, P., Liu, D., Miao, L. and Chu, B., 2008. Ion microprobe
2613 zircon U-Pb age and geochemistry of the Myanmar jadeitite. *Journal of the Geological*
2614 *Society*, 165(1): 221-234.

2615 Shi, G., Lei, W., He, H., Ng, Y.N., Liu, Y., Liu, Y., Yuan, Y., Kang, Z. and Xie, G., 2014.
2616 Superimposed tectono-metamorphic episodes of Jurassic and Eocene age in the jadeite
2617 uplift, Myanmar, as revealed by 40 Ar/39 Ar dating. *Gondwana Research*, 26(2): 464-474.

2618 Shi, H. and Li, C.-F., 2012. Mesozoic and early Cenozoic tectonic convergence-to-rifting transition
2619 prior to opening of the South China Sea. *International Geology Review*, 54(15): 1801-1828.

2620 Simmons, N., Myers, S., Johannesson, G., Matzel, E. and Grand, S., 2015. Evidence for long -
2621 lived subduction of an ancient tectonic plate beneath the southern Indian Ocean.
2622 *Geophysical Research Letters*, 42(21): 9270-9278.

2623 Simmons, N.A., Forte, A.M., Boschi, L. and Grand, S.P., 2010. GyPSuM: A joint tomographic
2624 model of mantle density and seismic wave speeds. *Journal of Geophysical Research: Solid*
2625 *Earth* (1978–2012), 115(B12).

2626 Smyth, H.R., Hamilton, P.J., Hall, R. and Kinny, P.D., 2007. The deep crust beneath island arcs:
2627 Inherited zircons reveal a Gondwana continental fragment beneath East Java, Indonesia.
2628 *Earth and Planetary Science Letters*, 258(1-2): 269-282.

- 2629 Soeria-Atmadja, R., Noeradi, D. and Priadi, B., 1999. Cenozoic magmatism in Kalimantan and its
2630 related geodynamic evolution. *Journal of Asian Earth Sciences*, 17(1): 25-45.
- 2631 Spasojevic, S. and Gurnis, M., 2012. Sea level and vertical motion of continents from dynamic
2632 earth models since the Late Cretaceous. *AAPG bulletin*, 96(11): 2037-2064.
- 2633 Spasojevic, S., Liu, L. and Gurnis, M., 2009. Adjoint models of mantle convection with seismic,
2634 plate motion, and stratigraphic constraints: North America since the Late Cretaceous.
2635 *Geochemistry, Geophysics, Geosystems*, 10(5).
- 2636 Stampfli, G.M. and Borel, G.D., 2002. A plate tectonic model for the Paleozoic and Mesozoic
2637 constrained by dynamic plate boundaries and restored synthetic oceanic isochrons. *Earth
2638 and Planetary Science Letters*, 196(1-2): 17-33.
- 2639 Stauffer, P.H., 1983. Unraveling the mosaic of Paleozoic crustal blocks in Southeast Asia.
2640 *Geologische Rundschau*, 72(3): 1061-1080.
- 2641 Steinberger, B. and Calderwood, A.R., 2006. Models of large-scale viscous flow in the Earth's
2642 mantle with constraints from mineral physics and surface observations. *Geophysical Journal
2643 International*, 167(3): 1461-1481.
- 2644 Steinberger, B. and O'Connell, R.J., 1998. Advection of plumes in mantle flow: implications for
2645 hotspot motion, mantle viscosity and plume distribution. *Geophysical Journal International*,
2646 132(2): 412-434.
- 2647 Steinberger, B. and Torsvik, T.H., 2008. Absolute plate motions and true polar wander in the
2648 absence of hotspot tracks. *Nature*, 452(7187): 620-623.
- 2649 Steinberger, B., Torsvik, T.H. and Becker, T.W., 2012. Subduction to the lower mantle-a
2650 comparison between geodynamic and tomographic models. *Solid Earth*, 3(2): 415.
- 2651 Stern, R.J., Reagan, M., Ishizuka, O., Ohara, Y. and Whattam, S., 2012. To understand subduction
2652 initiation, study forearc crust: To understand forearc crust, study ophiolites. *Lithosphere*,
2653 4(6): 469-483.
- 2654 Sukamoto, R. and Westermann, G., 1992. The Jurassic of the Circum- Pacific. Indonesia and Papua
2655 New Guinea. Cambridge University Press.
- 2656 Tapponnier, P., Peltzer, G., Le Dain, A.Y., Armijo, R. and Cobbold, P., 1982. Propagating
2657 extrusion tectonics in Asia: New insights from simple experiments with plasticine. *Geology*,
2658 10(12): 611-616.
- 2659 Taylor, B. and Hayes, D.E., 1980. The tectonic evolution of the South China Basin. The tectonic
2660 and geologic evolution of Southeast Asian seas and islands: 89-104.
- 2661 Taylor, B. and Hayes, D.E., 1983. Origin and history of the South China Sea basin. The Tectonic
2662 and Geologic Evolution of Southeast Asian Seas and Islands: Part 2: 23-56.
- 2663 Torsvik, T.H., Müller, R.D., van der Voo, R., Steinberger, B. and Gaina, C., 2008. Global plate
2664 motion frames: toward a unified model. *Reviews of Geophysics*, 46(3).
- 2665 Tovaglieri, F. and George, A.D., 2014. Stratigraphic architecture of an Early–Middle Jurassic
2666 tidally influenced deltaic system (Plover Formation), Browse Basin, Australian North West
2667 Shelf. *Marine and Petroleum Geology*, 49: 59-83.
- 2668 Treloar, P.J., Petterson, M.G., Jan, M.Q. and Sullivan, M., 1996. A re-evaluation of the stratigraphy
2669 and evolution of the Kohistan arc sequence, Pakistan Himalaya: implications for magmatic
2670 and tectonic arc-building processes. *Journal of the Geological Society*, 153(5): 681-693.
- 2671 Turcotte, D.L. and Oxburgh, E.R., 1972. Mantle convection and the new global tectonics. *Annual
2672 Review of Fluid Mechanics*, 4(1): 33-66.
- 2673 Valenti, G.L., 1993. P'nyang Field: discovery and geology of a gas giant in the western Papuan Fold
2674 Belt, Western Province, Papua New Guinea, *Proceedings of the Second PNG Petroleum
2675 Convention*, pp. 413-430.
- 2676 van der Meer, D.G., Spakman, W., van Hinsbergen, D.J.J., Amaru, M.L. and Torsvik, T.H., 2010.
2677 Towards absolute plate motions constrained by lower-mantle slab remnants. *Nature
2678 Geoscience*, 3: 36-40.

2679 van der Meer, D.G., Zeebe, R.E., van Hinsbergen, D.J.J., Sluijs, A., Spakman, W. and Torsvik,
 2680 T.H., 2014. Plate tectonic controls on atmospheric CO₂ levels since the Triassic.
 2681 Proceedings of the National Academy of Sciences, 111(12): 4380-4385.
 2682 van der Voo, R., Spakman, W. and Bijwaard, H., 1999a. Mesozoic subducted slabs under Siberia.
 2683 Nature, 397(6716): 246-249.
 2684 van der Voo, R., Spakman, W. and Bijwaard, H., 1999b. Tethyan subducted slabs under India.
 2685 Earth and Planetary Science Letters, 171(1): 7-20.
 2686 van Dongen, M., Weinberg, R.F., Tomkins, A.G., Armstrong, R.A. and Woodhead, J.D., 2010.
 2687 Recycling of Proterozoic crust in Pleistocene juvenile magma and rapid formation of the Ok
 2688 Tedi porphyry Cu–Au deposit, Papua New Guinea. Lithos, 114(3–4): 282-292.
 2689 van Hinsbergen, D.J.J., Lippert, P.C., Dupont-Nivet, G., McQuarrie, N., Doubrovine, P.V.,
 2690 Spakman, W. and Torsvik, T.H., 2012. Greater India Basin hypothesis and a two-stage
 2691 Cenozoic collision between India and Asia. Proceedings of the National Academy of
 2692 Sciences, 109(20): 7659-7664.
 2693 van Hinsbergen, D.J.J., Steinberger, B., Doubrovine, P.V. and Gassmüller, R., 2011. Acceleration
 2694 and deceleration of India–Asia convergence since the Cretaceous: roles of mantle plumes
 2695 and continental collision. Journal of Geophysical Research - Solid Earth, 116(B06101).
 2696 van Hunen, J. and Allen, M.B., 2011. Continental collision and slab break-off: a comparison of 3-D
 2697 numerical models with observations. Earth and Planetary Science Letters, 302(1): 27-37.
 2698 van Leeuwen, T.M., 1981. The geology of southwest Sulawesi with special reference to the Biru
 2699 area. The geology and tectonics of Eastern Indonesia, 2: 277-304.
 2700 van Ufford, A.Q. and Cloos, M., 2005. Cenozoic tectonics of New Guinea. AAPG bulletin, 89(1):
 2701 119-140.
 2702 Veevers, J.J., 2004. Gondwanaland from 650–500 Ma assembly through 320 Ma merger in Pangea
 2703 to 185–100 Ma breakup: supercontinental tectonics via stratigraphy and radiometric dating.
 2704 Earth-Science Reviews, 68(1-2): 1-132.
 2705 Vérard, C., Flores, K. and Stampfli, G., 2012. Geodynamic reconstructions of the South America–
 2706 Antarctica plate system. Journal of Geodynamics, 53: 43-60.
 2707 von Rad, U. and Exon, N.F., 1983. Mesozoic-Cenozoic sedimentary and volcanic evolution of the
 2708 starved passive continental margin off northwest Australia. In: J. Watkins and C. Drake
 2709 (Editors), Studies in Continental Margin Geology: AAPG Mem., pp. 252-281.
 2710 von Rad, U., Exon, N.F. and Haq, B.U., 1992. 46. Rift-To-Drift History Of The Wombat Plateau,
 2711 Northwest Australia: Triassic To Tertiary Leg 122 Results.
 2712 Wajzer, M., Barber, A. and Hidayat, S., 1991. Accretion, collision and strike-slip faulting: the
 2713 Woyla group as a key to the tectonic evolution of North Sumatra. Journal of Southeast
 2714 Asian Earth Sciences, 6(3-4): 447-461.
 2715 Wakita, K., 2000. Cretaceous accretionary–collision complexes in central Indonesia. Journal of
 2716 Asian Earth Sciences, 18(6): 739-749.
 2717 Wakita, K. and Metcalfe, I., 2005. Ocean plate stratigraphy in East and Southeast Asia. Journal of
 2718 Asian Earth Sciences, 24(6): 679-702.
 2719 Wakita, K., Miyazaki, K., Zulkarnain, I., Sopaheluwakan, J. and Sanyoto, P., 1998. Tectonic
 2720 implications of new age data for the Meratus complex of south Kalimantan, Indonesia.
 2721 Island Arc, 7(1 - 2): 202-222.
 2722 Wang, P., 2004. Cenozoic Deformation and the History of Sea - Land Interactions in Asia.
 2723 Continent-Ocean Interactions Within East Asian Marginal Seas: 1-22.
 2724 Wen, D.-R., Chung, S.-L., Song, B., Iizuka, Y., Yang, H.-J., Ji, J., Liu, D. and Gallet, S., 2008a.
 2725 Late Cretaceous Gangdese intrusions of adakitic geochemical characteristics, SE Tibet:
 2726 petrogenesis and tectonic implications. Lithos, 105(1): 1-11.
 2727 Wen, D.-R., Liu, D., Chung, S.-L., Chu, M.-F., Ji, J., Zhang, Q., Song, B., Lee, T.-Y., Yeh, M.-W.
 2728 and Lo, C.-H., 2008b. Zircon SHRIMP U–Pb ages of the Gangdese Batholith and
 2729 implications for Neotethyan subduction in southern Tibet. Chemical Geology, 252(3): 191-
 2730 201.

2731 Wennekers, J.H.L., 1958. South Sumatra Basinal Area: Far East, SP 18: Habitat of Oil. AAPG
 2732 Special Volumes, pp. 1347-1358.
 2733 Wessel, P., Smith, W.H.F., Scharroo, R., Luis, J. and Wobbe, F., 2013. Generic Mapping Tools:
 2734 Improved Version Released. *Eos, Transactions American Geophysical Union*, 94(45): 409-
 2735 410.
 2736 Whittaker, J.M., Müller, R.D., Sdrolias, M. and Heine, C., 2007. Sunda-Java trench kinematics, slab
 2737 window formation and overriding plate deformation since the Cretaceous. *Earth and*
 2738 *Planetary Science Letters*, 255(3): 445-457.
 2739 Widiyantoro, S., Kennett, B. and Van der Hilst, R., 1998. Extending shear-wave tomography for the
 2740 lower mantle using S and SKS arrival-time data. *Earth, planets and space*, 50(11-12): 999-
 2741 1012.
 2742 Widiyantoro, S. and van der Hilst, R.D., 1996. Structure and evolution of subducted lithosphere
 2743 beneath the Sunda arc, Indonesia. *Science Reports*, 271(5255): 1566-1570.
 2744 Williams, S.E., Whittaker, J.M. and Müller, R.D., 2011. Full - fit, palinspastic reconstruction of the
 2745 conjugate Australian - Antarctic margins. *Tectonics*, 30(6): 21.
 2746 Worthen, J., Stadler, G., Petra, N., Gurnis, M. and Ghattas, O., 2014. Towards adjoint-based
 2747 inversion for rheological parameters in nonlinear viscous mantle flow. *Physics of the Earth*
 2748 *and Planetary Interiors*, 234: 23-34.
 2749 Worthing, M.A. and Crawford, A.J., 1996. The igneous geochemistry and tectonic setting of
 2750 metabasites from the Emo Metamorphics, Papua New Guinea; a record of the evolution and
 2751 destruction of a backarc basin. *Mineralogy and Petrology*, 58(1-2): 79-100.
 2752 Wu, J., Suppe, J., Lu, R. and Kanda, R., 2016. Philippine Sea and East Asian plate tectonics since
 2753 52 Ma constrained by new subducted slab reconstruction methods. *Journal of Geophysical*
 2754 *Research: Solid Earth*.
 2755 Xu, C., Boucot, A., Scotese, C. and Junxuan, F., 2012. Pangaean aggregation and disaggregation
 2756 with evidence from global climate belts. *Journal of Palaeogeography*, 1: 5-13.
 2757 Yang, S., Hu, S., Cai, D., Feng, X., Chen, L. and Gao, L., 2004. Present-day heat flow, thermal
 2758 history and tectonic subsidence of the East China Sea Basin. *Marine and petroleum geology*,
 2759 21(9): 1095-1105.
 2760 Yang, T., Gurnis, M. and Zahirovic, S., 2016. Mantle - induced subsidence and compression in SE
 2761 Asia since the early Miocene. *Geophysical Research Letters*.
 2762 Yin, A. and Harrison, T.M., 2000. Geologic evolution of the Himalayan-Tibetan orogen. *Annual*
 2763 *Review of Earth and Planetary Sciences*, 28(1): 211-280.
 2764 Yirgu, G., Ebinger, C.J. and Maguire, P.K.H., 2006. The afar volcanic province within the East
 2765 African Rift System: introduction. *Geological Society, London, Special Publications*,
 2766 259(1): 1-6.
 2767 Yoshida, M. and Hamano, Y., 2015. Pangea breakup and northward drift of the Indian subcontinent
 2768 reproduced by a numerical model of mantle convection. *Scientific reports*, 5.
 2769 Yumul, G.P., Dimalanta, C.B., Marquez, E.J. and Queaño, K.L., 2009. Onland signatures of the
 2770 Palawan microcontinental block and Philippine mobile belt collision and crustal growth
 2771 process: A review. *Journal of Asian Earth Sciences*, 34(5): 610-623.
 2772 Yuwono, Y.S., Priyomarsono, S., Maury, R.C., Rampnoux, J.P., Soeria-Atmadja, R., Bellon, H. and
 2773 Chotin, P., 1988. Petrology of the Cretaceous magmatic rocks from Meratus Range,
 2774 southeast Kalimantan. *Journal of Southeast Asian Earth Sciences*, 2(1): 15-22.
 2775 Zahirovic, S., Flament, N., Müller, R.D., Seton, M. and Gurnis, M., In Press. Large fluctuations of
 2776 shallow seas in low-lying Southeast Asia driven by mantle flow. *Geochem. Geophys.*
 2777 *Geosys.*
 2778 Zahirovic, S., Müller, R.D., Seton, M. and Flament, N., 2015. Tectonic speed limits from plate
 2779 kinematic reconstructions. *Earth and Planetary Science Letters*, 418: 40-52.
 2780 Zahirovic, S., Müller, R.D., Seton, M., Flament, N., Gurnis, M. and Whittaker, J., 2012. Insights on
 2781 the kinematics of the India-Eurasia collision from global geodynamic models. *Geochemistry*
 2782 *Geophysics Geosystems*, 13(Q04W11).

2783 Zahirovic, S., Seton, M. and Müller, R., 2014. The Cretaceous and Cenozoic tectonic evolution of
2784 Southeast Asia. *Solid Earth (EGU)*, 5: 227-273.

2785 Zaman, H., Otofuji, Y.-i., Khan, S.R. and Ahmad, M.N., 2013. New paleomagnetic results from the
2786 northern margin of the Kohistan Island Arc. *Arabian Journal of Geosciences*, 6(4): 1041-
2787 1054.

2788 Zaman, H. and Torii, M., 1999. Palaeomagnetic study of Cretaceous red beds from the eastern
2789 Hindukush ranges, northern Pakistan: palaeoreconstruction of the Kohistan–Karakoram
2790 composite unit before the India–Asia collision. *Geophysical Journal International*, 136(3):
2791 719-738.

2792 Zaw, K., Meffre, S., Lai, C.-K., Burrett, C., Santosh, M., Graham, I., Manaka, T., Salam, A.,
2793 Kamvong, T. and Cromie, P., 2014. Tectonics and metallogeny of mainland Southeast
2794 Asia—A review and contribution. *Gondwana Research*, 26(1): 5-30.

2795 Zhang, K.-J., Zhang, Y.-X., Tang, X.-C. and Xia, B., 2012. Late Mesozoic tectonic evolution and
2796 growth of the Tibetan plateau prior to the Indo-Asian collision. *Earth-Science Reviews*,
2797 114(3): 236-249.

2798 Zhao, D., Maruyama, S. and Omori, S., 2007. Mantle dynamics of Western Pacific and East Asia:
2799 insight from seismic tomography and mineral physics. *Gondwana Research*, 11(1): 120-131.

2800 Zhong, S., Zuber, M.T., Moresi, L. and Gurnis, M., 2000. Role of temperature-dependent viscosity
2801 and surface plates in spherical shell models of mantle convection. *Journal of Geophysical*
2802 *Research*, 105(B5): 11063.

2803

2804